

Editor-in-Chief B.E.Paton

EDITORIAL BOARD

Yu.S. Borisov, A.Ya. Ishchenko,
B.V. Khitrovskaya (*exec. secretary*),
V.F. Khorunov, I.V. Krivtsun,
S.I. Kuchuk-Yatsenko (*vice-chief editor*),
V.I. Kyrian, Yu.N. Lankin,
V.N. Lipodaev (*vice-chief editor*),
L.M. Lobanov, A.A. Mazur,
O.K. Nazarenko, I.K. Pokhodnya,
V.D. Poznyakov, I.A. Ryabtsev,
K.A. Yushchenko,
A.T. Zelnichenko (*exec. director*)

**INTERNATIONAL EDITORIAL
COUNCIL**

N.P. Alyoshin (Russia)
Guan Qiao (China)
V.I. Lysak (Russia)
B.E. Paton (Ukraine)
Ya. Pilarczyk (Poland)
O.I. Steklov (Russia)
G.A. Turichin (Russia)
M. Zinigrad (Israel)
A.S. Zubchenko (Russia)

Founders

E.O. Paton Electric Welding Institute
of the NAS of Ukraine,
International Association «Welding»

Publisher

International Association «Welding»

Translators:

A.A. Fomin, O.S. Kurochko,
I.N. Kutianova, T.K. Vasilenko
Editor
N.A. Dmitrieva
Electron galley
D.I. Sereda, T.Yu. Snegiryova

Address

E.O. Paton Electric Welding Institute,
International Association «Welding»
11, Bozhenko Str., 03680, Kyiv, Ukraine
Tel.: (38044) 200 60 16, 200 82 77
Fax: (38044) 200 82 77, 200 81 45
E-mail: journal@paton.kiev.ua
www.patonpublishinghouse.com
URL: www.rucont.ru

State Registration Certificate
KV 4790 of 09.01.2001
ISSN 0957-798X

Subscriptions

\$348, 12 issues per year,
air postage and packaging included.
Back issues available.

All rights reserved.

This publication and each of the articles
contained herein are protected by copyright.
Permission to reproduce material contained in
this journal must be obtained in writing from
the Publisher.

CONTENTS

SCIENTIFIC AND TECHNICAL

- Pokhodnya I.K., Ignatenko A.V., Paltsevich A.P. and Sinyuk V.S.* Hydrogen-induced cold cracks in welded joints of high-strength low-alloyed steels (Review) 2
- Gajvoronsky A.A.* Influence of diffusible hydrogen on delayed cracking resistance of high-carbon steel welded joints 14
- Makhnenko V.I.* Problems of examination of modern critical welded structures 21
- Milenin A.S.* On planning of repair of pressurised main pipelines based on the results of in-pipe diagnostics 29
- Rybakov A.A., Semyonov S.E. and Filipchuk T.N.* Properties of the weld metal of two-sided welded joints on pipes made from increased-strength microalloyed steels 39
- Yushchenko K.A., Gakh I.S., Zadery B.A., Zvyagintseva A.V. and Karasevskaya O.P.* Influence of weld pool geometry on structure of metal of welds on high-temperature nickel alloy single crystals 45

INDUSTRIAL

- Khaskin V.Yu.* Development of laser welding of aluminium alloys at the E.O. Paton Electric Welding Institute (Review) 51
- Sergeeva E.V.* Friction stir welding in aerospace industry (Review) 56
- Dobrushin L.D., Pekar E.D., Bryzgalin A.G. and Illarionov S.Yu.* Method for measurement of dynamic strains in explosion welding 61

«The Paton Welding Journal» abstracted and indexed in Ukrainian refereed journal «Source», RJ VINITI «Welding» (Russia), INSPEC, «Welding Abstracts», ProQuest (UK), EBSCO Research Database, CSA Materials Research Database with METADEX (USA), Questel Orbit Inc. Weldasearch Select (France); presented in Russian Science Citation Index & «Google Scholar»; abstracted in «Welding Institute Bulletin» (Poland) & «Rivista Italiana della Saldatura» (Italy); covered in the review of the Japanese journals «Journal of Light Metal Welding», «Journal of the Japan Welding Society», «Quarterly Journal of the Japan Welding Society», «Journal of Japan Institute of Metals», «Welding Technology».



HYDROGEN-INDUCED COLD CRACKS IN WELDED JOINTS OF HIGH-STRENGTH LOW-ALLOYED STEELS (Review)

I.K. POKHODNYA, A.V. IGNATENKO, A.P. PALTSEVICH and V.S. SINYUK

E.O. Paton Electric Welding Institute, NASU

11 Bozhenko Str., 03680, Kiev, Ukraine. E-mail: office@paton.kiev.ua

Possibility of development of hydrogen-induced cold cracks in welded joint depends on series of interconnected and complex physical phenomena. Work represents a short review of investigations carried out in the E.O. Paton Electric Welding Institute on study of processes of hydrogen absorption by metal, its diffusion in the welded joint considering kinetics of temperature gradient, hydrogen traps and residual stresses. Peculiarities of hydrogen diffusion in strain-free and plastically deformed metal were studied by experiment-calculated methods. Results of experiment-calculation investigations and mathematical modeling of mechanisms of generation and growth of hydrogen-induced cracks in welded joints on micro- and macrolevel are stated. It is shown with high reliability that interaction of hydrogen with dislocations makes the basis of mechanism of hydrogen embrittlement. Hydrogen influences nucleation and growth of microcracks in metal making coalescence of dislocations easier that result in localizing of plastic strain under effect of hydrogen. As it is showed by computer modelling of development of microdefects in metal, the reduction of grain size, at other factors being equal, increases metal sensitivity to negative influence of hydrogen. Mechanism of crack growth in metal containing hydrogen is proposed considering effect of hydrogen-enhanced localized plasticity. 64 Ref., 12 Figures.

Keywords: brittle fracture, hydrogen embrittlement model, hydrogen-enhanced localized plasticity, residual stresses, BCC metals, grain size, hydrogen diffusion

Steel is one the most effective structural materials. More than 20 bln t of steel are used in different parts and structures in present time. 1550 mln t of steel were manufactured in the world in 2012, and in further 40 years volume of production would hypothetically increase by 50–100 % [1]. At that welding remains one of the most widespread methods for obtaining of permanent metal joints. As far as the requirements to strength of source materials and quality of obtained joints constantly rise in a course of time, it could be supposed that problems existing in development of more safe and long-term welded joints would be relevant and economic importance of scientific investigations directed on solution of given problems would permanently increase.

High-strength low-alloyed (HSLA) steels due to increasing requirements to service characteristics of welded structures are used in machine building, construction engineering, shipbuilding and pipeline construction. There is a risk of appearance of cold cracks in zone of welded joint in welding of HSLA steels. It was determined that one of the main factors promoting formation

of cold cracks is hydrogen absorbed by liquid metal from arc plasma. The results of carried out experimental and theoretical investigations show that hydrogen-induced cold cracks (HICC) are the consequence of more general physical effect, i.e. hydrogen embrittlement (HE) under specific conditions of thermal-deformation welding cycle [2].

Possibility of development of HICC in the welded joint depends on series of interconnected and complex physical phenomena. For their study the processes of hydrogen absorption by metal, diffusion of hydrogen in welded joint allowing for kinetics of temperature gradient, hydrogen traps and residual stresses were investigated as well as mathematical modeling of mechanisms of formation and growth of HICC on micro- and macrolevel was performed, and experiment-calculated investigations of mechanisms of HICC formation in welded joints were carried out at the E.O. Paton Electric Welding Institute.

Forms of hydrogen in iron and steels. Characteristics and state of hydrogen in metal volume are to be known for deep understanding of HE mechanism. Experimentally stated that process of hydrogen dissolution in iron follows the Sieverts' law, i.e. under thermodynamic equilibrium a concentration of dissolved hydrogen is directly proportional to square root of value of



its pressure in gas phase. This means that hydrogen like other biatomic gases is absorbed in form of atoms.

In spite of the fact that atomic hydrogen is the simplest substance soluble in iron, corresponding methods of calculation of its state based on different theories have not yet been developed. It is assumed that dissolved hydrogen can be in several forms, i.e. protonic, anionic and atomic. Occurrence of metallic bonding characterizing by sharing of valence electrons of iron and hydrogen electron takes place between atoms in metal during formation of protonic form. However, experimental observations of directed movement of hydrogen under effect of electric field do not provide precise answer to question about charge state of hydrogen in metal [3, 4]. The effect of transfer will be determined by particle charge [3] only in absence of interaction between the particles of migrating component and charge carrier in metal.

Quantum mechanical calculations were used for analyzing of possibility of existence of different forms of charge state of hydrogen depending on parameters of electron interaction in «hydrogen-metal» system [5]. It was concluded based on obtained results that protons H^+ , neutral atoms H^0 and negative ions H^- can be present in metal simultaneously with different possibilities. In authors' opinion, the main question lies in the fact in what condition the hydrogen will have the maximum effect on physico-mechanical properties. In V.I. Shvacko opinion [6] this conclusion causes doubts on alternative problem formulation about charge state of hydrogen in metal, but does not clear the situation itself. Conclusion about necessity to concentrate on determination of the most active form of hydrogen virtually means return to initial statement of problem since problem about charge state of hydrogen has appeared exactly from the necessity of determination of mechanism of its abnormal effect on metal properties.

Calculating electron structure of iron-hydrogen FCC system, the authors [7] came to the conclusion that density of valence electrons increases near hydrogen atom, i.e. negative charge is concentrated around hydrogen atoms. Calculations also showed from point of view of electron theory of metals that density of free electrons around the atoms of hydrogen being present in dislocations increases as well. This results in increase of dislocation mobility and reduction of distance between them in dislocation cluster [8].

It was shown using method of secondary ionic emission that hydrogen diffusing from metal

depth has negatively charged state on the surface [9, 10].

Model, according to which atoms of hydrogen introduced in metal lattice are localized in void of that or another type and make oscillatory motions near equilibrium position in accordance to atomic structure of solid solution, obtained wide distribution in authors' opinion [11]. Potential holes for atoms of hydrogen located in quasi equilibrium conditions are sufficiently deep (against their average kinetics energy). Such a model, apparently, describes the most significant peculiarities of the solution, i.e. in such form it provides the possibility accurately, by order of magnitude, calculate diffusion coefficients and explain the reasons of their exponential dependence on temperature, that is approved by direct experiments.

Hydrogen absorption. Processes of absorption of gases by electrode metal and weld pool develop significantly in welding of steels under conditions of high temperatures of arc discharge and high rates of heating and cooling of metal. Increase of hydrogen concentration in metal rises a risk of initiation of cold cracks in welded joint and, as a result, failure of whole welded structure [2, 12]. Thus, one of the main solutions of problem of HICC prevention is a fundamental investigation of hydrogen behavior in welding, searching of ways of reduction of its content in the weld metal and development of new welding consumables based on obtained results.

Content of H_2 and H_2O in arc atmosphere, metal temperature, presence of layer of slag and its properties, kinetics of electrode melting and transfer of electrode metal in the weld pool are mainly used for determination of hydrogen absorption by molten metal. High partial pressure of molecular and atomic hydrogen in arc gap as well as temperature of liquid metal at the end of electrode and weld pool provide for intensive hydrogen absorption. Experimentally showed that high rate of cooling of drops of electrode metal allows registering high contents of hydrogen [13].

Performance of experimental investigations on interaction of hydrogen with metal at the end of electrode and weld pool under conditions of arc welding is significantly complicated due to high temperatures, dissociation and ionized state of gases and, as a result, high reaction speeds [14-17]. Therefore, physical and mathematical models of processes, based on ideas about existence of local thermodynamic equilibrium in arc column, were developed and applied for investigation of processes of hydrogen absorption by



metal in arc welding. Mathematical model of process of hydrogen absorption by metal proposed in [14–16] is based on system of equations of gas dynamics and equation, which describes molecular interaction in thin Knudsen layer adjacent to metal surface, as well as equation of hydrogen mass transfer in metal. Evaporation of metal from drop surface was considered in calculation of absorption of hydrogen by drop of electrode metal. It is shown that reduction of arc temperature increases efficiency of hydrogen bonding by fluorine and oxygen. It was determined that effect of abnormal absorption of hydrogen by metal interacting with plasma of arc discharge is defined by degree of molecular dissociation in plasma volume, which depends on energy of molecular dissociation and temperature of plasma, and not by absorption of accelerated charged particles.

Maximum solubility in contact of iron with hydrogen under conditions of thermodynamic equilibrium is observed at $T = 2600$ K. Further increase of temperature results in reduction of hydrogen solubility caused by intensive iron evaporation. Calculation, proved by experiment, showed that absorption of hydrogen from plasma of arc discharge multiply exceeds (more than 10 times) absorption under equilibrium conditions at $T = 2000$ K, and is determined by degree of hydrogen dissociation depending on arc temperature. Also, monotonous reduction of content of hydrogen in iron is observed with increase of its temperature due to iron evaporation in contact with $\text{Ar} + \text{H}_2$ plasma.

Entering of fluorine compounds in composition of welding consumables is one of the most efficient methods of reduction of hydrogen absorption by liquid metal. Thermodynamic analysis of behavior of HF in arc zone was carried out in work [18]. HF and OH are completely dissociated in accordance with radial distribution of temperature in central high-temperature region at $T = 6200$ K. HF is not dissociated at column periphery (2500 K) that shows the possibility of hydrogen bonding by fluorine in arc zone.

Thermodynamic approach was also used for analysis of processes of bonding of hydrogen being in gas phase in a form of water vapors (at $P = 1 \cdot 10^5$ Pa pressure) by slags of $\text{TiO}_2\text{--CaO--CaF}_2$, $\text{Al}_2\text{O}_3\text{--CaO--CaF}_2$, $\text{SiO}_2\text{--CaO--CaF}_2$ system. It is shown that minimum content of hydrogen in metal is typical for $\text{TiO}_2\text{--CaO--CaF}_2$ and $\text{Al}_2\text{O}_3\text{--CaO--CaF}_2$ slag systems depending on CaO content in slag melt [19, 20]. In $\text{Al}_2\text{O}_3\text{--CaO--CaF}_2$ system weight fraction of CaO has no influence on hydrogen content in metal. Ad-

dition of SiF_4 in gas phase has effective influence on decrease of hydrogen content in metal due to reaction of HF formation and reduction of partial pressure of hydrogen.

Presence of mainly fluorosilicate compounds and anhydrous hydrogen fluoride was detected by mass-spectrometric investigations [21] of fluorides included in gases emitted from arc zone in welding by flux-cored wires which contain CaF_2 , SiO_2 , MgO , CaO , ZrO_2 . Composition of forming gases [22] was investigated in process of arc heating of CaF_2 specimen at $T = 147$ K. HF, which was formed at interaction of CaF_2 and residual vapors of water in mass spectrometer, was found in mass spectrum of gases in both experiments.

Accurate data on concentration of hydrogen in weld metal is necessary for development of efficient measures of reduction of hydrogen absorption by liquid metal, control of quality of welding consumables, prevention of formation of cold cracks and pores. Mercury method based on ISO 3690:2000(E) is a widely used method applying eudiometers. Developed method of analysis of diffusion hydrogen with chromatographic ending provides the possibility of measurement of volumes of hydrogen emitted from specimen with high accuracy and sensitivity, as well as allow accelerating measurement of quantity of hydrogen due to specimen heating 30–50 times. Chromatographic method is introduced in GOST 23338–91.

Investigations of effect technological factors of welding on hydrogen quantity in the weld metal [23, 24] were carried out using developed method. It is determined that changes of welding speed and value of welding current for coated electrodes do not virtually change concentration of hydrogen in the weld metal, but at the same time, content of hydrogen related to deposited metal significantly rises with increase of welding speed. Thus, a conclusion can be made that a content of hydrogen in molten weld metal is necessary to be determined for accurate estimation of diffusion hydrogen. Average concentration of hydrogen in multilayer deposited metal does not exceed content of hydrogen in single-run weld metal.

One of the main methods for reduction of hydrogen content in weld metal is preliminary heat treatment of welding consumables, at which part of hydrogen in a form of H_2O is removed. Allowable temperatures of baking for coated electrodes make 400–450 °C, and for flux-cored wires are 250–270 °C and they do not allow removing all moisture present in components of welding



consumables. Temperature dependence of removal of H_2O and H_2 (up to $1000\text{ }^\circ\text{C}$) from gas-slag-forming and alloying components was investigated using thermal desorption analysis [25] which allowed determining methods of their treatment for reduction of level of potential hydrogen in welding consumables. Application of heat-treated components in composition of the coated electrodes provided obtaining of extremely low concentrations of diffusion hydrogen ($1.0\text{--}1.5\text{ ml}/100\text{ g}$) in the weld metal [26].

Hydrogen diffusion. Redistribution of hydrogen in metal of the welded joint takes place after its absorption by weld pool. Field of hydrogen concentration in the joint is necessary to be known for determining the zones of metal of welded joint susceptible to the highest risk of HICC initiation. Thus, nonstationary problem of hydrogen diffusion considering thermal-deformation cycle of welding, structural transformations and hydrogen traps [2] is solved in a general case.

Moving force of diffusion is a gradient of chemical potential, the value of which depends on hydrogen solubility in metal, diffusion coefficient, gradients of concentration and temperature, stressed state and plastic deformations [27]. At that, thermal-deformation cycle of welding results in significant inhomogeneity of hydrogen concentration field.

Diffusion of hydrogen in the weld metal and redistribution of hydrogen in welded joint after welding were studied experimentally and using mathematic modelling. Experiments on kinetics of removal of hydrogen, being absorbed in process of welding, from cylinder specimens of the weld metal were carried out, and dependence of speed of degassing V on quantity of hydrogen Q in specimen $V(Q)$ were obtained for determination of value of effective coefficient of hydrogen diffusion D_H . D_H was determined based on obtained experimental dependence $V(Q)$ using solution of reverse coefficient isothermal problem. $D_H = 1 \cdot 10^{-7}\text{ cm}^2/\text{s}$ for metal welds performed using rutile welding consumables at $T = 20\text{ }^\circ\text{C}$, and $D_H = 1 \cdot 10^{-6}\text{ cm}^2/\text{s}$ [28] was obtained for low-alloy killed welds.

Removal and redistribution of hydrogen in metal of welded joint take place after welding. Using results of experimental investigation [29] a mathematical model of redistribution of hydrogen between the weld metal and base metal [30] was developed, which allows determining current concentration of hydrogen in zones of welded

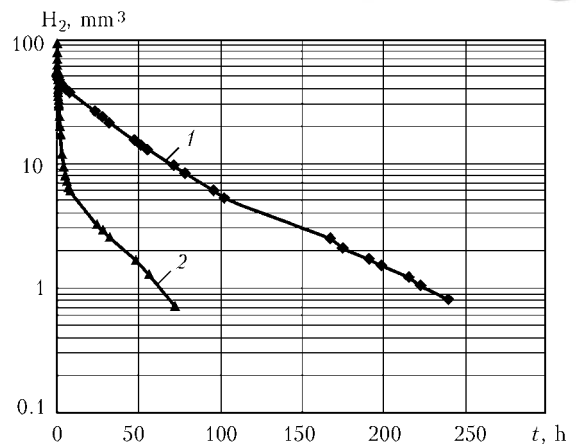


Figure 1. Results of experiments on kinetics of hydrogen removal from deformed (1) and underformed (2) specimen

joint considering hydrogen absorption by defects of metal crystalline structure. Applied stresses significantly influence on D_H value and hydrogen permeability of steel at plastic strain [31].

Plastic strain in fracture zone precedes as a rule metal failure. Plastic strain of weld metal and HAZ is possible as a result of thermal-deformation cycle of welding or due to external loading. In this case, interaction of hydrogen with formed dislocation structure takes place. The dislocations are reversible traps, which at metal temperature lower than $100\text{ }^\circ\text{C}$ start to provide significant effect on hydrogen diffusion. Besides, as follows below, basis of HE lies in interaction of hydrogen with mobile edge dislocations. Therefore, study of hydrogen diffusion in plastically deformed metal is of particular interest in scope of HE investigation.

Results of investigation of kinetics of hydrogen removal at room temperature are shown in Figure 1 [32]. Character of hydrogen diffusion in undeformed and plastically deformed metal has noticeable difference. As computer calculations based on experimental data showed, D_H remains constant in plastically deformed metal virtually during the whole degassing processes. Therefore, completely all hydrogen is bonded with dislocation structure to the moment of degassing beginning, and in order that hydrogen atom can move out from the metal it firstly needs to overcome energy barrier and detach from dislocation holding it. Respectively, D_H value in deformed metal is determined by average energy of bonding of hydrogen atoms with dislocations and does not change in the degassing processes.

According to calculations, D_H changes by several orders (Figure 2) in undeformed specimen in a process of dissociation. Only part of hydrogen is bonded with dislocation structure in the

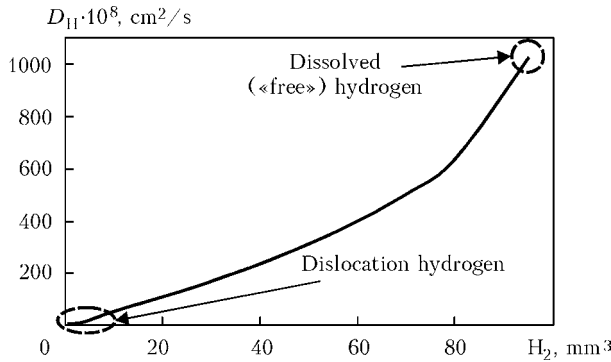


Figure 2. Calculation dependence of D_H on hydrogen content in metal

beginning of degassing in undeformed metal due to relatively small concentration of dislocations. Initially, when desorption of hydrogen not bonded with dislocations takes place, the dislocations have no significant effect on diffusion process and, respectively, on D_H value. But, as far as desorption takes place the portion of hydrogen, which was initially bonded with dislocation structure, increases in general flow of degassed gas. Thus, increase of time of degassing provides reduction of concentration of remained hydrogen, and rise of influence of dislocations on character of hydrogen diffusion in metal is observed. This leads to gradual reduction of D_H value and speed of specimen degassing. When hydrogen concentration is low, D_H value in undeformed metal is comparable with its value in deformed metal that confirms the conclusions about role of dislocation structure made before.

Work [33] proposes a mathematical model of hydrogen mass transfer in metal considering

traps, which describes redistribution of hydrogen between residual and diffusion one. Dislocations formed as a result of structural transformations in metal during cooling were considered as traps. Calculation of mass transfer of hydrogen in welded joint was carried out by finite element method from moment of beginning of weld metal solidification (Figure 3).

Local concentration of hydrogen C_H in weld center in moment of its solidification as well as during structural transformations rapidly increases due to solubility jump (see Figure 3). Concentration of residual hydrogen (bonded with dislocations) increases with cooling of metal up to 100 °C and depends on bond energy of traps with hydrogen E_b . Thus, at presence in metal of traps with $E_b = 20$ kJ/mol the quantity of residual hydrogen makes 0.5 cm³/100 g, and behavior of diffusion hydrogen does not significantly change.

In case of traps with $E_b = 30$ kJ/mol the quantity of residual hydrogen increases up to 2 cm³/100 g, and content of diffusion hydrogen rapidly reduces. After traps are saturated, significant delay of hydrogen diffusion takes place due to reduction of gradient of concentration of diffusion hydrogen as a result of its transfer in residual one. Thus, resulting reduction of local concentration of diffusion hydrogen in the weld center (in 10 h after welding) appears to be smaller than increase of residual one.

Hydrogen transfer by edge dislocations. Peculiarities of reversible hydrogen embrittlement (for example, temperature-speed dependence of metal sensitivity to hydrogen embrittlement) according to current representations are explained by interaction of hydrogen dissolved in metal with mobile edge dislocations [6, 34]. Mathematical model was proposed in [35] for description of process of hydrogen transfer by edge dislocations. Atom of hydrogen moving inside the metal as a result of interaction with lattice will have different potential energy in different moments of time. Possibility of transfer of interstitial atoms in specific adjacent void depends on metal temperature, potential energy of atom in initial and finite void. Based on concepts of microscopic theory of diffusion and considering that atom of hydrogen can jump in adjacent void only if it is not occupied by other atoms, the following system of equations describing diffusion of hydrogen in the field of mobile edge dislocation [36] can be obtained:

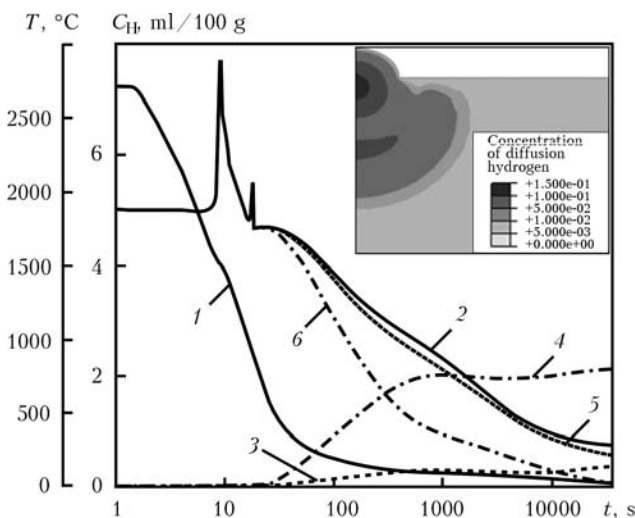


Figure 3. Dependence on time of temperature T (1) and hydrogen concentration C_H : 2 – diffusion (without traps); 3, 4 – in traps with $E_b = 20$ and 30 kJ/mol, respectively; 5, 6 – diffusion with $E_b = 20$ and 30 kJ/mol, respectively (concentration of diffusion hydrogen in 10 h after welding is shown in the right upper corner)



$$\begin{cases} j_x = -D \left[\frac{\partial u_D}{\partial x} p(1-p) + \frac{\partial p}{\partial x} \right] + V_0 p, \\ j_y = -D \left[\frac{\partial u_D}{\partial y} p(1-p) + \frac{\partial p}{\partial y} \right] + V_0 p, \\ \frac{\partial(j_x)}{\partial x} + \frac{\partial(j_y)}{\partial y} = 0, \end{cases}$$

where J_x and J_y are the flow of hydrogen along x and y axes, respectively; D is the coefficient of hydrogen diffusion in defect-free metal; u_D is the potential of interaction of hydrogen with edge dislocation; $p = C/C_v$ is the hydrogen concentration related to number of voids; C_v is the number of voids in volume unit; V_0 is the speed of movement of edge dislocation with conditions at infinity: $p = p_0 = C/C_v$; $J_x = V_0 C_0/C_v = V_0 p_0$; $J_y = 0$ at $(x^2 + y^2) \rightarrow \infty$.

Effect of metal temperature, speed of movement of edge dislocations and concentration of diffusion hydrogen on quantity of hydrogen transferred by dislocations was investigated. The calculations showed that dependence of quantity of hydrogen transported by edge dislocation N on temperature has maximum in field of room temperature (Figure 4). It is determined that increase of speed of edge dislocation movement or reduction of diffusion hydrogen concentration decreases quantity of transported hydrogen and maximum of $N(T)$ curve is shifted in area of higher temperatures [36]. Since movement of dislocation is an elementary act of plastic deformation then increase of speed of plastic deformation rises speed of dislocation movement. The results of calculation are well matched with experimental data, i.e. increase of speed of plastic deformation reduces metal sensitivity to HE, and minimum of brittle strength of specimens containing hydrogen is shifted in area of higher temperatures [12].

Mechanical investigations. Works [37–39] proposed new physically based criterion characterizing the degree of reduction of brittle strength of metal under effect of hydrogen, and procedure of its determination was developed on data of mechanical tests. In contrast to comparison criteria used earlier, new criterion has clear physical content determined by metal structure. Application of this procedure allows estimating the degree of metal HE by means of performance of the simplest uniaxial tensile tests of standard specimens.

Works [40–43] show that measure of brittle strength of metal is a value of microcleavage resistance R_{mce} , i.e. minimum stress of brittle frac-

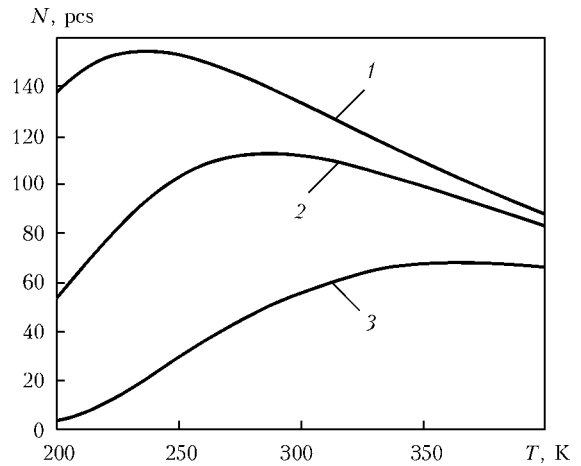


Figure 4. Dependence of hydrogen quantity N transported by section of mobile edge dislocation on temperature of specimen and speed of its movement $V_0 = 1 \cdot 10^{-3}$ (1), $1 \cdot 10^{-2}$ (2) and $1 \cdot 10^{-1}$ (3) m/s

ture at uniaxial tension deformed per certain degree e . Since R_{mce} value is structurally determined in relation to temperature, then change of R_{mce}^H/R_{mce} relation depending on temperature reflects influence of hydrogen on this value. Peculiarities of R_{mce} value marked in [40–43] allow expressing degree of reduction of brittle strength of metal under effect of hydrogen δ_H through decrease of value of critical fracture stress σ_{1C} in specimen waist:

$$\delta_H = \frac{R_{mce}^H}{R_{mce}} \approx \frac{\sigma_{1C}^H}{\sigma_{1C}},$$

where R_{mce}^H and σ_{1C}^H are the characteristics of metal containing hydrogen.

σ_{1C} for concerned temperature interval should be calculated based on data of mechanical tests for determination of δ_H parameter. Estimation of δ_H value is obtained after dividing at fixed e and $\sigma_{1C}^H/\sigma_{1C}$.

Results of experimental investigations of hydrogen effect on mechanism of metal fracture are given in work [44]. Thermodesorption analysis determined that residual hydrogen which is bonded with formed dislocations and microcracks (Figure 5) is generated in metal containing diffusion hydrogen as a result of plastic deformation. Thus, density of dislocations increases and microdefects are formed as a result of plastic deformation of metal that leads to hydrogen redistribution.

Specimens from VSt3sp (killed) steel containing $7 \text{ cm}^3/100 \text{ g}$ of hydrogen were stretched to different degrees of plastic deformation for studying of effect of hydrogen on mechanisms of nucleation and growth of microdefects in metal. After preliminary deformation the hydrogen was

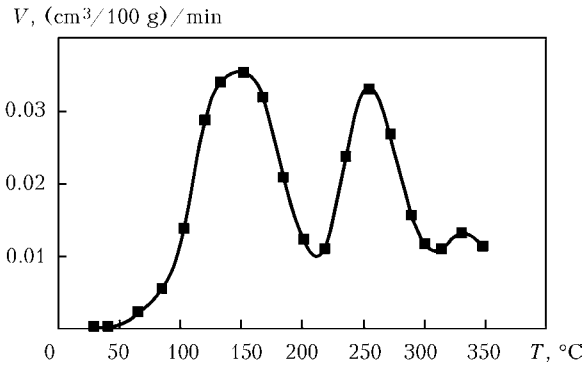


Figure 5. Spectrum of thermodesorption of residual hydrogen for VSt3sp steel specimen, containing $8.5 \text{ cm}^3/100 \text{ g}$ of diffusion hydrogen, after fracture

removed and specimens were stretched up to failure. The specimens containing no hydrogen were subjected to identical cycle of testing. Hydrogen provides no significant effect on mechanical properties of VSt3sp steel (Figure 6, *a*) up to 10 % deformation of specimen, and increase of deformation from 15 up to 17 % results in significant effect of hydrogen on metal failure (Figure 6, *b*, *c*). Brittle microcrack, the growth of which takes place on tough mechanism after hydrogen removal (Figure 6, *d*), was found on the fracture surface of specimens with $7 \text{ cm}^3/100 \text{ g}$ content of hydrogen and preliminary deformation.

Deformation of metal containing hydrogen results in nucleation and growth of microdefects in it that significantly influence mechanical properties. Effect of hydrogen rapidly increases in achieving of certain level of plastic deformation. Presence of hydrogen on dislocations facilitates their coalescence that results in microcrack nucleation at lower external stress.

Mechanism of hydrogen embrittlement of iron and steel. Formation of HICC in welded joints from HSLA steels are determined by peculiarities of structural transformations in weld metal and HAZ, value of residual tensile stresses and concentration of hydrogen in metal [9, 45]. Mechanism of more general physical phenomenon of degradation of mechanical properties of metal under effect of dissolved hydrogen, i.e. hydrogen embrittlement [9], is necessary to be considered for detection of mechanism of HICC formation under conditions of thermal-deformation cycle of welding.

Hydrogen at plastic strain is transported to place of crack nucleation by mobile dislocations. Dislocation theory proposes a number of models of dislocation reorganizations which can result in formation of extremely sharp nucleation sub-microcrack [46]. One of them is Zener–Stroh

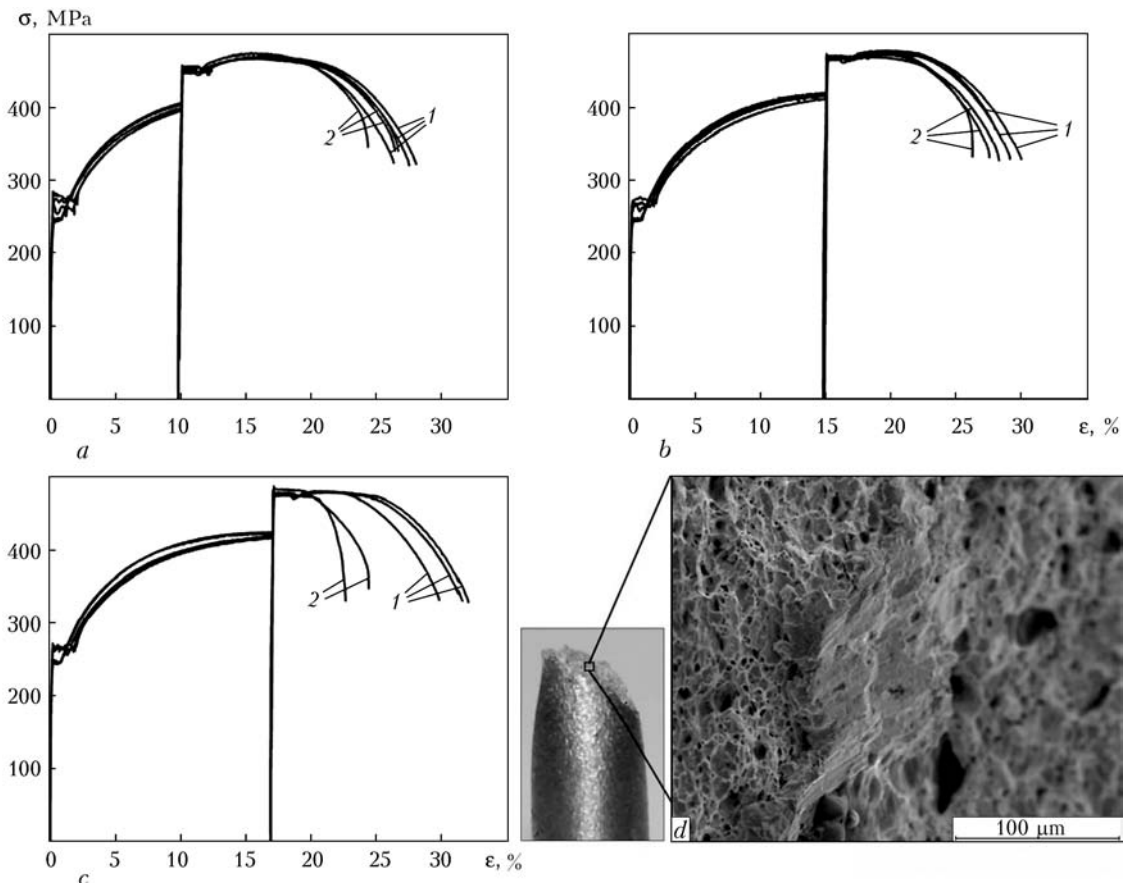


Figure 6. Tensile diagrams for VSt3sp steel specimens with preliminary deformation ϵ_{pr} of 10 (*a*), 15 (*b*) and 17 (*c*) % (*1, 2* – specimens containing no hydrogen and containing it respectively), and microstructure of microcrack (*d*)

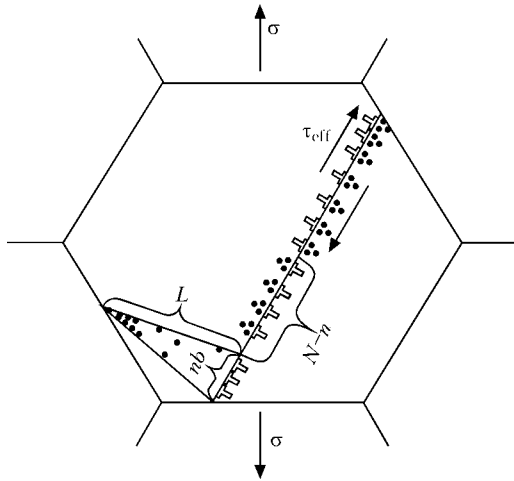


Figure 7. Scheme of microcrack formation: σ – external tensile stresses; τ_{eff} – tangential stresses acting in slide plane of dislocations; L – length of submicrocracks; N – total quantity of edge dislocations in plain cluster; n – quantity of dislocations merged in submicrocrack; b – modulus of Burgers vector

model, according to which cluster of dislocations is formed in a place of stop of slip band and occurrence of tensile stress takes place in its top, which under certain force conditions is developed in microcrack (Figure 7). Presence of hydrogen around the dislocations results in nucleation of submicrocrack at lower stress due to facilitation of dislocation coalescence.

If stability of microcrack is lost in a process of nucleation, then brittle fracture of metal will take place [47, 48]. If crack does not lose stability, then its further growth will depend on peculiarities of development of local plastic strain in zone around microcrack tip and hydrogen concentration [49, 50] (Figure 8).

Presence of hydrogen results in change of morphology of plastic area due to localized plastic strain [51–53]. New microdefect [54] (Figure 9) is nucleated in shear band near microcrack tip under hydrogen effect.

Change of character of microplastic strain around micropores or nonmetallic inclusions under effect of hydrogen promotes transfer from

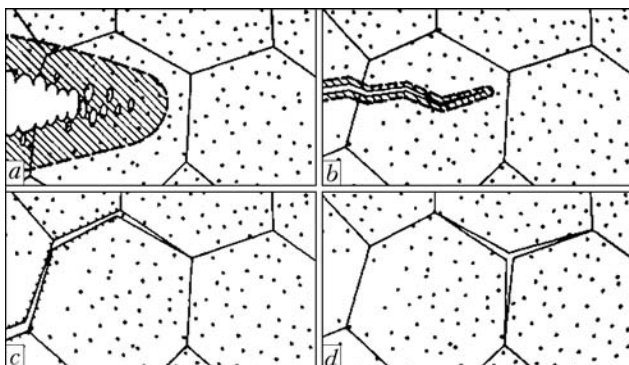


Figure 8. Mechanism of crack growth: *a* – tough; *b* – quasi-brittle; *c, d* – intergranular

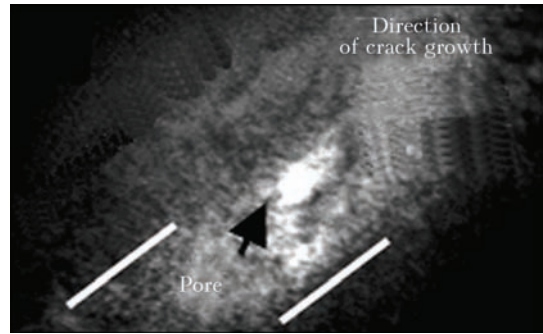


Figure 9. Formation of micropore in specimen from IN903 steel containing hydrogen [54]

tough to brittle fracture due to hydrogen-enhanced localized plastic strain [55, 56] (Figure 10).

Thus, critical factors on the stage of microcrack development are the main tensile stresses and quantity of hydrogen transferred by dislocations to the place of defect formation (determined by concentration of diffusion hydrogen, temperature, speed of deformation and dislocation density in metal). Mechanism of microcrack growth (tough or brittle), if it does not lose stability in the moment of its nucleation, is determined by stress intensity factor and hydrogen concentration in the crack tip.

Plastic strain of metal results in increase of number of mobile dislocations that, in turn, leads to redistribution of diffusion hydrogen between the lattice and reversible traps-dislocations. Hydrogen, transferred by dislocations to place of microcrack nucleation, will be molized inside the latter.

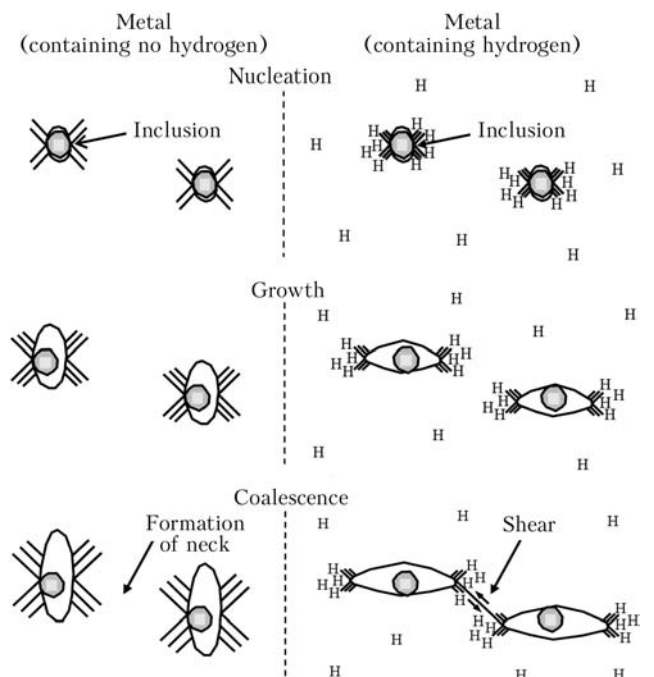


Figure 10. Scheme of nucleation, growth and merging of micropores in tough metal fracture

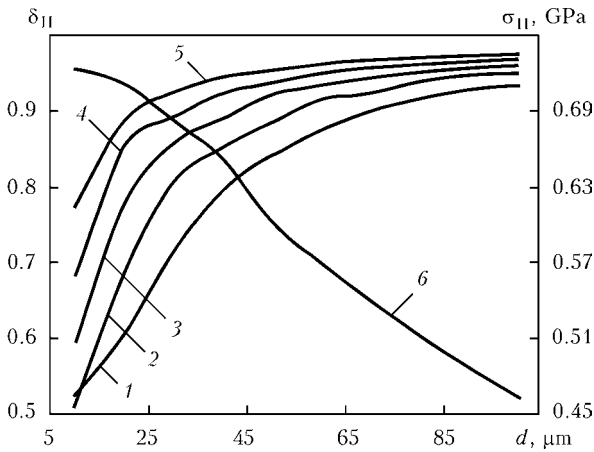


Figure 11. Dependence of degree of reduction of brittle strength of iron $\delta_H = \sigma_H / \sigma_0$ on grain size d at $T = 250$ (1), 275 (2); 300 (3), 325 (4) and 350 (5) K (σ_0, σ_H – fracture stress of iron grain containing no hydrogen and containing it, respectively), and dependence σ_H of on d at $T = 300$ K (6)

Model of nucleation and growth of submicrocrack in metal grain on microcleavage mechanism was proposed considering the model of hydrogen transfer by dislocations. The main mechanism of metal embrittlement by hydrogen is effect of hydrogen-enhanced localized plasticity [47] which is considered through change of elastic energy of edge dislocations and submicrocrack induced by accumulation of hydrogen atoms around them. The effect indicated above significantly reduces value of stress necessary for grain fracture. Proposed mathematical model [57, 58] considers metal temperature, grain size in which submicrocracks appear, complex stressed state, physical characteristics of metal, mobility and concentration of diffusion hydrogen, speed of movement of edge dislocations and influence hydrogen-enhanced localized plasticity. Multi-factor model allows describing such peculiarities of reversible hydrogen embrittlement as tempera-

ture-speed dependence of value of fracture stress of metal containing hydrogen.

Computer modeling of influence of metal grain orientation in relation to external stresses on value of fracture stress was carried out [59]. The optimum angle of inclination between slip plane of edge dislocations and main tensile stress α_{opt} equals 45° . It is determined that number of dislocations in cluster reduces with deviation of inclination of slip plane of edge dislocations from optimum angle or increase of complex stressed state of metal. Appearance of cluster of edge dislocations in slip plane is completely impossible under certain conditions. Such a dependence between α_{opt} corresponds with conclusions of dislocation theory. It is determined that relative effect of hydrogen on metal brittle strength increases with rise of complex stressed state of metal, however, absolute value of fracture stress of hydrogen-containing metal grain increases.

Hydrogen-enhanced localized plasticity of metal significantly reduces value of stress which is necessary to be applied for grain fracture [57, 60]. In some cases decrease of metal strength can achieve 40–50 % (Figure 11). It was determined using calculations that, at other factors being equal, decrease of metal grain results in increase of degree of metal HE, however, absolute value of fracture stress of hydrogen-containing metal rises with grain decrease (see Figure 11, curve 6). Thus, increase of steel strength due to decrease of metal grain is reasonable only to certain extent, which depends on number of hydrogen as well as sensitivity of steel to HE under given conditions. Calculation results correspond with presented experimental data which were obtained for Armco-iron and low-carbon steel [12, 61].

One of the most possible mechanisms of macrocrack development in metal is formation microdefect in front of crack tip and its further coalescence with crack (Figure 12) [58, 62]. Area of plastic strains is formed in metal in front of tip of growing crack under effect of stress. In a process of crack growth this results in formation of plastically deformed metal under its surface, the thickness of which depends on applied stress, i.e. the higher stress which is necessary to be applied for formation of microdefect in front of crack tip, the thicker is the layer. Energy necessary for macrocrack growth consists from two parts, namely energy of formation of free surfaces, and energy of near-surface plastically deformed metal. In metal containing no hydrogen specific energy necessary for formation of such a layer is several orders higher than the specific energy of free surfaces of crack [63]. Stress nec-

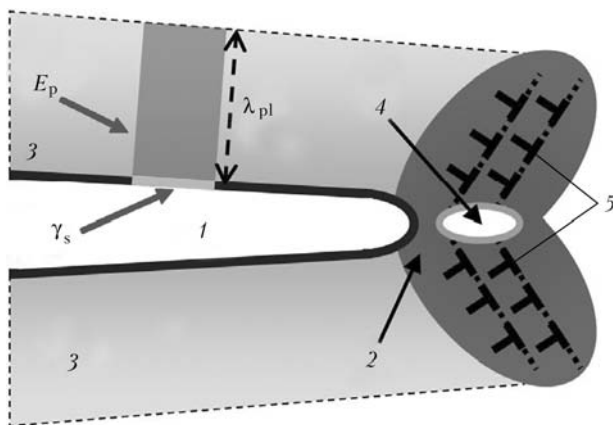


Figure 12. Scheme of growth of macrocrack in metal containing hydrogen: 1 – macrocrack; 2 – area of plastic deformations; 3 – subsurface layer of plastically deformed metal; 4 – microdefect; 5 – dislocation cluster; E_p – energy necessary for plastic strain of layer of metal of λ_{pl} thickness; γ_s – specific surface energy



essary for formation of microdefect in front of tip of macrocrack significantly reduces due to effect of hydrogen-enhanced localized plasticity. Effect of hydrogen-enhanced localized plasticity reduces the most energy-consuming constituent of macrocrack growth, i.e. formation of near-surface layer. Therefore, development of macrocrack should take place more brittle, with lower energy consumption in hydrogen-containing metal with BCC lattice that is observed in experiments [2, 12, 64].

Conclusions

1. Physical model of saturation of metals by gases being in contact with low-temperature plasma was developed. The model is build on the basis of kinetics theory of gases and considers movement of ions, atoms and molecules in plasma volume, adsorption and desorption of gas on metal surface as well as diffusion transfer of dissolved gas in metal melt.
2. It is shown that activation of molecules in plasma (excitation, dissociation, ionization) increases speed of dissolution by several orders in comparison with equilibrium conditions.
3. It is determined that entering of fluorine compounds in composition of welding consumables results in HF formation. Thermal-dynamic analysis showed that HF is substantially dissociated in larger part of arc section (high-temperature). Bonding of fluorine by hydrogen takes place in arc periphery that results in reduction of hydrogen absorbed by weld pool. Presence of HF in arc zone was experimentally proved.
4. New chromatographic methods for analysis of hydrogen in metal of welds, welding consumables and their components were proposed. Chromatographic method for analysis of diffusion hydrogen with degassing temperature up to 150 °C was entered in GOST 23338–91.
5. Method for reduction of hydrogen content in coated electrode welding and submerged arc welding providing extremely low concentrations of diffusion hydrogen in weld metal was proposed.
6. It is stated based on experiment-calculation investigations of kinetics of degassing of hydrogen from the weld metal that dependence of coefficient of diffusion on concentration of hydrogen is character for undeformed metal whereas it is not observed in deformed specimen. This is well settled in scope of ideas about dislocations as hydrogen traps.
7. It is determined that formation of hydrogen-induced cold cracks in welded joints is representation of HE under specific conditions of thermal-deformation welding cycle. Therefore, solving of problem of HICC should be based on accurate knowledge of mechanism of HE of metal of the welded joint.
8. It is shown with high reliability that interaction of hydrogen with dislocations makes a basis of mechanism of HE. Hydrogen influences on nucleation and growth of microcracks in metal facilitating coalescence of dislocations that result in localized plastic strain under effect of hydrogen.
9. Effect of hydrogen on nucleation of microcrack in macrolevel appears in a form of reduction of normal tensile stresses necessary for its nucleation. Further growth of microcrack takes place on quasi-brittle mechanism due to formation of new microdefect in its tip under hydrogen effect.
10. It is shown with the help of computer calculations that quantity of hydrogen transferred by dislocations to the place of microdefect nucleation depends on speed of dislocation movement, metal temperature and has maximum in area of room temperatures. This is agreed with experimentally stated temperature-speed dependence of reversible HE having minimum in area of room temperature.
11. Modeling of growth of submicrocrack in metal grain considering effect of hydrogen-enhanced localized plasticity showed that metal becomes more brittle and sensitive to HE with reduction of size of grain, however, absolute value of fracture stress increases.
12. It is shown that removal of hydrogen from metal as well as its redistribution between diffusion and residual ones due to presence in metal of hydrogen traps take place in welded joint cooling. Increase of bond energy of traps and hydrogen reduces diffusion of the latter and increases quantity of residual hydrogen.

1. <http://www.worldsteel.org>
2. Pokhodnya, I.K., Yavdoshchin, I.R., Paltsevich, A.P. et al. (2004) *Metallurgy of arc welding*. Kiev: Naukova Dumka.
3. Beloglazov, S.M. (1975) *Hydrogenation of steel in electrochemical processes (Review)*. Leningrad: LGU.
4. Kasatkin, O.G. (1994) Peculiarities of hydrogen embrittlement of high-strength steels in welding (Review). *Avtomatich. Svarka*, **1**, 3–7.
5. Yuhnovsky, P.I., Tkachev, V.I. (1987) About state of hydrogen in metal. *Fiz.-Khimich. Mekhanika Materialov*, **4**, 107–108.
6. Shvachko, V.I. (2002) *Reversible hydrogen brittleness of bcc iron alloys — structural steels*: Syn. of Thesis for Dr. of Phys.-Math. Sci. Degree. Kharkiv.
7. Teus, S.M., Shivanyuk, V.N., Shanina, V.D. et al. (2007) Effect of hydrogen on electronic structure of fcc iron in relation to hydrogen embrittlement of austenite steels. *Phys. Status Solids A*, **204**(12), 4249–4258.



8. Gavriljuk, V.G., Shivanyuk, V.N., Shanina, B.D. (2005) Change in the electron structure cause by C, N and H atoms in iron and its effect on their interaction with dislocations. *Acta Materialia*, **53**, 5017–5024.
9. Pokhodnya, I.K., Shvachko, V.I. (1997) Physical nature of hydrogen-induced cold cracks in welded joints of structural steels. *Avtomatich. Svarka*, **5**, 3–12.
10. Pokhodnya, I.K. (1998) Problems of welding of high-strength low alloy steels. In: *Current materials science of 21st century*: Transact. Kiev: Naukova Dumka, 31–69.
11. Geld, P.V., Ryabov, R.A. (1974) *Hydrogen in metals and alloys*. Moscow: Metallurgiya.
12. Kolachev, B.A. (1985) *Hydrogen brittleness of metals*. Moscow: Metallurgiya.
13. Yavdoshchin, I.R. (1969) *Investigation and development of universal electrodes with rutile coating*: Syn. of Thesis for Cand. of Techn. Sci. Degree. Kiev.
14. Pokhodnya, I.K., Shvachko, V.I., Portnov, O.M. (2000) Mathematical modelling of absorption of gases by metal during welding. *The Paton Welding J.*, **7**, 11–16.
15. Pokhodnya, I.K. (2003) Mathematical modelling of processes of interaction of metal with gases in arc welding. *Ibid.*, **2**, 2–9.
16. Pokhodnya, I.K., Portnov, O.M. (2003) Mathematical modelling of absorption of gases by electrode drop metal. *Ibid.*, **6**, 2–5.
17. Pokhodnya, I.K., Portnov, O.M., Shvachko, V.I. (2001) Computer modeling of hydrogen absorption by electrode metal drop under its intensive evaporation. In: *Proc. of 6th Seminar on Numeric Analysis of Weldability* (Graz, Oct. 2001). Graz: TU of Graz, 895–902.
18. Pokhodnya, I.K., Shvachko, V.I., Utkin, S.V. (1998) Calculated assessment of hydrogen behavior in arc discharge. *Avtomatich. Svarka*, **9**, 4–7.
19. Pokhodnya, I.K., Tsybulko, I.I., Orlov, L.N. (1993) Influence of slag composition on hydrogen content in liquid metal during CO₂ welding. *Ibid.*, **11**, 8–14.
20. Tsybulko, I.I. (1993) Calculation of thermodynamic equilibrium in metallurgical system gas-slag-metal. In: *Proc. of 2nd Int. Seminar on Numeric Analysis of Weldability* (Graz-Segau, 10–12 Sept. 1993). Graz: TU of Graz.
21. Pokhodnya, I.K., Shvachko, V.I., Ustinov, V.G. et al. (1972) Mass-spectrometric examinations of fluorides emitted in arc welding. *Avtomatich. Svarka*, **6**, 10–12.
22. Pokhodnya, I.K., Shvachko, V.I. (1981) Formation of hydrogen fluoride in arc discharge. *Ibid.*, **2**, 11–13.
23. Pokhodnya, I.K., Paltsevich, A.P., Yavdoshchin, I.R. (1986) Influence of methods of weld metal sampling for determination of diffusion-mobile hydrogen content in it. *Ibid.*, **1**, 24–28.
24. Pokhodnya, I.K., Paltsevich, A.P., Yavdoshchin, I.R. (1988) Influence of welding conditions on hydrogen content in welds made with electrodes of basic type coatings. *Ibid.*, **3**, 19–22.
25. Paltsevich, A.P. (1999) Chromatographic method of hydrogen content evaluation in electrode coating components. *Ibid.*, **6**, 46–48.
26. Pokhodnya, I.K., Paltsevich, A.P. (2003) Examination of potential content of hydrogen. In: *Abstr. for Int. Conf. on Current Problems of Welding and Resource of Structures* (Kiev, 24–27 Nov. 2003). Kiev: PWI, 67.
27. Panasyuk, V.V. (1991) *Mechanics of quasi-brittle fracture of materials*. Kiev: Naukova Dumka.
28. Paltsevich, A.P. (1988) *Development of methods of hydrogen content reduction in welds for new coated electrodes and flux-cored wires of basic type*: Syn. of Thesis for Cand. of Techn. Sci. Degree. Kiev.
29. Pokhodnya, I.K., Demchenko, L.I., Paltsevich, A.P. et al. (1976) Kinetics of diffusion redistribution of hydrogen between weld metal and base metal in arc welding. *Avtomatich. Svarka*, **8**, 1–5.
30. Pokhodnya, I.K., Demchenko, V.F., Demchenko, L.I. (1979) *Mathematical modeling of gas behavior in welds*. Kiev: Naukova Dumka.
31. Pokhodnya, I.K., Pavlyk, V.A., Shvachko, V.I. (1993) Effect of heat treatment and deformation on hydrogen diffusion and permeability of 10KhN3DM type steel. In: *Metallurgy of welding and consumables*. St.-Petersburg: StPGTU, 158–160.
32. (2011) *Development of materials for welding of technological equipment of mining and smelting and fuel and energy complexes*. Pt 1: Study by methods of experimental and numerical modeling of hydrogen behavior in weld metal of higher strength under conditions of thermal-deformation cycle of welding: Final report No. 0107U0022787. Kiev: PWI.
33. Sinyuk, V.S., Stepanyuk, S.N. (2009) Interaction of hydrogen with dislocation structure of structural steel welded joints. In: *Proc. of Sci. Conf. on Mechanics of Fracture Materials and Strength of Structures* (23–27 June, 2009, Lviv). Lviv: FMI, 999–1002.
34. Stepanyuk, S.M. (2001) *Reversible hydrogen embrittlement in welding of high strength low-alloy steels*: Syn. of Thesis for Cand. of Techn. Sci. Degree. Kyiv.
35. Shvachko, V.I., Ignatenko, A.V. (2007) Model of transportation of hydrogen with dislocations. *The Paton Welding J.*, **2**, 24–26.
36. Ignatenko, A.V. (2007) Mathematical model of transportation of hydrogen by edge dislocation. *Ibid.*, **9**, 23–27.
37. Pokhodnya, I.K., Shvachko, I.V., Kotrechko, S.A. et al. (1999) A new method for quantitative determination of sensitivity of steels to hydrogen embrittlement. *Int. J. Mater. Sci.*, **34**(4), 538–543.
38. Shvachko, V.I., Stepanyuk, S.M., Pokhodnya, I.K. (2000) The evaluation methods of HSLA steels susceptibility to hydrogen embrittlement. In: *Proc. of 4th Int. Conf. on HSLA Steels* (Xi'an, China, Oct. 30–Nov. 2, 2000). Beijing: Metallurg. Industry Press, 453–458.
39. Pokhodnya, I.K., Meshkov, Yu.Ya., Shvachko, V.I. et al. *Method of quantitative determination of level of hydrogen embrittlement of structural steels and welds*. Appl. 5040067. Int. Cl. G 01 n 17/00. Fil. 01.07.91.
40. Meshkov, Yu.Ya. (1981) *Physical principles of strength of steel structures*. Kiev: Naukova Dumka.
41. Meshkov, Yu.Ya., Pakharenko, G.A. (1985) *Structure of metal and brittleness of steel products*. Kiev: Naukova Dumka.
42. Meshkov, Yu.Ya., Serditova, T.N. (1989) *Fracture of wrought steel*. Kiev: Naukova Dumka.
43. Kotrechko, S.A., Meshkov, Yu.Ya., Mettus, G.S. (1990) To problem of tough and brittle states of polycrystalline metals. *Metallofizika*, **12**(6), 3–13.
44. Sinyuk, V.S., Pokhodnya, I.K., Paltsevich, A.P. et al. (2012) Experimental study of the mechanism of hydrogen embrittlement of metals with the bcc lattice. *The Paton Welding J.*, **5**, 8–11.
45. Tsaryuk, A.K., Brednev, V.I. (1996) Problem of cold crack prevention. *Avtomatich. Svarka*, **1**, 36–40.
46. Vladimirov, V.I. (1984) *Physical nature of metal fracture*. Moscow: Metallurgiya.
47. Birnbaum, H.K., Sofronis, P. (1994) Hydrogen-enhanced localized plasticity – a mechanism for hydrogen-related fracture. *Mat. Sci. and Eng. A*, **174**, 191–202.
48. Kotrechko, S.A., Meshkov, Yu.Ya. (2008) *Ultimate strength*. Kiev: Naukova Dumka.
49. Pokhodnya, I.K., Shvachko, V.I., Utkin, S.V. (2002) Effect of hydrogen on equilibrium of dislocation submicrocrack in α -iron. *Fiz.-Chimich. Mekhanika Materialiv*, **1**, 7–14.
50. Beachem, C.D. (1972) A new model for hydrogen-assisted cracking (hydrogen embrittlement). *Metallurg. Transact.*, **3**, 259–273.
51. Gedeon, S.A., Eagar, T.W. (1990) Assessing hydrogen-assisted cracking fracture modes in high-strength steel weldments. *Welding J.*, **6**, 213–219.



52. Sofronis, P., Liang, Y., Aravas, N. (2001) Hydrogen induced shear localization of the plastic flow in metals and alloys. *Eur. J. Mech. – A: Solids*, **20**, 857–872.
53. Liang, Y., Sofronis, P., Aravas, N. (2003) On the effect of hydrogen on plastic instabilities in metals. *Acta Materialia*, **51**, 2717–2730.
54. <http://www.icf.11.com/proceeding/EXTENDED/5638.pdf>
55. Liang, Y., Sofronis, P., Dodds, R.H. (2004) Interaction of hydrogen with crack-tip plasticity: Effect of constraint on void growth. *Mat. Sci. and Eng. A*, **366**, 397–411.
56. Ahn, D.C., Sofronis, P., Dodds, R.H. (2007) On hydrogen-induced plastic flow localization during void growth and coalescence. *Int. J. Hydrogen Energy*, **32**, 3734–3742.
57. Ignatenko, O.V., Pokhodnya, I.K. (2011) Influence of hydrogen-enhanced localized plasticity and grain size on the strength of bcc metal. In: *Proc. of 2nd Ukrain.-Greek Symp. on Fracture Mechanics of Materials* (3–7 Oct. 2011, Lviv). Lviv: FMI.
58. Ignatenko, A.V., Pokhodnya, I.K., Paltsevich, A.P. et al. (2012) Dislocation model of hydrogen-enhanced localizing of plasticity in metals with bcc lattice. *The Paton Welding J.*, **3**, 15–19.
59. <http://dfmn2011.imetran.ru/2011/index.php>
60. Ignatenko, O.V., Pokhodnya, I.K., Stepanyuk, S.M. et al. (2010) Principles of hydrogen cracking of welded joints of high strength low alloy steels. In: *Fundamental problems of hydrogen energy*. Kyiv: KIM, 340–360.
61. Ostash, O.P., Vitvitsky, V.I. (2011) Duality of hydrogen effect on mechanical behavior of steels and structural optimization of their hydrogen resistance. *Fiz.-Chimich. Mekhanika Materialov*, **4**, 4–19.
62. Ignatenko, A.V., Sinyuk, V.S. (2012) Influence of hydrogen-enhanced localized plasticity and complex-stressed state on strength of metal. In: *Proc. of 6th Int. Conf. on Mathematical Modelling and Information Technologies in Welding and Related Processes* (Katsiveli, 29 May–1 June 2012). Kiev: PWI, 35–36.
63. Panasyuk, V.V. (1968) *Ultimate equilibrium of brittle bodies with cracks*. Kiev: Naukova Dumka.
64. Morozov, L.S., Chechulin, B.B. (1967) *Hydrogen brittleness of metals*. Moscow: Metallurgiya.

Received 27.03.2013



INFLUENCE OF DIFFUSIBLE HYDROGEN ON DELAYED CRACKING RESISTANCE OF HIGH-CARBON STEEL WELDED JOINTS

A.A. GAJVORONSKY

E.O. Paton Electric Welding Institute, NASU

11 Bozhenko Str., 03680, Kiev, Ukraine. E-mail: office@paton.kiev.ua

Influence of diffusible hydrogen in deposited metal on the change of resistance to and nature of delayed fracture of HAZ metal in welded joints of high-strength wheel steel of grade 2 with 0.58 wt.% C was studied. «Pencil» method was used to determine diffusible hydrogen content in the deposited metal in CO₂ welding by PP-AN180MN flux-cored wire, the amount of which can vary in the range from 0.3 up to 2.2 cm³/100 g. At testing by the implant method the influence of diffusible hydrogen on the change of critical stress values at delayed fracture of wheel steel joints was evaluated. Scanning electron microscopy methods were used to study the influence of diffusible hydrogen on the nature of HAZ metal fracture; characteristic fracture zones and structural component parameters were determined. It is established that at diffusible hydrogen content in the deposited metal on the level of 0.3 cm³/100 g delayed fracture resistance of the joints is the highest, and depending on structural condition of metal of HAZ overheated zone critical fracture stresses are equal to (0.35–0.45) $\sigma_{0.2}$. Fracture occurs predominantly in the brittle mode along the boundaries and through the grain body, fraction of tough structural component is not more than 20 %. At increase of diffusible hydrogen content HAZ metal becomes brittle and delayed fracture resistance decreases. The most abrupt drop of critical stress characteristics to 0.1 $\sigma_{0.2}$ value is characteristic for the metal of HAZ with martensite-bainite structure, which has 70 % of martensite. 13 Ref., 2 Tables, 6 Figures.

Keywords: arc welding, diffusible hydrogen, wheel steel, delayed fracture, HAZ, structure

Cold cracking in high-strength steel welded joints is known to proceed by delayed fracture mechanism. This requires presence of quenched metal structure (martensite, bainite) with a high level of inner stresses and diffusion-mobile hydrogen which, accumulating in structural discontinuities, increases local stress level. This way, diffusible hydrogen leads to further embrittlement of the structure, and initiates formation of microcracks in the metal. Further on under the impact of residual stresses formed in the joint in welding, microcracks develop into macrocracks [1–5]. Here, geometrical stress raisers in the joints such as undercuts, lacks-of-fusion, lacks-of-penetration in the root have a great influence, being the sites of residual stress localizing, where the probability of cold cracking is the highest [6].

It is obvious that hydrogen is one of the main factors in cold cracking in welded joints of high-strength steels. Hydrogen influence on the process of delayed fracture of metal is accounted for by dislocation model, which is described in detail in [5, 7, 8]. According to this model, atomic hydrogen present in the welded joint accumulates in propagating dislocations and lowers ductile

properties of metal, energy of crack initiation and propagation at its fracture under the impact of external loading. It is also established that hydrogen influence becomes stronger with increase of metal strength.

Saturation of molten weld metal by atomic hydrogen, change of its solubility in the metal depending on temperature are described in [1]. So, hydrogen solubility in γ -iron is approximately equal to 8.2 cm³/100 g at the temperature of 1200 °C, and in α -iron at 500 °C this characteristic is only 0.6 cm³/100 g. Therefore, when at joint cooling structural $\gamma \rightarrow \alpha$ transformations proceed in weld metal, hydrogen solubility abruptly decreases and it diffuses into the ambient medium, including the adjacent region of HAZ metal. It is impossible to experimentally determine diffusible hydrogen content in HAZ metal.

In this connection, most of the researchers consider diffusible hydrogen content in deposited metal for comparative assessment of hydrogen influence on cold cracking resistance of high-strength steel welded joints. «Pencil» and chromatography methods are most often used for this purpose [1–3, 9]. For instance, it was established with application of «pencil» method that, depending on moisture level in welding consumables, diffusible hydrogen content in deposited metal in welding with solid wires in shielding



gases can reach 3, in manual arc welding 12 and in submerged-arc welding 8 cm³/100 g [1, 2].

Hydrogen content in HAZ metal can be assessed with a certain degree of approximation with application of calculation methods, allowing for kinetics of structural transformations in the welded joint. In [10] it was established that at initial content of diffusible hydrogen in the weld metal on the level of 10 cm³/100 g, local amount of atomic (diffusible) and molecular (residual) hydrogen in the HAZ metal of joints of high-strength low-alloyed (HSLA) steel at cooling by the specified thermal cycle to 60 °C (welding heat input of 9.1 kJ/cm) can be within 1.09–1.59 and 0.38–1.68 cm³/100 g, respectively. Changes of its concentration within the above limits depend on structural state of metal.

At formation of martensite-bainite structure content of diffusible and residual hydrogen in the HAZ metal is equal to 1.30 and 0.79 cm³/100 g, and in bainite-ferrite structure it is 1.49 and 1.68 cm³/100 g, respectively. As is seen, calculated local hydrogen concentrations in HAZ metal of the joints differ only slightly at its fixed content in the weld metal and constant welding heat input. Here diffusible hydrogen content in the HAZ metal is approximately 7 times lower than its initial content in the weld metal. However, even with such low and approximately same amount of it in the HAZ metal, the structure and ductile properties of which differ depending on TDWC conditions, delayed cracking resistance of HSLA steels is different.

In the case of arc welding of high-strength wheel steels, carbon content in which is higher than 0.5 %, quenching structures with higher dislocation density form in the HAZ metal. As a result, strength properties of the metal become higher, and ductile properties decrease [11–13]. It can be anticipated that in this case even negligible local hydrogen concentrations will lead to more essential changes of HAZ metal properties than in welding of HSLA steels. However, as investigations of weldability of high-strength steels with more than 0.5 % C began to be conducted comparatively recently, experimental data on hydrogen influence on delayed cracking resistance of welded joints of this type of steels are not available.

The objective of this work was investigation of the influence of diffusion-mobile hydrogen content in the deposited metal on the change of resistance to and nature of delayed fracture in HAZ metal of welded joints of high-strength wheel steel under static loading. Used as research material was wheel steel of grade 2 (GOST

10791) of the following composition, wt.%.: 0.58 C; 0.44 Si; 0.77 Mn; 0.10 Ni; 0.05 Cr; 0.012 S; 0.011 P.

Quantitative evaluation of delayed fracture resistance of HAZ metal was performed with application of Implant method [2, 3]. Unlike the traditional method, samples-inserts from the studied steel of 6 mm diameter were made without notches [13]. HSLA steel 20 mm thick was used as technological plates. Samples after welding and their natural cooling to 50 °C were loaded by constant load. Comparative testing was performed with application of mechanized CO₂ welding by experimental 2 mm flux-cored wire PP-AN180MN (weld metal alloying of 10KhGSFT system) at welding current $I_w = 220$ –250 A and arc voltage $U_a = 26$ V. Heat input at welding speed $v_w = 16.7$ m/h was $Q_w = 8.9$ kJ/cm, and at $v_w = 11$ m/h it was 13.6 kJ/cm. Welding of Implant samples was performed without preheating ($T_{pr} = 20$ °C). Here, HAZ metal cooling rate in the temperature range of 600–500 °C ($w_{6/5}$) was equal to 25–30 and 12–14 °C/s, respectively, and time of cooling from 800 to 100 °C ($\tau_{8/1}$) was 170 and 260 s, respectively.

It is obvious that metal structure in HAZ overheated zone will change depending on welding heat input and joint cooling rate. Specially conducted metallographic investigations showed that structure of wheel steel of grade 2 in as-delivered condition is represented by pearlite-ferrite mixture (Figure 1, *a*) with grain size $D_{gr} = 20$ –75 μm and microhardness $HV0.1-1990$ –2450 MPa. Ferrite fringes of size $h_f = 5$ –10 μm are located along the grain boundaries. Under the conditions of welding, when cooling rate is equal to $w_{6/5} = 25$ –30 °C/s, a mixed martensite-bainite structure forms in the HAZ metal overheated zone (Figure 1, *b*), in which the amount of martensite is 70 %, and structural component microhardness is $HV0.1-4340$ –6990 MPa. At $w_{6/5} = 12$ –14 °C/s martensite-bainite structure also forms in the HAZ metal overheated zone (Figure 1, *c*), but with prevailing fraction of bainite (80 %) with structural component microhardness $HV0.1-3340$ –3680 MPa. Grain size in HAZ metal overheated zone is $D_{gr} = 63$ –94 μm (point 4 and 5 to GOST 5639).

At testing by Implant method, hydrogen content in the deposited metal was varied by changing the temperature of flux-cored wire baking and time of its soaking in air before welding. Amount of diffusible hydrogen $[H]_{dif}$ in the deposited metal was determined by «pencil» method, using a mixture of glycerin and distilled

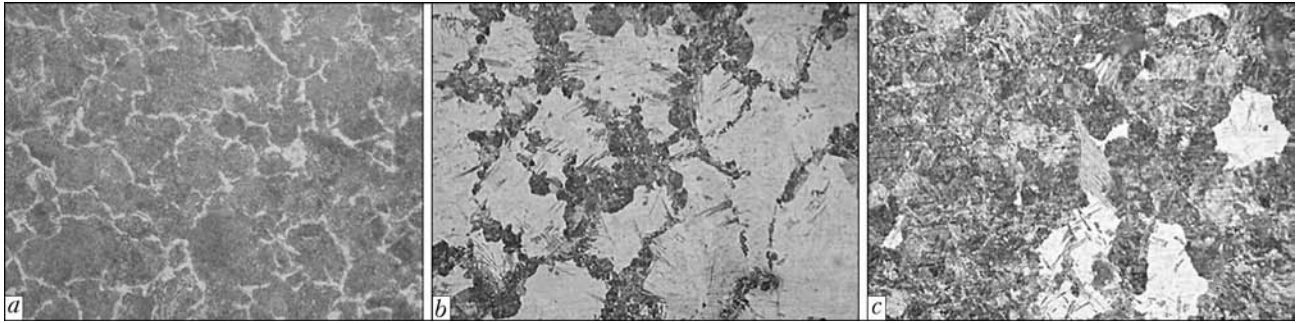


Figure 1. Microstructure ($\times 500$, reduced 2 times) of HAZ metal of grade 2 wheel steel: *a* – base metal; *b* – $w_{6/5} = 25-30$; *c* – $12-14\text{ }^\circ\text{C/s}$

water as blocking liquid. $[H]_{\text{dif}}$ content in the deposited metal depending on the conditions of preparation of flux-cored wire PP-AN180MN before welding was as follows, $\text{cm}^3/100\text{ g}$: baking at $230\text{ }^\circ\text{C}$ for 2.5 h – 0.3; baking at $230\text{ }^\circ\text{C}$ for 1 h – 0.5; baking at $230\text{ }^\circ\text{C}$ for 1 h, seasoning in air for 7 days – 1; baking at $230\text{ }^\circ\text{C}$ for 1 h, seasoning in air for 14 days – 1.3; baking at $200\text{ }^\circ\text{C}$ for 2.5 h – 1.5; baking at $150\text{ }^\circ\text{C}$ for 2.5 h – 1.8; without baking – 2.2.

It follows from the above data that in flux-cored wire CO_2 welding of high-strength carbon steels joints, it is possible to achieve a lower content of diffusible hydrogen in the weld metal, which is equal to $0.3\text{ cm}^3/100\text{ g}$ under the condition of pre-baking of the wire at $230\text{ }^\circ\text{C}$ for 2.5 h. This value $[H]_{\text{dif}}$ is several times lower than in submerged-arc welding with solid wires. In welding with flux-cored wire, which was baked for 1 h, and its seasoning for 14 days in air (moisture level of up to 75 %), $[H]_{\text{dif}}$ in weld metal rises up to $1.3\text{ cm}^3/100\text{ g}$. At lowering of baking temperature from 230 to $150\text{ }^\circ\text{C}$ and in

welding with wire not subjected to heat treatment, diffusible hydrogen content in the deposited metal is the highest – $1.8-2.2\text{ cm}^3/100\text{ g}$.

Figure 2 gives data on the change of delayed fracture resistance of HAZ metal in joints of wheel steel of grade 2, depending on welding heat input and diffusible hydrogen content in the deposited metal, varying from 0.3 up to $0.5\text{ cm}^3/100\text{ g}$. As is seen from the above material, critical stresses σ_{cr} , at which Implant samples do not fail, are the highest at minimum $[H]_{\text{dif}}$ values. In welding at heat input $Q_w = 8.9\text{ kJ/cm}$ ($w_{6/5} = 25-30\text{ }^\circ\text{C/s}$), they are equal to 250 MPa, and at $Q_w = 13.6\text{ kJ/cm}$ ($w_{6/5} = 12-14\text{ }^\circ\text{C/s}$) σ_{cr} rise up to 320 MPa.

Change of delayed fracture resistance values at constant $[H]_{\text{dif}} = 0.3\text{ cm}^3/100\text{ g}$ is influenced by structural state of metal in HAZ overheated zone. As was shown above, in welding of wheel steel in the modes, when $Q_w = 13.6\text{ kJ/cm}$, martensite-bainite structure of lower hardness forms in HAZ overheated zone. Amount of martensite in the structure is not higher than 20 %. Metal becomes more ductile, has better resistance to microcrack initiation and propagation and critical fracture stresses rise by 30 %.

It should be also noted that at $Q_w = 13.6\text{ kJ/cm}$ HAZ metal stays longer in temperature interval of $800-100\text{ }^\circ\text{C}$ at cooling ($\tau_{8/1}$ is 1.5 times higher) than at $Q_w = 8.9\text{ kJ/cm}$. This can also promote increase of delayed fracture resistance due to development of hydrogen diffusion processes in HAZ metal.

At increase of diffusible hydrogen content in the deposited metal up to $0.5\text{ cm}^3/100\text{ g}$ delayed fracture resistance of wheel steel HAZ metal decreases. This occurs more intensively in the case of welding at $Q_w = 8.9\text{ kJ/cm}$ ($w_{6/5} = 25-30\text{ }^\circ\text{C/s}$), when 70 % of martensite forms in the HAZ metal structure. Critical fracture stresses decrease from 250 to 150 MPa (by 40 %). In welding with a higher heat input (13.6 kJ/cm) and formation of predominantly bainitic structure in HAZ metal overheated zone, σ_{cr} decrease by 20 % to the level of 260 MPa.

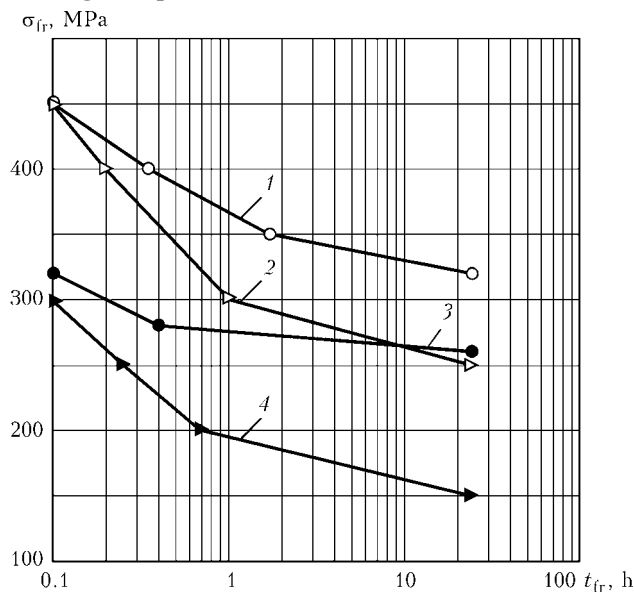


Figure 2. Influence of diffusible hydrogen on delayed fracture resistance of HAZ metal of grade 2 wheel steel: 1, 2 – $[H]_{\text{dif}} = 0.3$; 3, 4 – $0.5\text{ cm}^3/100\text{ g}$; 1, 3 – $Q_w = 13.6$; 2, 4 – 8.9 kJ/cm



As is seen, a slight increase of diffusible hydrogen in the deposited metal led to an essential lowering of the indices of delayed fracture resistance of HAZ metal. As shown in [13], in welding of joints of wheel steel with carbon content of 0.58 %, a structure, in which dislocation density can reach values $\rho = 5-8 \cdot 10^{10} \text{ cm}^{-2}$, forms in the HAZ metal overheated zone. Therefore, a comparatively small excess of the content of atomic hydrogen, which accumulates in dislocations with such density level in higher strength metal, leads to marked embrittlement of HAZ metal. This is indicated by comparative testing of Implant samples, in which welding heat input was equal to 8.9 kJ/cm at load level of 300 MPa (see Figure 1): time of HAZ metal fracture at $[H]_{\text{dif}} = 0.3$ and $0.5 \text{ cm}^3/100 \text{ g}$ in the weld metal is equal to 60 and 6 min, respectively.

Generalized results of investigation of the influence of diffusible hydrogen content in the deposited metal on delayed fracture resistance values of HAZ metal in welded joints of wheel steel of grade 2 (0.58 % C) are given in Figure 3. As is seen, subsequent increase of $[H]_{\text{dif}}$ content in the weld up to $1.0-1.5 \text{ cm}^3/100 \text{ g}$ leads to lowering of delayed fracture resistance of HAZ metal, but these changes proceed smoothly. So, at increase of diffusible hydrogen in the deposited metal by $1.0 \text{ cm}^3/100 \text{ g}$ (from 0.5 up to 1.5), σ_{cr} values for HAZ metal of wheel steel joints, made in the modes with $Q_w = 13.6 \text{ kJ/cm}$, decrease by approximately another 12 % (from 260 to 220 MPa), and in welding with $Q_w = 8.9 \text{ kJ/cm}$ – by 24 % (from 150 to 90 MPa). Here also the influence of structural factor is manifested. Embrittlement of more hardened HAZ metal at increase of diffusible hydrogen proceeds to a greater degree.

At increase of $[H]_{\text{dif}}$ up to $1.8 \text{ cm}^3/100 \text{ g}$ delayed fracture resistance of HAZ metal of wheel steel joints, which were welded at $Q_w =$

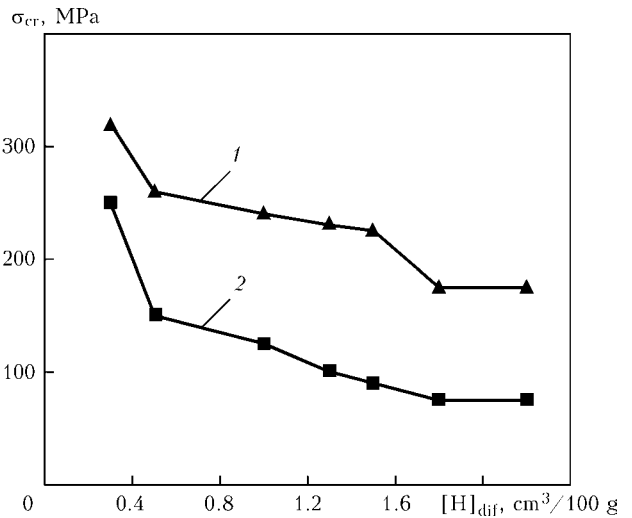


Figure 3. Influence of diffusible hydrogen content in the deposited metal on critical fracture stress of HAZ metal in joints of grade 2 wheel steel in welding with PP-AN180MN wire: 1 – $Q_w = 13.6$; 2 – 8.9 kJ/cm

$= 8.9 \text{ kJ/cm}$, decreases by 6 % to values $\sigma_{\text{cr}} = 75 \text{ MPa}$. This is the limit value of critical stresses under these conditions of welding, which is equal to approximately 0.1 of HAZ metal yield point ($\sigma_{0.2}$ of about 715 MPa [12]), and further on at increase of diffusible hydrogen content in the deposited metal to $2.2 \text{ cm}^3/100 \text{ g}$, this value does not change. Total lowering of critical fracture stresses of HAZ metal in wheel steel joints at $Q_w = 8.9 \text{ kJ/cm}$ at increase of $[H]_{\text{dif}}$ content from 0.3 up to $2.2 \text{ cm}^3/100 \text{ g}$ in the deposited metal was equal to 70 %.

For HAZ metal of joints welded at $Q_w = 13.6 \text{ kJ/cm}$, σ_{cr} value changes in a somewhat different manner at $[H]_{\text{dif}}$ increase from 1.5 up to $1.8 \text{ cm}^3/100 \text{ g}$. As is seen from Figure 3, lowering of critical fracture stresses is equal to 14 % (from 220 to 175 MPa). This is, probably, related to the fact that under these welding conditions, when predominantly bainitic structure forms in the overheated zone of HAZ metal in wheel steel joints, its oversaturation with atomic

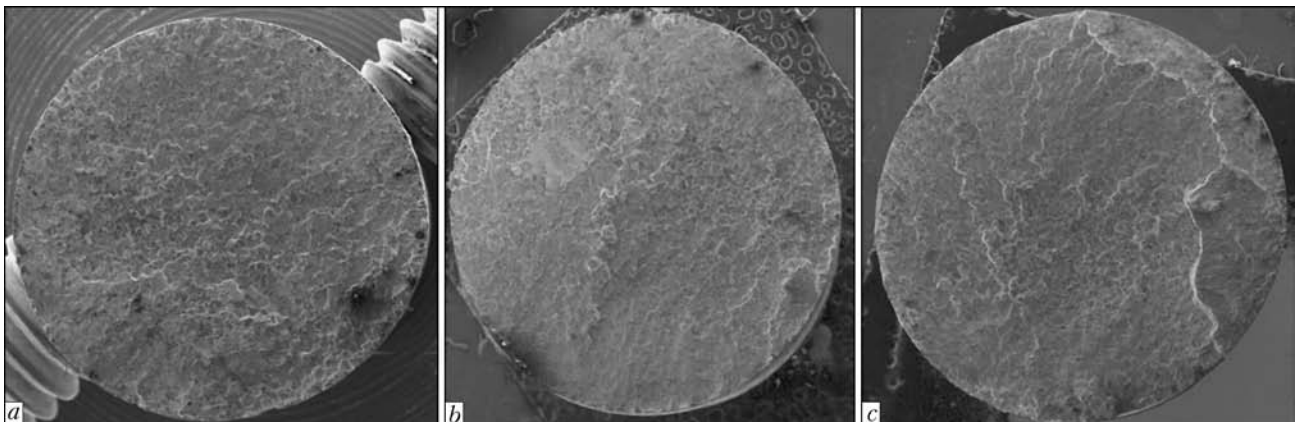


Figure 4. Fractures ($\times 25$) of Implant samples of grade 2 wheel steel in welding with PP-AN180MN wire at $Q_w = 13.6 \text{ kJ/cm}$: a – $[H]_{\text{dif}} = 0.3$; b – 0.5 ; c – $2.2 \text{ cm}^3/100 \text{ g}$



Table 1. Parameters of testing Implant samples of wheel steel for investigations of fracture surface ($Q_w = 13.6 \text{ kJ/cm}$)

$[H]_{\text{dif}}, \text{ cm}^3/100 \text{ g}$	$\sigma_{\text{cr}}, \text{ MPa}$	$\sigma_{\text{fr}}, \text{ MPa}$	$t_{\text{fr}}, \text{ h}$
0.3	320	350	1.5
0.5	260	320	0.1
1.5	220	250	4.5
2.2	175	200	4.5

hydrogen takes place and ductile properties of the metal decrease more abruptly. At further increase of diffusible hydrogen content in the deposited metal to $2.2 \text{ cm}^3/100 \text{ g}$ this value does not change, either. Total lowering of critical stresses of HAZ metal fracture in wheel steel joints at increase of $[H]_{\text{dif}}$ content from 0.3 up

to $2.2 \text{ cm}^3/100 \text{ g}$ was equal to 45 % for these welding conditions.

Fractures of Implant samples of wheel steel, which were welded at $Q_w = 13.6 \text{ kJ/cm}$ with different content of diffusible hydrogen in the deposited metal, were studied by scanning electron microscopy methods*.

The Philips scanning electron microscope SEM-515, fitted with energy-dispersive spectrometer of LINK system, was used. Loading parameters at testing of Implant samples of wheel steel, which were selected for fracture surface studies, are given in Table 1.

Fractures of Implant samples of wheel steel of grade 2 are shown in Figure 4. It is established that fracture runs, mainly, in the brittle mode. Characteristic fracture zones are observed on

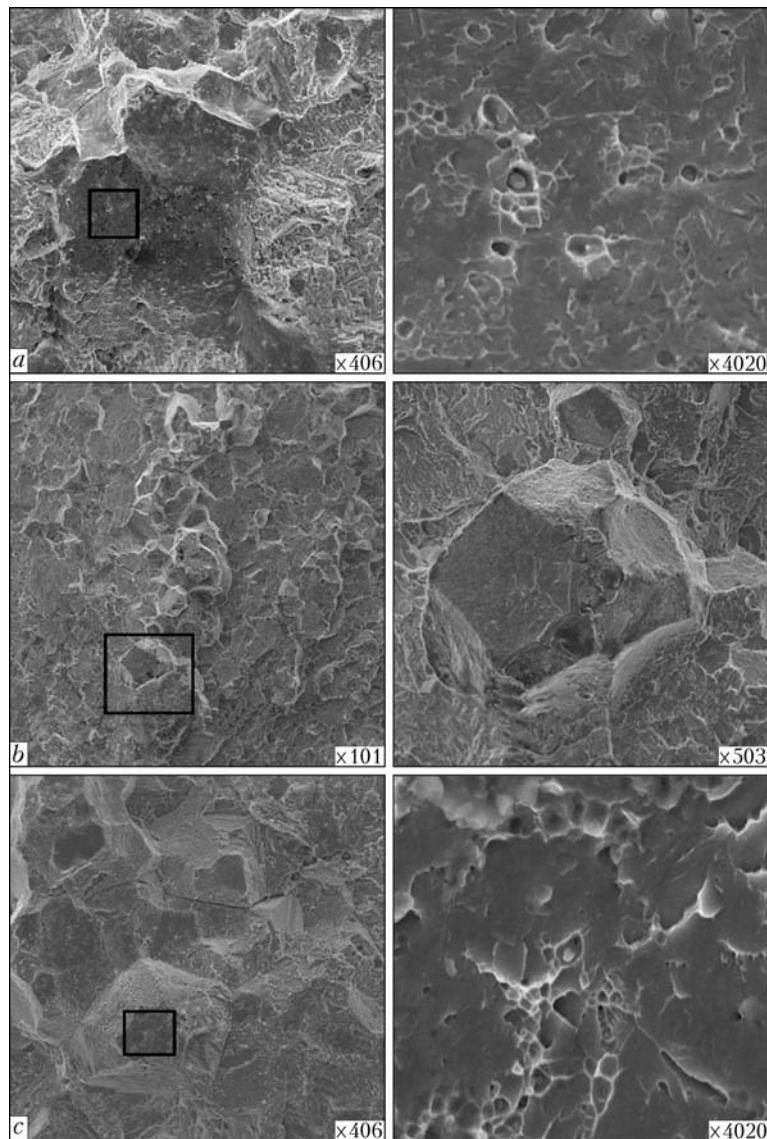


Figure 5. Fragments of fracture surface of HAZ metal in the region of initiation and delayed propagation of microcracks: *a* – $[H]_{\text{dif}} = 0.3$; *b* – 0.5; *c* – $2.2 \text{ cm}^3/100 \text{ g}$

* Investigations were performed by L.I. Markashova, E.N. Berdnikova and T.A. Alekseenko.



Table 2. Fracture structure at delayed fracture of HAZ metal of grade 2 wheel steel

[H] _{dif} , cm ³ /100 g	Zone I				Zone II					
	Brittle intergranular		Brittle intragranular		Brittle intergranular		Brittle intragranular		Tough	
	V, %	D _f , μm	V, %	D _f , μm	V, %	D _f , μm	V, %	D _f , μm	V, %	D _f , μm
0.3	20	30/100	80	50/100	20	60/100	60	40/60	20	0.5/2
0.5	40	50/120	60	50/100	15	50/120	80	40/60	5	0.5/2
1.5	60	50/120	40	50/100	40	50/100	60	50/80	–	–
2.2	80	50/100	20	50/80	40	50/100	60	40/80	–	–

fracture surface, which can be conditionally divided into local regions of microcrack initiation and their delayed propagation (zone I), regions of accelerated microcrack propagation up to macrolevel (zone II), and final fracture regions (zone III). Zone distribution is of a local nature, crack initiation and propagation occurs simultaneously in several sites, and fracture regions al-

ternate. Investigations at microlevel showed that, depending on diffusible hydrogen content in the deposited metal and loading level, microrelief of HAZ metal fracture surface is different. Generalized results of investigations are given in Figures 5, 6 and Table 2.

It is established that microcrack initiation in the HAZ metal of wheel steel joints proceeds in

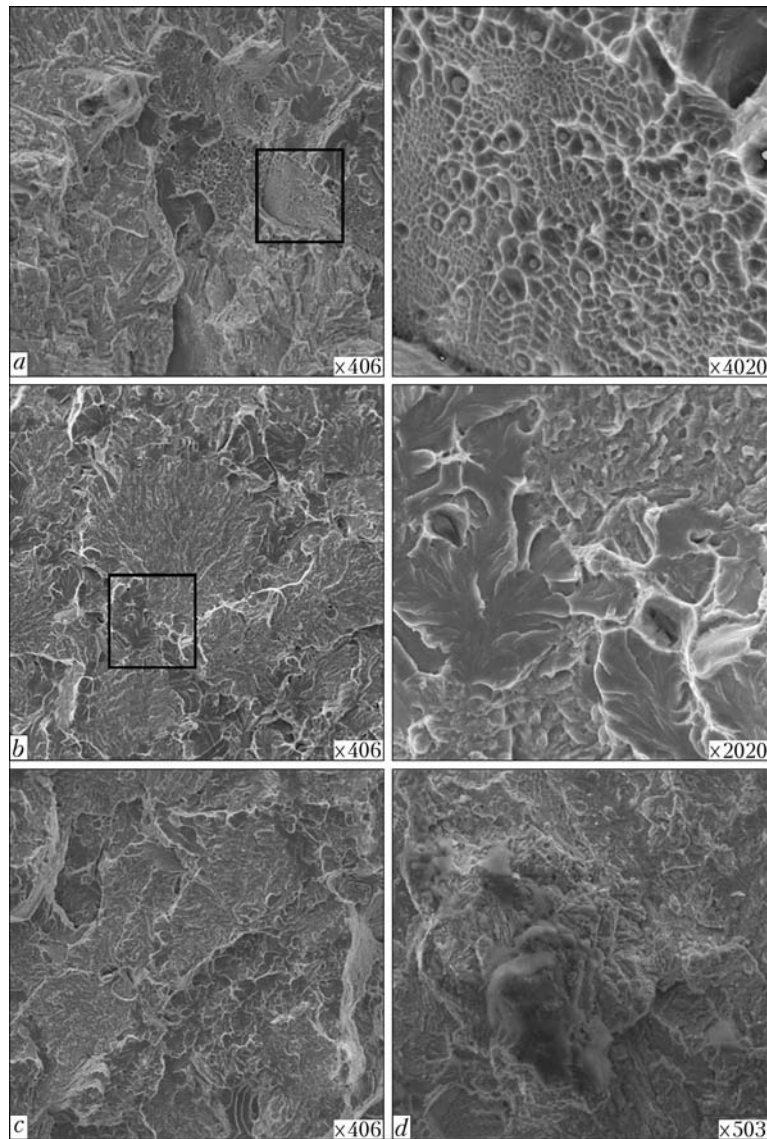


Figure 6. Fragments of fracture surface of HAZ metal in regions of accelerated development of microcracks (a, b) and final fracture (c, d): a, c – [H]_{dif} = 0.3; b, d – 2.2 cm³/100 g



the brittle mode along grain boundaries. In fracture zone I with all welding variants, local regions of brittle intergranular fracture are observed, which are the sites of microcrack initiation (Figure 5, *a-c*). Further on, under the impact of stresses, microcracks propagate both along the boundaries and through the grain body: fracture in this zone is characterized as intergranular and intragranular cleavage. Size of cleavage facets D_f is equal to approximately 30–100 μm . Depending on diffusible hydrogen content in the deposited metal, ratio of these kinds of fracture changes. With increase of $[\text{H}]_{\text{dif}}$ content from 0.3 up to 2.2 $\text{cm}^3/100\text{ g}$, volume fraction V of intergranular cleavage rises from 20 up to 80 %, while fraction of intragranular cleavage decreases, respectively (see Table 3). In this zone also secondary cracks were detected, the length of which is equal to 250 μm at $[\text{H}]_{\text{dif}} = 2.2\text{ cm}^3/100\text{ g}$.

After the crack has reached its critical size, accelerated development of microcracks into macrocracks begins. Alongside intergranular and intragranular cleavage, local regions of tough fracture with facet size of about 0.5–2.0 μm are observed along the boundaries of some grains (Figure 6, *a*). At $[\text{H}]_{\text{dif}} = 0.3\text{ cm}^3/100\text{ g}$ volume fraction of tough fracture is up to 20 %, at $[\text{H}]_{\text{dif}} = 0.5\text{ cm}^3/100\text{ g}$ it is 5 %, and at subsequent increase of diffusible hydrogen content in the deposited metal accelerated crack development runs solely in the brittle mode (Figure 6, *b*).

In the final fracture zone, fracture mode and size of structural elements differ from those of other fracture zones. This predominantly is intragranular quasibrittle fracture with facet size of approximately 10–20 μm , and at increase of $[\text{H}]_{\text{dif}}$ content fracture mode practically does not change (Figure 6, *c, d*).

Thus, conducted investigations showed that:

- in welding with flux-cored wire of PP-AN180MN type, it is possible to ensure lower (0.3 $\text{cm}^3/100\text{ g}$) content of diffusible hydrogen in the deposited metal («pencil» method) that is much lower than in welding with solid wires in shielding gases and under a layer of flux. At such $[\text{H}]_{\text{dif}}$ value delayed fracture resistance of HAZ metal in joints of high-strength wheel steel with carbon content of 0.58 % is the highest. Critical fracture stresses, depending on structural state of the metal of HAZ overheated zone, were equal to approximately (0.35–0.45) $\sigma_{0.2}$. Fracture occurs predominantly in the brittle mode along the boundaries and in the body of grains, with not more than 20 % fraction of tough structural component;

- at increase of diffusible hydrogen content in the deposited metal by 0.2 $\text{cm}^3/100\text{ g}$ (from 0.3 to 0.5) HAZ metal becomes brittle, and delayed fracture resistance of welded joints drops abruptly. Degree of this influence is determined by structural state of metal in HAZ overheated zone. At formation of martensite-bainite structure of higher strength and lower ductility (70 % of martensite, $w_{6/5} = 25\text{--}30\text{ }^\circ\text{C/s}$) critical fracture stresses decrease by 40 %, when a predominantly bainitic structure forms (80 % of bainite, $w_{6/5} = 12\text{--}14\text{ }^\circ\text{C/s}$) they decrease by 20 %. Here the fraction of tough component in the fracture is not higher than 5 %;

- at increase of diffusible hydrogen content in the deposited metal up to 1.8–2.2 $\text{cm}^3/100\text{ g}$ further embrittlement of HAZ metal proceeds and critical fracture stresses decrease to minimum values of (0.10–0.25) $\sigma_{0.2}$. Fracture runs solely in the brittle mode along the boundaries and in the body of grains, fraction of brittle intergranular cleavage in the zone of microcrack initiation and delayed propagation rises from 20 up to 80 %.

1. Kozlov, R.A. (1969) *Hydrogen in welding of hull steels*. Leningrad: Sudostroenie.
2. Makarov, E.L. (1981) *Cold cracks in welding of alloyed steels*. Moscow: Mashinostroenie.
3. Hrivnak, I. (1984) *Weldability of steels*. Moscow: Mashinostroenie.
4. Kasatkin, O.G. (1994) Peculiarities of hydrogen embrittlement of high strength steels in welding. *Avtomatich. Svarka*, **1**, 3–7.
5. Pokhodnya, I.K., Shvachko, I.V. (1997) Physical nature of hydrogen induced cold cracks in welded joints of structural steels. *Ibid.*, **5**, 3–12.
6. Makhnenko, V.I. (2006) *Resource of safety service of welded joints and assemblies of current structures*. Kiev: Naukova Dumka.
7. Shvachko, I.V., Ignatenko, A.V. (2007) Model of transportation of hydrogen with dislocations. *The Paton Welding J.*, **2**, 24–26.
8. Ignatenko, A.V., Pokhodnya, I.K., Paltsevich, A.P. et al. (2012) Dislocation model of hydrogen-enhanced localizing of plasticity in metals with bcc lattice. *Ibid.*, **3**, 15–19.
9. Pokhodnya, I.K., Paltsevich, A.P. (1980) Chromatographic method for determination of diffusion hydrogen content in welded joints. *Avtomatich. Svarka*, **1**, 37–39.
10. Makhnenko, V.I., Korolyova, T.V., Lavrinets, I.G. (2002) Effect of microstructural transformations on redistribution of hydrogen in fusion welding of structural steels. *The Paton Welding J.*, **2**, 6–13.
11. Kiselyov, S.N., Voronin, N.N., Kuzmina, G.D. et al. (2000) Investigation of thermal processes and structure formation in twin-arc surfacing of railway wheels on the base of computer modeling. *Svarochn. Proizvodstvo*, **3**, 3–8.
12. Gajvoronsky, A.A., Poznyakov, V.D., Sarzhevsky, V.A. et al. (2010) Influence of thermodeformational cycle of hardfacing on the structure and properties of railway wheels at their reconditioning. *The Paton Welding J.*, **5**, 15–18.
13. Gajvoronsky, A.A., Poznyakov, V.D., Markashova, L.I. et al. (2012) Influence of deposited metal composition on structure and mechanical properties of reconditioned railway wheels. *Ibid.*, **8**, 16–22.

Received 06.03.2013



PROBLEMS OF EXAMINATION OF MODERN CRITICAL WELDED STRUCTURES

V.I. MAKHNENKO*

E.O. Paton Electric Welding Institute, NASU
11 Bozhenko Str., 03680, Kiev, Ukraine. E-mail: office@paton.kiev.ua

An important stage of diagnostics of the state of critical welded structures is prediction of their residual life based on strength analysis by limiting state. In the absence of crack-like raisers spontaneous macrofailure of structural elements in a number of cases is the result of plastic instability, related to porosity initiation and development. This work deals with the main problems of modelling tough fracture of welded structures and proposes methodological basis for description of mechanisms of their limiting state. In particular, complex finite element models of simultaneous development of 3D stress-strain state of elastoplastic material with strengthening and pore formation have been developed. Condition of initiation of tough fracture pores is determined by limit value of Odqvist parameter, and pore development — by Rice–Tracey law. Thus, limiting state of a structure at developed plastic flow of metal is due to discontinuity growth, local redistribution of load and reduction of actual load-carrying cross-section. Application of the proposed methodology was illustrated by examples of calculation of limiting inner pressure of pipeline elements, allowing for initial stress-strain state at site and repair welding, structural inhomogeneity, and surface defects of local wall thinning. It is shown that in the absence of geometrical raisers, physical inhomogeneity has little influence on limiting load at static loading of the considered welded structures. This is in agreement with the available experience of pipeline system operation that proves applicability of developed approaches of numerical analysis for effective solution of practical problems of diagnostics of the state of modern welded structures. 12 Ref., 1 Table, 4 Figures.

Keywords: *tough fracture, pore formation, mathematical modelling, stress-strain state, limit load*

Practical experience all over the world shows that periodical technical examination of the state of modern critical structures is the most effective measure, ensuring reliability of their operation. Technical examination of such structures consists of a whole number of stages, among which technical diagnostics of the state and appropriate prediction of safe residual operating life have a special place. Continuous development of diagnostic means and technologies allows obtaining every year more and more accurate data on the state of various structures, in particular welded structures. Advance of technical diagnostics stimulates respective development of methods of predicting safe residual operating life. A lot of attention in this case is given to modern development of computational engineering, as well as numerical methods of modelling continuum deformations and concurrent processes of fracture mechanics. For welded structures, for which strength analysis is usually performed by limiting state, extremely important for solving practical

problems of prediction of safe residual operating life, based on concrete data of technical diagnostics, is development of methods of mathematical modeling of deformation processes up to states close to the limiting state and mathematical description of limiting state mechanisms, that is by far not always reduced to comparison of calculated maximum stresses or deformations with limiting values for the given structural material under the respective loading conditions. In other words, unlike strength analysis by allowable stresses (deformations), calculation by limiting loads requires, as a rule, application of more precise methods of non-linear mechanics of deformation (allowing for physical or geometrical non-linearity, or for one and the other simultaneously), as well as involvement of respective criteria of formation of discontinuity (fracture), depending on loading conditions, material properties, etc., determining the fracture mode.

Over the last decades brittle fracture is believed to be the best studied in this respect that can be related to a number of factors, of which the following are the most important: large-scale negative consequences of such failures, small differences between prior deformation of fracture zone and the elastic one, i.e. urgency at relatively simple initial parameters. Nonetheless, creation of modern, quite rigorous linear theory of fracture

* Under the author's guidance E.A. Velikoivanenko, G.F. Rozyinka and N.I. Pivtorak also participated in this work.



mechanics of bodies with cracks and approximate non-linear theory for the same purpose took several decades. At prediction of safe residual operating life of critical welded structures with detected (or hypothetical) crack-like defects, modern theories of fracture mechanics of bodies with cracks allow solving a number of practical tasks [1, 2, etc.] under various loading conditions (static, cyclic, temperature, in aggressive medium, etc.). Popularity of modern theories of fracture mechanics of bodies with cracks is determined, primarily, by absence of the need for detailed analysis of stress-strain state in the «hot zone» along a quite indeterminate crack border, operating with the respective integral characteristics of the following type:

- stress intensity factor K_j ($j = I, II, III$) and its critical value $K_{j,c}$, $\text{MPa}\cdot\text{m}^{1/2}$;
- released energy per a unit of crack growth length J_j and its critical value $J_{j,c}$, J/m ;
- crack opening displacement δ and its critical value δ_c , mm ;
- reference stresses σ_{ref} , determining the state of plastic collapse along the crack border at a specified yield limit σ_y of material in this zone, MPa .

Algorithms for calculation of these characteristics, as well as experimental procedures for determination of their critical values, have been quite profoundly studied, particularly for K_j and σ_{ref} [2, 3, etc.], as well as for J_j that determines minimum deviations of various investigation results on limiting loads for specific tasks.

In case of absence of a crack-like defect and sufficiently tough material of welded structure, for instance, thinning of bearing wall of a welded pressure vessel or pipeline, calculations by ad-

missible stresses can lead to tough fractures of the type of plastic instability [4] that is characteristic for high-strength steels with a small coefficient of deformation strengthening. Such calculation data are by far not always confirmed by experience that is due to additional mechanisms of compensation of section reduction at tension.

Process of pore formation at developed plastic flow of structural steels is universally recognized as one of such mechanisms. In the general form, regularities of pore initiation and development processes, as well as the influence of pore formation on deformation processes and fracture have been defined, mainly, on the basis of experimental investigations already in the 1970s. However, their actual application [5–8, etc.] is rather complicated and requires a number of material characteristics that can be obtained only through combination of experiment and calculations (actually, on rather simple samples [5]). Nonetheless, the real progress of development of computational engineering and methods of solving deformation problems in 3D definition, allowing for physical and geometrical non-linearity, noticeably changes the opinions on realization of complex mathematical models. Respective developments are performed in various organizations, including PWI — for welded structures. Main postulates of such development and some cases of its application when solving practical problems are given below.

The work is based on simultaneous consideration of deformation and pore formation processes in an arbitrary 8-node finite element (FE), used to simulate a continuum in an orthogonal system of coordinates x, y, z . Within the considered FE (Figure 1), distribution of stresses, strains and temperatures is taken to be uniform.

Porosity develops at a certain level of plastic deformations, characterized by Odqvist parameter κ_s :

$$\kappa_s = \int d\varepsilon_i^p, \tag{1}$$

where $d\varepsilon_i^p = \frac{\sqrt{2}}{3} \sqrt{d\varepsilon_{ij}^p d\varepsilon_{ij}^p}$; $d\varepsilon_{ij}^p$ are the components of plastic deformation increment tensor ($i, j = x, y, z$).

Pores formed in FE are uniformly distributed through its volume V_{FE} ; volume fraction of discontinuity ρ_V is determined by the ratio of volumes of pores V_{pore} and entire finite element V_{FE} .

Accordingly, condition of the start of pore formation process in a concrete FE is given by the following equation:

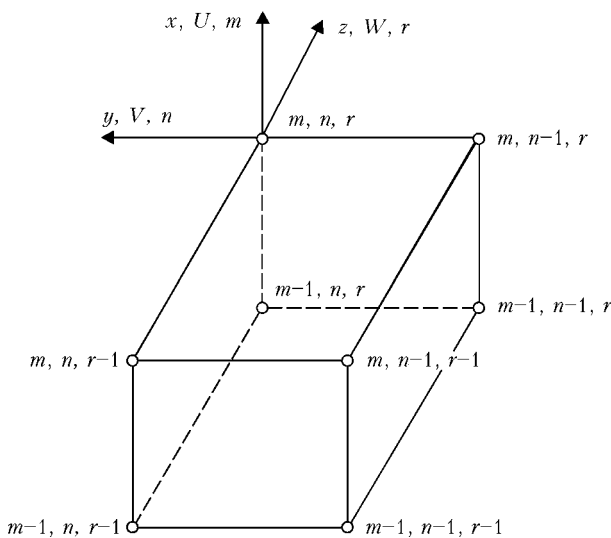


Figure 1. Schematic of finite element in x, y, z coordinate system, with displacement in the respective directions V, U, W and node numbering m, n, r



$$\begin{cases} \rho_V = 0 & \text{at } \kappa < \kappa_s, \\ \rho_V \geq \rho_V^s & \text{at } \kappa \geq \kappa_s, \end{cases} \quad (2)$$

where ρ_V^s is the conditional initial volume fraction of pores.

By analogy with ρ_V concept, the following characteristics are introduced: ρ_S – relative area of pores in FE cross-section, i.e.

$$\rho_S = \frac{S_{\text{pore}}}{S_{\text{FE}}} \quad (3)$$

and ρ_l – relative length of FE linear size, taken up by pores, i.e.

$$\rho_l = \frac{l_{\text{pore}}}{l_{\text{FE}}} \quad (4)$$

There exists a connection $\rho_V = 3\rho_l$ between ρ_V , ρ_S and ρ_l , $\rho_S = 2\rho_l$ at $\rho_l \ll 1$.

Pores initiating in FE grow with development of plastic deformations by Rice–Tracey law [5], i.e.

$$d\rho_l = \rho_l K_1 \exp\left(K_2 \frac{\sigma_m}{\sigma_i}\right) d\varepsilon_i^p, \quad (5)$$

where $\sigma_m = \frac{1}{3}(\sigma_{xx} + \sigma_{yy} + \sigma_{zz})$ is the mean normal stress in the given FE; $\sigma_i = \sqrt{\frac{1}{2}\sigma_{ij}\sigma_{ij}}$ is the stress intensity in this FE; σ_m/σ_i is the characteristic of stressed state rigidity; $K_1 = 0.28$; $K_2 = 1.5$.

It follows from (5) that value $d\rho_l$ is the relative increment of FE linear dimensions due to porosity, i.e. increment of deformation tensor components can be given by the following sum:

$$\begin{aligned} d\varepsilon_{ij} &= d\varepsilon_{ij}^e + d\varepsilon_{ij}^p + \delta_{ij}(d\varepsilon_T + d\rho_l), \\ \delta_{ij} &= 1 \text{ at } i = j, \delta_{ij} = 0 \text{ at } i \neq j, \end{aligned} \quad (6)$$

where $d\varepsilon_{ij}^e$, $d\varepsilon_{ij}^p$, $\delta_{ij}d\varepsilon_T$, $\delta_{ij}d\rho_l$ are the components of deformations increment due to stresses by Hooke’s law, plastic deformation, change of temperature and porosity, respectively.

Proceeding from the method of successive tracing of development of elastoplastic deformations and the assumption that at the tracing step σ_m/σ_i value changes only slightly, relationship (5) becomes

$$\ln \frac{\rho_l}{(\rho_l)^*} = K_1 \exp\left(K_2 \frac{\sigma_m}{\sigma_i}\right) (\kappa - \kappa^*), \quad (7)$$

where index *) refers this value to the previous tracing step.

Accordingly, after $\rho_l = (\rho_l)^* + \Delta\rho_l$ substitution into (7)

$$\Delta\rho_l = (\rho_l)^* \left\{ \exp\left[K_1 \exp\left(K_2 \frac{\sigma_m}{\sigma_i} \right) (\kappa - \kappa^*) \right] - 1 \right\}, \quad (8)$$

$(\kappa^*) > \kappa_s$.

Substitution of Δ for d operator in (6) allowing for (8) yields an expression for total deformation increment $\Delta\varepsilon_{ij}$, allowing for pore growth in this FE per tracing step. Further on the algorithm of solution of deformation problem corresponds to that from [1, 5].

At realization of plastic flow conditions the following dependence is used:

$$\sigma_i = \sigma_s(T, \kappa)(1 - 2\rho_l), \quad (9)$$

where $\sigma_s(T, \kappa)$ are the deforming stresses in the material at temperature T and Odqvist parameter κ to (1).

Equations of constraint between tensor σ_{ij} and $\Delta\varepsilon_{ij}$ are as follows:

$$\begin{aligned} \Delta\varepsilon_{ij} &= \psi(\sigma_{ij} - \delta_{ij}\sigma_m) + \delta_{ij}(K\sigma_m + \Delta\varepsilon_T + \Delta\rho_l) - b_{ij}, \\ b_{ij} &= \frac{1}{2G}(\sigma_{ij} - \delta_{ij}\sigma_m)^* + (K\sigma_m)^*, \quad (i, j = x, y, z), \end{aligned} \quad (10)$$

where $K = \frac{1 - 2\nu}{E}$; E is the Young’s modulus; ν is the Poisson’s ratio; $G = \frac{E}{2(1 + \nu)}$ for material of this FE; ψ is the function of material state, determined by yield condition, i.e.

$$\psi = \frac{1}{2G} \text{ if } \sigma_i < \sigma_s(T, \kappa)(1 - 2\rho_l); \quad (11)$$

$$\psi > \frac{1}{2G} \text{ if } \sigma_i = \sigma_s(T, \kappa)(1 - 2\rho_l);$$

$\sigma_i > \sigma_s(T, \kappa)(1 - 2\rho_l)$ state is inadmissible.

Plastic deformations are determined from the following equation:

$$\Delta\varepsilon_{ij} = \left(\psi - \frac{1}{2G} \right) (\sigma_{ij} - \delta_{ij}\sigma_m), \quad (i, j = x, y, z). \quad (12)$$

Realization of conditions (11) is performed in each tracing step iteratively, using (12), (1), (7), (8) and respective dependence $\sigma_s(T, \kappa)$ on κ and T [5]. At each iteration by ψ , stresses σ_{ij} are found from (10):

$$\sigma_{ij} = \frac{1}{\psi} \left(\Delta\varepsilon_{ij} + \delta_{ij} \frac{\psi - K}{K} \Delta\varepsilon \right) + J_{ij}, \quad (13)$$

where



$$\Delta \varepsilon = \frac{\Delta \varepsilon_{xx} + \Delta \varepsilon_{yy} + \Delta \varepsilon_{zz}}{3},$$

$$J_{ij} = \frac{1}{\psi} \left[(b_{ij} - \delta_{ij} b) + \delta_{ij} \left(K \sigma^* - \frac{\Delta \varepsilon_T + \Delta \rho_l}{K} \right) \right],$$

$$b = \frac{1}{3} (b_{xx} + b_{yy} + b_{zz}).$$

Tensor $\Delta \varepsilon_{ij}$ and displacement increment vector ΔU_i are connected by the following relationship:

$$\Delta \varepsilon_{ij} = \frac{1}{2} (\Delta U_{i,j} + \Delta U_{j,i}), \quad (14)$$

where the comma in the index corresponds to differentiation within FE, i.e. in the system of coordinates x, y, z (see Figure 1). From (14) at $\Delta \varepsilon_{ij} \ll 1$ it follows that

$$\Delta \varepsilon_{xx} = \frac{\Delta U_{m,n,r} - \Delta U_{m-1,n,r}}{x_{m,n,r} - x_{m-1,n,r}},$$

$$\Delta \varepsilon_{yy} = \frac{\Delta V_{m,n,r} - \Delta V_{m,n-1,r}}{y_{m,n,r} - y_{m,n-1,r}},$$

$$\Delta \varepsilon_{zz} = \frac{\Delta W_{m,n,r} - \Delta W_{m,n,r-1}}{z_{m,n,r} - z_{m,n,r-1}},$$

$$\Delta \varepsilon_{xy} = \frac{1}{2} \times$$

$$\times \left[\frac{\Delta U_{m,n,r} - \Delta U_{m,n-1,r}}{y_{m,n,r} - y_{m,n-1,r}} + \frac{\Delta V_{m,n,r} - \Delta V_{m-1,n,r}}{x_{m,n,r} - x_{m-1,n,r}} \right],$$

$$\Delta \varepsilon_{xz} = \frac{1}{2} \times$$

$$\times \left[\frac{\Delta U_{m,n,r} - \Delta U_{m,n,r-1}}{z_{m,n,r} - z_{m,n,r-1}} + \frac{\Delta W_{m,n,r} - \Delta W_{m-1,n,r}}{x_{m,n,r} - x_{m-1,n,r}} \right],$$

$$\Delta \varepsilon_{yz} = \frac{1}{2} \times$$

$$\times \left[\frac{\Delta U_{m,n,r} - \Delta U_{m,n,r-1}}{z_{m,n,r} - z_{m,n,r-1}} + \frac{\Delta W_{m,n,r} - \Delta W_{m,n-1,r}}{y_{m,n,r} - y_{m,n-1,r}} \right],$$

where $x_{m,n,r}, y_{m,n,r}, z_{m,n,r}, \dots$ are the coordinates of FE components (see Figure 1) allowing for their changes at differentiation, i.e.

$$x_{m,n,r} = x_{m,n,r}^* + \Delta U_{m,n,r},$$

$$y_{m,n,r} = y_{m,n,r}^* + \Delta V_{m,n,r},$$

$$z_{m,n,r} = z_{m,n,r}^* + \Delta W_{m,n,r}. \quad (16)$$

Stress tensor components (13) satisfy static equations for inner FE and respective limiting conditions. In its turn, components of ΔU_i ($\Delta U, \Delta V, \Delta W$) vector meet the respective conditions on the boundary.

Resolving system of algebraic equations relative to displacement increment vector in FE nodes at each step of tracing and iteration by ψ is determined as a result of minimizing the (functional Lagrange variation principle) [9]:

$$E_1 = -\frac{1}{2} \sum_V (\sigma_{ij} + J_{ij}) \Delta \varepsilon_{ij} V_{m,n,r} + \sum_{S_p} P_i \Delta U_i \Delta S_p^{m,n,r}, \quad (17)$$

where \sum_V is the operator of summation by inner FE; \sum_{S_p} is the operator of summation by surface FE, in which components of force vector P_i ($i = x, y, z$) are assigned, i.e. system of equations

$$\frac{\partial E_1}{\partial \Delta U_{m,n,r}} = 0, \quad \frac{\partial E_1}{\partial \Delta V_{m,n,r}} = 0,$$

$$\frac{\partial E_1}{\partial \Delta W_{m,n,r}} = 0 \quad (18)$$

allows deriving a solution for increments of displacement vector in each step of tracing and iteration by ψ for the respective FE. State of plastic instability for the considered FE at the specific tracing step is determined by the value of function ψ .

It follows from (12), (13) that at increase of function ψ , plastic deformation increments $\Delta \varepsilon_{ij}^p$ grow and stresses σ_{ij} decrease. If in the previous tracing step Odqvist parameter κ^* , and plastic instability develops at deformation ε_f , then, equating $\kappa^* + \Delta \varepsilon_i^p = \varepsilon_f$, we can evaluate $\left(\psi - \frac{1}{2G} \right)_{cr}$ values, above which the process of plastic instability is quite real in this FE, i.e.

$$\left(\psi - \frac{1}{2G} \right)_{cr} \geq \frac{\varepsilon_f - \kappa^*}{1.5 \sigma_i} \approx \frac{\varepsilon_f - \kappa^*}{1.5 \sigma_s(\kappa, T)}. \quad (19)$$

Thus, condition (19) can be considered to be the upper constraint for function ψ in terms of plastic instability. In other words, if the iteration process by ψ in the considered FE at a given loading step yields rising ψ values higher than ψ_{cr} by (19), then it can be assumed that the element is not able to take the load in this step, $\psi \rightarrow \infty$ and $\sigma_{ij} \rightarrow 0$, respectively.

Another variant of loss of performance of this FE is also possible: true maximum principal stresses $\frac{\sigma_1}{1 - 2\rho_l}$ exceed cleavage stresses S_c , that is possible at high deformation strengthening of

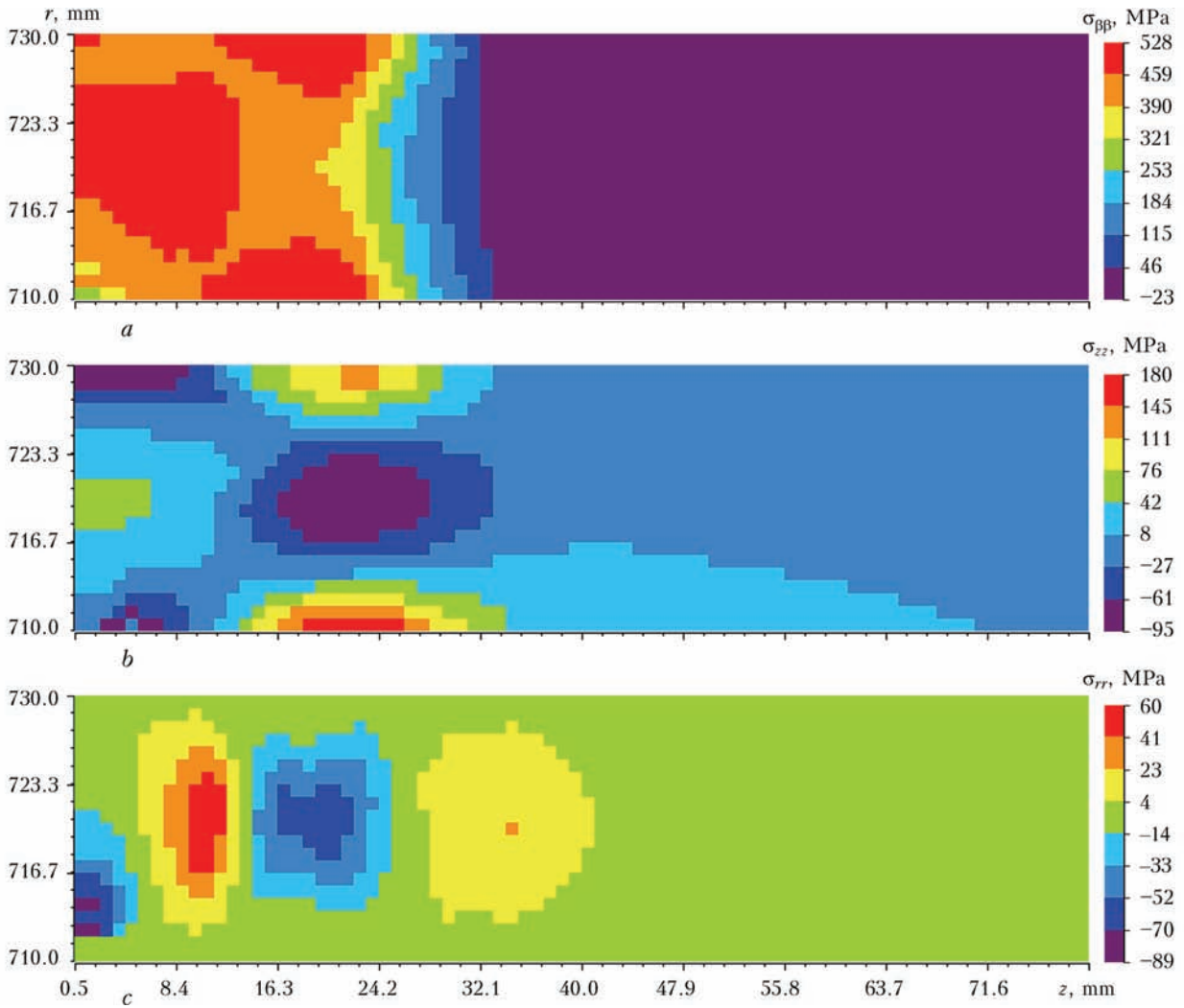


Figure 2. Distribution of residual stresses in the zone of circumferential weld: *a* – circumferential $\sigma_{\beta\beta}$; *b* – longitudinal σ_{zz} ; *c* – radial σ_{rr}

material. In this case, it should be also assumed that at this tracing step and in all the subsequent ones this element cannot take the load, i.e. $\psi \rightarrow \infty$, $\sigma_{ij} \rightarrow 0$.

Eventually, we can define two main conditions, when a given FE irreversibly loses its ability to take the load:

$$\psi > \frac{1}{2G} + \frac{\varepsilon_f - \kappa^*}{1.5\sigma_s(\kappa, T)} \text{ is the plastic instability;}$$

$$\frac{\sigma_1}{1 - 2\rho_l} > S_c \text{ is the cleavage fracture.} \quad (20)$$

If the process of the above «zeroing» to conditions (20) proceeds at this loading step, covering an ever greater number of adjacent FE, and does not allow moving to the next step, then this step determines the limit load of «spontaneous fracture».

Such an approach requires additional knowledge of process parameters:

κ_s, ρ_V^s are the parameters of pore initiation;

ε_f, S_c are the parameters of finite element «zeroing».

For structural steels values S_c are quite well-known [1, etc.]. As regards ε_f , recommendations of [5, 8] can be used, connecting ε_f to rigidity of stressed state σ_m/σ_i by empirical dependencies of type [8]

$$\varepsilon_f = 0.07 + 2.99 \exp(-1.5\sigma_m/\sigma_i) \dots \quad (21)$$

In the absence of experimental data for κ_s and ρ_V^s , $0.005 < \kappa_s < 0.03$ and $0.01 < \rho_V^s < 0.05$ can be approximately taken. Here it should be taken into account that at the stage of developed pore formation (close to limiting state) influence of possible errors of selection of initial κ_s, ρ_V^s values on derived solution decreases markedly.

Given below is a number of examples of application of the above-described approach for pipe $2R \times \delta = 1420 \times 20$ mm from steel X70 loaded by inner pressure.

The following steel properties were assumed: yield limit $\sigma_y = 490$ MPa, Young's modulus $E =$

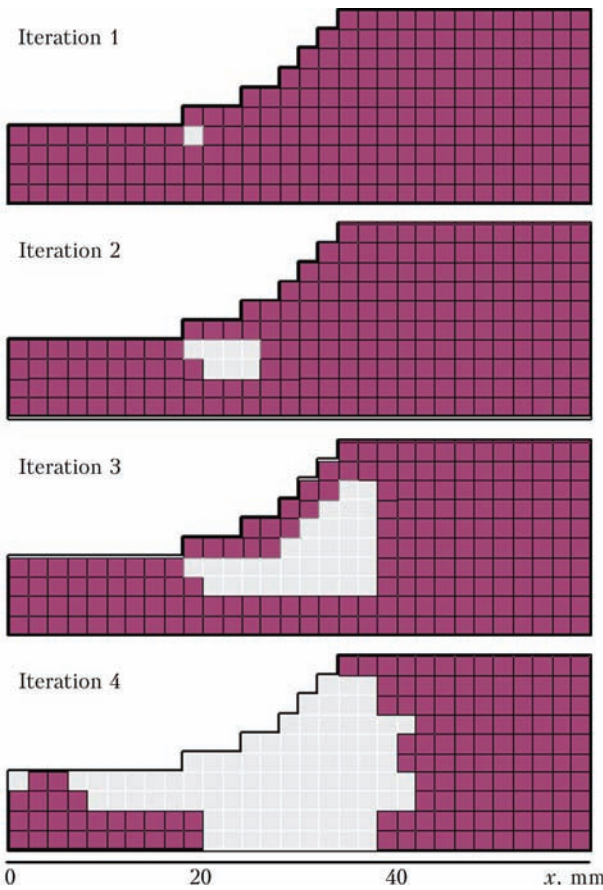


Figure 3. Development of macrofracture by the mechanism of plastic instability in the longitudinal section of surface defect of pipeline element at $P = 17.7$ MPa (finite elements, which have lost their load-carrying capacity, are shown in grey): iteration 1 – macrocrack initiation; 2, 3 – defect development; 4 – violation of pipe wall integrity

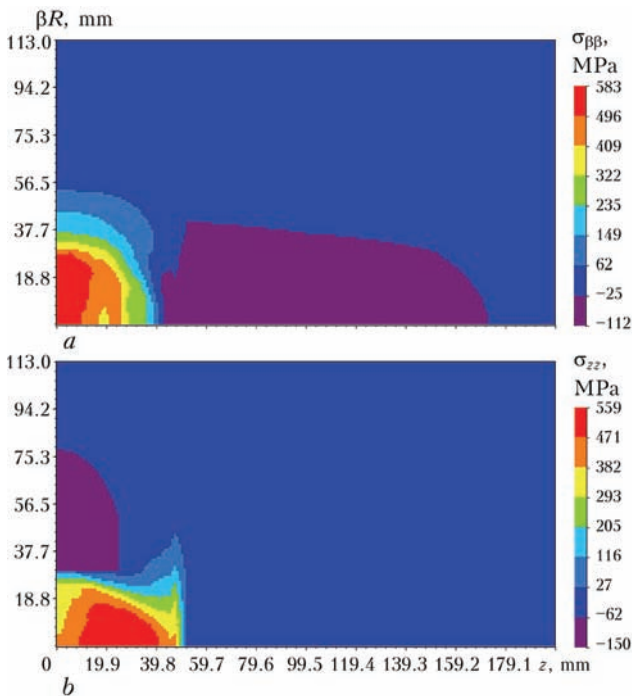


Figure 4. Residual stresses after arc welding up of thinning defect $s \times c \times a = 66 \times 40 \times 14$ mm in $2R \times \delta = 1420 \times 20$ mm pipe from steel X70 on outer surface $r = 70$ mm: a – circumferential $\sigma_{\beta\beta}$; b – longitudinal σ_{zz}

$= 2 \cdot 10^5$ MPa, cleavage stress $S_c = 1000$ MPa, $\sigma_s(\kappa) = \sigma_y + A\kappa^m$, where $A = \sigma_T^{1-m} F^m$ and $m = 0.14$ are the coefficients. Metal microstructure is ferritic-pearlitic.

Case 1. Pipe, geometrically ideal and physically uniform in the initial condition, is loaded by inner pressure P . Stresses $\sigma_{\beta\beta}$, σ_{rr} , σ_{zz} arising in pipe wall are non-uniformly distributed at $P \neq 0$ across wall thickness that causes certain physical inhomogeneity, which is manifested at pore initiation ($\kappa > \kappa_s = 0.01$) and growth, because of different values σ_m/σ_i and fracture mechanisms. However, as shown by our calculations, this non-uniformity is small, therefore, at $P = 19.4$ MPa porosity is found through the entire volume, and at $P = 19.5$ MPa spontaneous fracture both by the mechanism of plastic instability and by microcleavage takes place.

Limit load of $19.4 < P_{lim} < 19.5$ MPa is close to the actual upper limit load for steel X70 in the absence of stress raisers, either geometrical or physical.

Case 2. Conditions are the same, as in Case 1, but pipe metal has residual (initial) balanced stresses σ_{ij}^{res} , shown in Figure 2, i.e. maximum stresses $\sigma_{\beta\beta}$ are on the level of yield limit (490 MPa) that is characteristic, in particular, for stressed state in the vicinity of circumferential site welds.

According to calculations, limiting state corresponds to limit load $19.21 < P_{lim} < 19.22$ MPa, i.e. compared to the previous case lowering on the level of up to 2 % (in absence of raisers and without any essential development of dissipated damage of metal in welding heating area) confirms the known postulate that under static loading of steel structures the influence of residual stresses on the limit load is negligible.

Case 3. Conditions are the same, as in Case 1, but structural inhomogeneity (typical distribution of microstructural components of pipe steel in the area of circumferential site weld: martensite – 0.32–0.35, bainite – 0.67–0.64, ferrite-pearlite – 0.02–0.01 with inhomogeneity width of about 15 mm) and changes of mechanical properties of material of the respective FE, related to this inhomogeneity, are in place [10]. Results of calculation of limit load are indicative of the fact that within microstructural (phase) inhomogeneity, caused by welding temperature cycle, no noticeable changes in the limit static load take place, but fracture mode changes as follows: plastic instability in the volume of structural inhomogeneity and microcleavage in the homogeneous part of the structure that is also in quite good agreement with the experimental data.



This work dealt with quite a number of similar examples of variation of residual (balanced) stress distributions of the type of welding stresses, as well as microstructural changes and their combinations, which, however, do not change the conclusion following from Cases 1–3 that in the absence of geometrical raisers the considered physical inhomogeneity has little influence on limit load at static loading of steel welded structures. Here it should be noted that the factor of the influence of structural transformations and kinetics of stress-strain state of metal in the area of the weld and HAZ in welding on characteristics of pore initiation ($\kappa_s, \varepsilon_f, S_c$) and degree of dissipated damage ρ_V^s requires additional investigations.

Case 4. A typical problem is assessment of the state of structures with geometrical non-uniformity of the type of pipe wall thinning, which in this Case is solved with the same assumptions as in [11], but at greater deformations. Thinning of ellipsoidal shape on the pipe outer surface is described by the following equation in the cylindrical system of coordinates r, β, z :

$$\left(\frac{R-r}{a}\right)^2 + \left(\frac{2\beta r}{c}\right)^2 + \left(\frac{2z}{s}\right)^2 = 1, \quad (22)$$

where a, c, s are the overall dimensions of thinning by wall thickness (a), around the circumference (c), along pipe axis (s); $\beta = 0$ and $z = 0$ in the plane of symmetry.

For the considered pipe at working pressure $P = 7.5$ MPa a case of external surface defect was analyzed. Defect dimensions were $s = 66$ mm, $a = 14$ mm, $c = 40$ mm that is allowable [2]. It should be noted that the above value of operating pressure allows for safety factors typical for the conditions of operation of pipeline elements (2–3). Therefore calculation of limiting state in this case requires detailed modeling of fracture processes in the raiser area. As shown by investigations within the above-described methodology,

limiting state of a pipe with a defect is reached at the pressure of 17.7 MPa by the mechanism of plastic instability. Nature of spontaneous fracture in the area of geometrical anomaly is determined by the order, in which FE lose their ability to take the load according to (20). Proceeding from the results of calculations (Figure 3), fracture initiates on the periphery of a surface defect and develops in its longitudinal section under the impact of circumferential stresses in the pipe wall.

Case 5. One of the technological processes of restoration of load-carrying capacity of pipes with detected defects of local thinning type is surfacing by welding [12]. In this case operational loss of pipe wall metal is compensated by deposited metal and overall dimensions of the structure are restored to normative values. Here residual welding stresses develop in the area of repaired defect, the influence of which on load-carrying capacity of the pipe requires additional investigations. In particular, developed procedure of evaluation of limiting state of structures by tough fracture mechanism allows determination of limit pressure preceding spontaneous development of macrofractures in the region of local non-uniformity of the stressed state. Figure 4 gives the results of calculation of characteristic residual stresses in the field of welding up a defect of ellipsoidal shape, parameters of which are given in Case 4. These data illustrate high local stresses, reaching the yield limit of the considered steel. Here limit pressure, at which plastic instability of such a pipe develops, is equal to $P = 19.4$ MPa by the results of computational investigation that, alongside the conclusions of Case 3 on insignificant influence of structural inhomogeneities on the kinetics of initiation and development of tough fracture pores, confirms the effectiveness of defect repair by surfacing in terms of safe residual operating life of a pipeline element.

Results of calculation of limit loads of pipeline elements ($2R \times \delta = 1420 \times 20$ mm) under the impact of inner pressure depending on structure initial state

Initial structure state	Fracture pressure, MPa	Fracture mode
Uniform structure	19.5	Microcleavage
Presence of local residual stresses characteristic for site circumferential welds	19.2	Microcleavage
Structural inhomogeneity of welds	19.5	Plastic instability in structural inhomogeneity zone, microcleavage in the uniform part
Geometrical inhomogeneity of the type of semielliptical wall thinning	17.7	Plastic instability in defect peripheral part
Presence of local residual stresses induced by repair welding	19.4	Plastic instability in residual stress area



The Table gives comparative results of calculation of limiting state (Cases 1–5), which lead to the general conclusion that the influence of characteristic welding processes (site or repair welding) on pipeline element metal (structural transformations, residual stress-strain state) in terms of the magnitude of limit operating load is insignificant by tough fracture criteria.

Conclusions

1. Numerical procedure of investigation of processes of tough fracture of structures under external load impact was developed. For this purpose a model of pore initiation and development was constructed on the basis of finite element analysis of complex stress-strain state of structural elements at developed flow of material. Pores leads to lowering of structure load-carrying capacity, and as a result — to its spontaneous fracture. Proposed approach allows tracing of the kinetics of structure state right up to limiting state.

2. Typical cases of loading pipeline element by inner pressure are considered. It is shown that the influence of structural inhomogeneity of pipe steel, as well as initial stress-strain state induced, in particular, by site welding, on the limiting load that can be taken by such a structure is insignificant.

3. Limiting states were studied according to tough fracture mechanism of pipeline section with an external ellipsoidal defect of the type of local wall thinning, in particular, after repair by surfacing. It is shown that in terms of development of tough fracture such a kind of repair does

not lower the load-carrying capacity of the restored structural element, despite the high residual stresses in the repaired defect area.

1. Makhnenko, V.I. (2006) *Resource of safe service of welded joints and assemblies of current structures*. Kiev: Naukova Dumka.
2. (2000) *Fitness-for-service*. American Petroleum Institute Recommended Practice 579. 1st ed.
3. Savruk, M.P. (1988) *Fracture mechanics and strength of materials*: Refer. Book. Vol. 2: Stress intensity factors in bodies with cracks. Ed. by V.V. Panasyuk. Kiev: Naukova Dumka.
4. Kurkin, S.A., Lukianov, V.F. (1967) On strength of welded vessels of high strength steels. *Svarochn. Proizvodstvo*, **9**, 1–3.
5. Karzov, G.P., Margolin, B.Z., Shvetsova, V.A. (1993) *Physico-mechanical modeling of fracture processes*. St.-Petersburg: Politekhnik.
6. McClinton, F., Argon, A. (1970) *Deformation and fracture of materials*. Moscow: Mir.
7. Rybin, V.V. (1986) *Large plastic deformations and fracture of metals*. Moscow: Metallurgiya.
8. Hancock, I., Mackenzie, A.C. (1976) On the mechanism of ductile failure a high strength steel subjected in multi-axial stress state. *J. Mech. Phys. Solids*, **24(213)**, 147–149.
9. Makhnenko, V.I. (1976) *Computational methods of investigation of welding stress and strain kinetics*. Kiev: Naukova Dumka.
10. Makhnenko, V.I., Velikoivanenko, E.A., Makhnenko, O.V. et al. (2000) Investigation of the influence of phase transformations on residual stresses in circumferential welding of pipes. *The Paton Welding J.*, **5**, 2–7.
11. Makhnenko, V.I., Velikoivanenko, E.A., Rozyuka, G.F. et al. (2012) Consideration of pore formation at estimation of limiting state in zone of pressure vessel wall thinning defect. *Ibid.*, **12**, 2–8.
12. Kiefner, J.F., Bruce, W.A., Stephens, D.R. (1994) *Pipeline repair manual*. Houston: Technical Toolboxes.

Received 19.02.2013



ON PLANNING OF REPAIR OF PRESSURISED MAIN PIPELINES BASED ON THE RESULTS OF IN-PIPE DIAGNOSTICS*

A.S. MILENIN

E.O. Paton Electric Welding Institute, NASU
11 Bozhenko Str., 03680, Kiev, Ukraine. E-mail: office@paton.kiev.ua

The world and national practice of operation of land main pipelines shows the trend to utilisation of different methods to repair them by welding without any interruption of transportation of a product. Planning of a certain repair method, which is an important stage of ensuring the efficiency and safety of restoration of a carrying capacity of defective regions in main pipelines, requires development of appropriate methodological principles for analysis of damage of a structure, estimation of admissibility of operation and prediction of remaining life. This study suggests a multilevel procedure for numeric analysis of results of in-pipe diagnostics of the state of linear parts of main pipelines, allowing for the specific character of repairing them without removal from service, and permitting optimisation of repair-and-renewal operations in lengthy regions of a pipeline on the basis of numeric ranking of defects of a different nature. It is suggested using different levels of ranking depending on the available data of technical diagnostics of the state of a specific linear region of a main pipeline: based on subdivision of all defects into admissibility groups by estimating the remaining safety factor in a region of a specific defect, or by calculating the probability of violation of integrity of a pipeline wall. A differing degree of conservatism of the suggested procedure depending on the completeness of the source data makes it possible to analyse the results of in-pipe diagnostics at the required accuracy and effectively plan removal of the detected defects by the methods of repair of pipelines without withdrawing them from service. 12 Ref., 10 Tables, 5 Figures.

Keywords: *main pipeline, repair without removing from service, in-pipe diagnostics, defect, planning, ranking*

Application of different methods for repair of main pipelines (MP) without removing them from service is one of the modern approaches to maintaining their serviceability. An interest in such technologies is caused, first of all, by economic benefits and an insignificant negative impact on the environment. In addition, this allows a long-term planning of local repair operations, which makes it possible to continuously maintain the safe operation of a pipeline at the required level [1–3].

Performing repair operations in active MP is associated with the following characteristic technological and methodological problems [4]:

- planning of local repair operations in lengthy regions of MP with a different degree of service damage in terms of minimisation of the risk of emergency situations;

- selection of repair parameters from the standpoints of ensuring safety of the repair operations performed on a pipeline under internal pressure;

- ensuring serviceability of regions of MP, the carrying capacity of which was restored by the repair methods without removal from service.

These problems should be solved in an integrated manner by including both development of new methodological principles of planning and optimisation of repair parameters, and implementation of science-intensive technologies for repair of defective regions of pressurised MP. Modern regulatory documents and practical recommendations are oriented primarily to overhaul of defective land MP, which does not allow taking into account the specific character of repair under pressure and effectively planning the repair-and-renewal operations, in particular, on the basis of results of in-pipe diagnostics (IPD) of the state of linear regions of MP. Such specific features include the problems of ranking of the defects detected during the IPD process, allowance for the natural spread of the available data on sizes and positions of defects and actual properties of metal of a pipeline, and selection of a repair method based on the maximal service life of a repaired structure. To allow for the characteristic

* The article is based on the paper presented at the 6th International Conference «Mathematical Modelling and Information Technologies in Welding and Related Processes» (29 May–1 June 2012, Katsiveli, Ukraine).

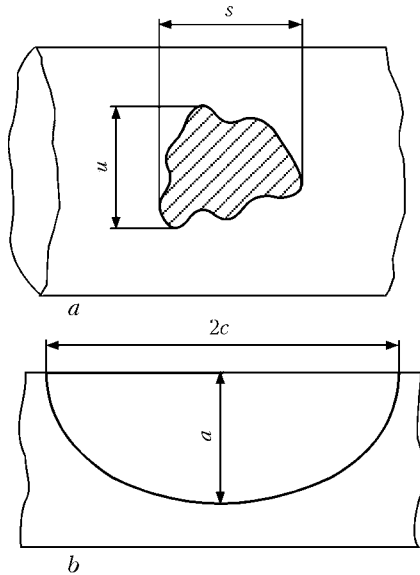


Figure 1. Schematic of defects of the type of local corrosion metal losses (a) and crack-like defects (b)

peculiarities of planning of the repair-and-renewal operations on MP without removing them from service, the E.O. Paton Electric Welding Institute of the NAS of Ukraine developed a multilevel procedure for ranking of the defects detected in technical diagnostics.

The main defects in MP are defects of the type of metal discontinuity of a corrosion or stress-corrosion nature (local and general loss of metal, stress-corrosion cracks), defects in welds (lacks of penetration, pores), and shape defects (dents) [5]. Their admissibility is specified by different national and industry standards, as well as codes based on deterministic criterion relationships. In this case, different safety and reliability factors [6–8] are used to allow for stochastic deviations of source data from the known values, this being a maximum conservative approach. For example, the limiting state of a MP region containing a defect of the corrosion thinning type (Figure 1, a) can be estimated on the basis of the deterministic criterion [9]

$$Y = t_{\min} - W\Delta t - t_p R_t, \quad (1)$$

where t_{\min} is the minimal residual thickness of the MP wall; t_p is the minimal admissible thickness of the MP wall determined either by design-service requirements to MP in a region under consideration, or by additional calculations; Δt is the time period under consideration; W is the uniform corrosion rate (conservatively, can be assumed to be equal to 1 mm/year); R_t is the shape function of the thinning defect determined as follows (see Figure 2, a):

$$R_t = \begin{cases} 0.2 \text{ at } \lambda = \frac{1.285s}{\sqrt{Dt_p}} \leq 0.3475, \\ \left(0.9 - \frac{0.9}{\sqrt{1.0 + 0.48\lambda^2}}\right) \left(1.0 - \frac{0.9}{\sqrt{1.0 + 0.48\lambda^2}}\right)^{-1} \\ \text{at } \lambda > 0.3475, \end{cases} \quad (2)$$

where D is the inner diameter of a pipe.

Term $Y > 0$ guarantees integrity of the defective region of MP under the considered conditions.

The most common deterministic criterion of admissibility of a crack-like defect (Figure 1, b) is the two-parameter criterion of brittle-tough fracture (Figure 2, b) having the following expression [10]:

$$Y = f(L_r) - K_r, \quad (3)$$

where

$$f(L_r) = \begin{cases} (1 - 0.14L_r^2)[0.3 + 0.7 \exp(-0.65L_r^6)] \\ \text{at } L_r \leq L_r^{\max} = \frac{\sigma_t + \sigma_y}{2\sigma_y}, \\ 0 \text{ at } L_r > L_r^{\max}; \end{cases} \quad (4)$$

$$K_r = \frac{K_I}{K_{IC}}; \quad L_r = \frac{\sigma_{\text{ref}}}{\sigma_y};$$

K_I is the stress intensity factor at a given point of contour of the surface semi-elliptical crack; and σ_{ref} is the reference stress in a defect region,

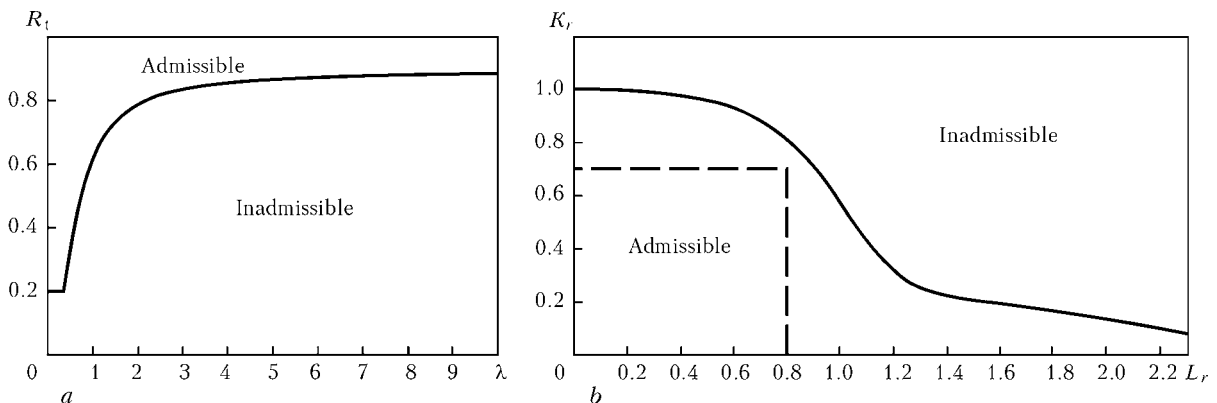


Figure 2. Criterion diagrams of admissibility of defects of the type of local corrosion metal losses (a) and crack-like defects (b)



Table 1. Selection of method for repair of defective regions in MP depending on the degree of development of damage [8]

Nature of defect and parameter	Repair method
Corrosion-mechanical damages:	Grinding
external $a \leq 0.2t$	Mounting of reinforcing structure
external $0.2t < a \leq 0.5t$	Same
external $0.5t < a \leq 0.8t$	»
external $a > 0.2t$; $t_{\min} \geq 5 \text{ mm}$	»
external $s \leq 100 \text{ mm}$ or group of closely located pits $a > 0.4t$	»
defects extending in circumferential direction $a > 0.2t$; $s \geq 1/6\pi D$	»
in zone of circumferential welds $a > 0.4t$	»
internal $a > 0.2t$	»
Cracks:	»
external $a < 0.2t$; $2c \leq 2\sqrt{Dt}$	Grinding

whose calculation procedure is described, in particular, in study [11].

Therefore, term $Y > 0$ is sufficient for the guaranteed admissibility of the defects under consideration.

In analysis of admissibility of the crack-like defect, after a certain period of time Δt it is necessary to make allowance for the probability of growth of the crack, namely:

$$\begin{cases} a(\Delta t) = a_0 + V_a \Delta t, \\ c(\Delta t) = c_0 + V_c \Delta t, \end{cases} \quad (5)$$

where a_0 and c_0 are the initial sizes of the crack; V_a and V_c are the rates of growth of the crack along the respective size, which can be estimated as follows:

$$V_{a, c}(K_I) = \begin{cases} V_{\max} & \text{if } K_I \geq K_{ISCC} \\ 0 & \text{if } K_I < K_{ISCC} \end{cases} \quad (6)$$

where V_{\max} is the maximal rate of growth of the crack determined from the diagram of static corrosion resistance of a material under given conditions.

It should be noted that, compared to the mentioned deterministic approaches, the use of the probability procedures to analyse the state of defective regions in MP allows correctly describing the probable spread of values of the source data based both on the existing experience in investigations of defective pipeline systems and on the technological characteristics of the applied equipment and specifics of the analysis.

The main methods for repair of pressurised MP are controlled grinding of surface defects, welding-up of the surface defects, and mounting of reinforcing structures (sleeves, bands) [12]. The choice of the repair technology is based on the degree of damage of a pipeline, as well as on

the efficiency of each specific method. Approaches specified in the actual regulatory documents [8] (Table 1), in particular, can be conservatively used for this purpose. To reduce conservatism of selection of a repair method, it is possible to model the repair process at specific technological parameters, and, on the basis of corresponding safety criteria, efficiency requirements and sufficient service life of the repaired region, to conclude on the possibility of using this or other method by restoring the carrying capacity of a defective structure.

As proved by practice, the quantity of geometric anomalies detected by IPD using flaw detectors may amount to several thousands (Figure 3). The order of their repair based on the existing deterministic regulations, which subdivide defects into certain groups by the degree of danger (up to four), may be ambiguous in a case of a large quantity of defects, because of the necessity to rank geometric anomalies within one group. Therefore, when planning repair of MP without its removal from service it is reasonable

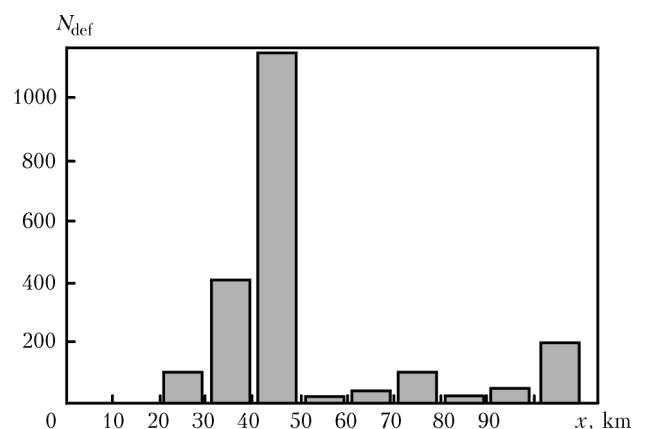


Figure 3. Diagram of distribution of the quantity of metal loss defects N_{def} according to the data of IPD of part of the «Urengoy-Centre 2» main gas pipeline



to use continuous ranking. Within the framework of the developed procedure, it is suggested using the following levels of estimation of the order of removing defects depending on the completeness of the available data and required conservatism:

- *level 1.* Subdivision of all defects into four groups as to their admissibility degree: insignificant, moderate, significant and critical;
- *level 2.* Estimation of the safety factor for the MP region containing a detected specific defect;
- *level 3.* Calculation of the probability of fracture of the pipeline wall within the zone of the considered defect.

According to ranking level 1, all the defects detected by IPD of a linear part of MP are subdivided into four groups by the degree of admissibility, according to National Standard DSTU-N BV.2.3-21:2008. In this case the priority of repair is determined by belonging to a group of the most dangerous defects. This approach is applied if all moderate defects can be technically removed in a period of up to six months, and significant defects – in a period of up to two months. The presence of critical defects provides for changing service conditions of a pipeline up to its complete shutoff. The determining parameter is safety factor n , which is calculated on the basis of the criterion of admissibility of the state of a region containing the certain type of a defect.

The safety factor for a 3D defect of the type of a local corrosion loss of metal is estimated on the basis of a modified diagram of the limiting state of a region (Figure 4, *a*), where function R_τ determined by normalising of function R_t has the following form:

$$R_\tau = \frac{1}{3.87R_t} - 0.292. \tag{7}$$

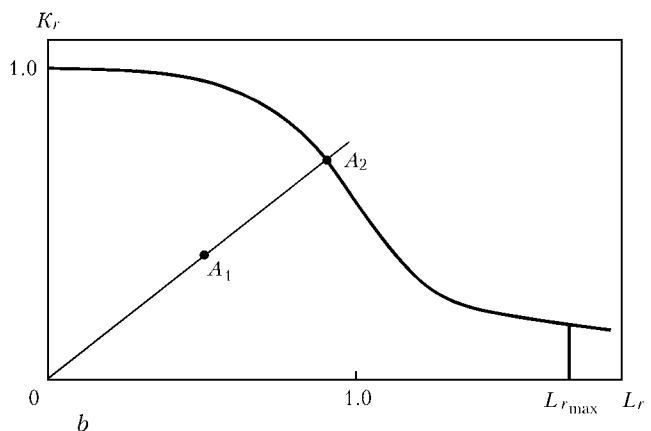
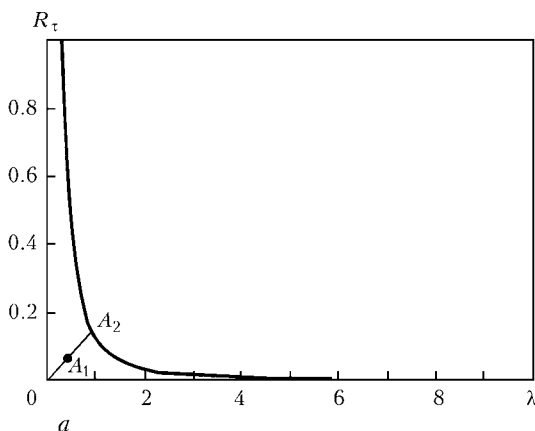


Figure 4. Determination of the value of safety factor for a part of MP with a defect of the type of local corrosion loss of metal (*a*) and crack-like defect (*b*)

If the state of a defect is described by position A_1 in the diagram, the safety factor is determined by relationship

$$n = \frac{OA_1}{OA_2}. \tag{8}$$

The length of segment OA_2 is determined either graphically or by numeric solution of the following equation with respect to coordinate λ of point A_2 :

$$\frac{R_\tau^{A_1}}{\lambda^{A_1}} - R_\tau(\lambda) = 0. \tag{9}$$

Safety factor for the crack-like defect is determined similarly to the above approach for the local corrosion loss of metal, but the limiting state curve in this case is a two-parameter diagram of admissibility of cracks (Figure 4, *b*). The safety factor is estimated by relationship of lengths of the segments according to formula (8). The length of segment OA_2 is determined either graphically or by numeric solution of the following equation with respect to coordinate L_r of point A_2 :

$$\frac{K_r^{A_1}}{L_r^{A_1}} - K_r(L_r) = 0. \tag{10}$$

For the MP defects of a different degree of admissibility the ranges of the values of safety factor n are as follows [6]:

- $n > k$ – insignificant;
- $1.1\sigma_t/\sigma_y \leq n < k$ – moderate;
- $1.1 \leq n < 1.1\sigma_t/\sigma_y$ – significant;
- $n < 1.1$ – critical,

where $k = 0.9k_1k_{app}/m$; m is the service factor of a pipeline; k_1 is the material reliability factor; k_{app} is the reliability factor of the pipeline for its application.



The first stage of ranking level 2 repeats level 1, according to which all the defects are subdivided into four groups by the degree of their admissibility at the time of their diagnostics. All the defects ranked as insignificant, moderate or significant are subject to planning of repair. Ranking within these groups is performed on the basis of the value of the calculated safety factor allowing for a natural growth of defects by using the corresponding procedures. Consideration of repair of critical defects is based on a certain change in service parameters of the defective region of MP (decrease of internal pressure) and transfer of a defect to a rank of significant or moderate. The priority of removal of each isolated (united) defect is based on minimisation of the determined values of the safety factor under specific service conditions: the lower the safety factor of the defective region, the higher is the priority of its repair.

Ranking level 3 is least conservative and makes it possible to allow for a natural spread of the source data in order to more accurately determine the order of removal of defects, which may change the admissibility degree within the considered period, as well as in a case of the insufficient information on geometric and service parameters of the defective region and/or mechanical characteristics of a pipeline material. In this case the ranking parameter is the probability of an emergency situation in the defective region under real service conditions, which is calculated by the Monte-Carlo method using the following algorithm:

- proceeding from the known densities of distribution of the source data, representative sampling of their specific values is found within the known variation ranges; it is assumed in this case that the probability of characteristic of a defect is random and varies from 0 to 1. Note that the representative sampling implies quantity N_s of equally probable combinations, which is sufficient for a stable value of the probability of fracture of a specific defect according to the chosen limiting state criterion;
- based on the deterministic criteria of fracture, the admissibility of a detected defect is determined for each set of geometric and service characteristics out of the representative sampling;
- calculation of the quantity of inadmissible states of a pipeline with specific defect N_i is made within the representative sampling. Therefore, the probability of the emergency situation, P_i , in a region of the isolated or plural defect implies relationship $P_i = N_i / N_s$;

- if necessary, the total probability of the emergency situation, $P_\Sigma = 1 - \Pi(1 - P_i)$, in a MP region with independent defects is determined to reveal the priority repair region.

Allowance for a stochastic deviation of values of different source data is described by using a truncated normal distribution (geometric sizes of a defect, strength properties of a pipeline material, corrosion rate) and Weibull distribution (crack resistance characteristics of a material). The order of repair at each time moment after diagnostics of the state of a linear MP region is determined by probability P_i : the higher the probability of the emergency situation, the higher is the repair priority.

The given methodology of analysis of the data base on the defects detected in IPD of the MP state was implemented in the form of a graphical user software package. Ranking of model defects in terms of the order of repair under pressure was performed as an example of its application (Table 2). Geometric and service parameters of the investigated linear part of MP are as follows:

Segment length L , m	2000
Internal diameter D , mm	1420
Wall thickness t , mm	20
Minimal admissible wall thickness t_{min} , mm	16
Pipeline material, steel 17G1S, MPa	$\sigma_y = 360$ $\sigma_t = 510$
Pressure at investigated region inlet P_{max} , MPa	7.5
Pressure at investigated region outlet P_{min} , MPa	6.5
Corrosion rate, mm/year, in region of:	
0–800 m	0.2
800–1400 m	0.4
1000–2000 m	(conservatively assumed value is 1)
There are no regular loads caused by imperfection of geometry of the considered region	

The results of calculation of the ranking parameters according to the suggested procedure for the model defects allowing for their development during further operation of MP at different time moments are given in Tables 3–6, respectively, and the priority of repair of each of the defective regions of MP according to different ranking levels is given in Table 7. It should be noted that the method of repair of a specific MP region determined according to Table 1 can be changed during development of a defect, and limiting values of the sizes within the specific repair method can serve as a reference for determination of the terms of repair from the standpoint of minimisation of costs and labour intensity of repair, whereas the ranking parameters make it possible to determine only the sequence of removal of defects.

It can be seen from distribution of the total probability of defects on a 10 m repair base determined according to level 3 and shown in Figure 5 that removal of all defects in the two,



Table 2. Parameters of model defects in linear part of MP

Defect No.	Type of defect	Position of defect		Size of defect, mm			Internal pressure in defect region of MP, MPa
		In length, m	In circumference, deg	Axial	Tangential	Radial	
1	Thinning	150	30	160	17	4.7	7.4
2		230	0	200	20	7	7.4
3		680	120	60	8	5	7.2
4		681	60	100	10	15	7.2
5		800	40	120	11	14.7	7.1
6		1150	90	80	15	8	6.9
7		1200	80	25	7	10	6.9
8		1200	10	35	5	13	6.9
9		1200	120	170	13	6	6.9
10		1370	0	95	11	15	6.8
11		1560	140	150	18	6	6.7
12		1710	30	50	26	9	6.7
13		1750	90	75	16	8	6.6
14		1780	0	45	8	8	6.5
15	Longitudinal crack	530	50	25	–	2	7.2
16		710	110	15	–	2	7.2
17		750	30	10	–	3	7.1
18		1100	70	6	–	1	7.0
19		1520	20	20	–	2	6.7

Table 3. Parameters of ranking of model defects and repair method at the time moment of diagnostics of MP

Defect No.	Admissibility group	Safety factor	Probability of fracture	Repair method
1	Insignificant	1.648299	0.011	Grinding
2	Critical	0.885463	0.4	Welding-up
3	Insignificant	2.933383	0	Grinding
4	Critical	0.666297	0.983	Welding-up
5	Same	0.603503	0.621	Same
6	Significant	1.523807	0.035	»
7	Insignificant	2.610481	0	Grinding
8	Same	1.618357	0.0777	Same
9	Significant	1.340008	0.198	Welding-up
10	Critical	0.694965	0.969	Same
11	Insignificant	1.626517	0.125	Grinding
12	Same	1.893557	0.003	Same
13	»	1.686921	0.0255	»
14	»	2.391991	0	»
15	Significant	1.534515	0.06273	Welding-up
16	Insignificant	1.540512	0.04391	Grinding
17	Significant	1.463110	0.116	Welding-up
18	Insignificant	1.730804	0.005535	Grinding
19	Same	1.651180	0.0246	Same



Table 4. Parameters of ranking of model defects and repair method after 1 year in service

Defect No.	Admissibility group	Safety factor	Probability of fracture	Repair method
1	Insignificant	1.552745	0.02	Grinding
2	Critical	0.859123	0.43	Welding-up
3	Insignificant	2.756573	0	Grinding
4	Critical	0.652421	0.992	Mounting of sealing sleeve
5	Same	0.592111	0.646	Welding-up
6	Significant	1.439648	0.0695	Same
7	Insignificant	2.511972	0	Grinding
8	Same	1.547994	0.0837	Same
9	Significant	1.224116	0.25	Welding-up
10	Critical	0.669225	0.985	Grinding
11	Significant	1.254279	0.273	Welding-up
12	Insignificant	1.699346	0.028	Grinding
13	Significant	1.478064	0.0857	Welding-up
14	Insignificant	2.073059	0.00125	Grinding
15	Significant	1.364442	0.3641	Welding-up
16	Same	1.356944	0.22386	Same
17	»	1.291293	0.2952	»
18	»	1.484581	0.09594	»
19	»	1.453562	0.18819	»

Table 5. Parameters of ranking of model defects and repair method after 2 years in service

Defect No.	Admissibility group	Safety factor	Probability of fracture	Repair method
1	Significant	1.465154	0.0365	Welding-up
2	Critical	0.839193	0.457	Same
3	Insignificant	2.622561	0	Grinding
4	Critical	0.638599	0.992	Mounting of sealing sleeve
5	Same	0.580757	0.672	Welding-up
6	Significant	1.371563	0.0963	Same
7	Insignificant	2.413463	0	Grinding
8	Significant	1.477631	0.162	Welding-up
9	Same	1.129953	0.309	Same
10	Critical	0.630616	0.995	Mounting of sealing sleeve
11	Same	1.060068	0.429	Welding-up
12	Significant	1.529412	0.608	Same
13	Same	1.317405	0.182	»
14	Insignificant	1.860438	0.0085	Grinding
15	Significant	1.180542	0.7651	Welding-up
16	Same	1.285151	0.51537	Same
17	Critical	1.091123	0.7515	»
18	Significant	1.310414	0.30134	»
19	Same	1.256049	0.37066	»



Table 6. Parameters of ranking of model defects and repair method after 3 years in service

Defect No.	Admissibility group	Safety factor	Probability of fracture	Repair method
1	Significant	1.393489	0.0632	Welding-up
2	Critical	0.819303	0.486	Same
3	Insignificant	2.489434	0	Grinding
4	Critical	0.624833	0.997	Mounting of sealing sleeve
5	Same	0.569441	0.689	Same
6	Significant	1.319313	0.145	Welding-up
7	Insignificant	2.364209	0.0005	Grinding
8	Significant	1.442449	0.234	Welding-up
9	Critical	1.05752	0.351	Same
10	Same	0.604877	0.997	Mounting of sealing sleeve
11	»	0.930594	0.564	Welding-up
12	Significant	1.40803	0.137	Same
13	Same	1.188877	0.308	»
14	Insignificant	1.674394	0.0415	Grinding
15	Critical	0.9414836	1	Welding-up
16	Significant	1.224571	0.96801	Same
17	Critical	0.834522	1	»
18	Significant	1.107456	0.69741	»
19	Critical	1.014003	0.92865	»

Table 7. Priority of removal of model defects according to different ranking levels

Defect No.	At the time of diagnostics			After 1 year in service			After 2 years in service			After 3 years in service			Type of defect
	Level 1	Level 2	Level 3	Level 1	Level 2	Level 3	Level 1	Level 2	Level 3	Level 1	Level 2	Level 3	
1	3	12	14	3	15	16	2	14	16	1	14	16	Thinning
2	1	4	4	1	4	4	1	4	8	1	4	10	
3	3	19	19	3	19	19	3	19	19	3	19	19	
4	1	2	1	1	2	1	1	3	2	1	3	4	
5	1	1	3	1	1	3	1	1	5	1	1	8	
6	2	7	11	2	10	14	2	13	15	1	13	14	
7	3	18	18	3	18	18	3	18	18	2	18	18	
8	3	10	8	3	14	13	2	15	14	3	16	13	
9	2	5	5	2	5	8	1	7	11	1	9	11	
10	1	3	2	1	3	2	1	2	1	1	2	3	
11	3	11	6	2	6	7	1	5	9	1	6	9	
12	3	16	16	3	16	15	2	16	6	2	15	15	
13	3	14	12	2	12	12	2	12	13	2	11	12	
14	3	17	17	3	17	17	3	17	17	3	17	17	
15	2	8	9	2	9	5	2	8	3	1	7	2	Cracks
16	3	9	10	2	8	9	2	10	7	2	12	5	
17	2	6	7	2	7	6	1	6	4	1	5	1	
18	3	15	15	2	13	11	2	11	12	2	10	7	
19	3	13	13	2	11	10	2	9	10	1	8	6	



Table 8. Characteristics of defects of the type of local thinning in a region of «Urengoy-Centre 2» gas pipeline

Defect No.	s, mm	u, mm	t_{min} , mm	Position in length of defect, m
1	330	200	16.0	2
2	210	200	16.8	250
3	350	350	15.7	450
4	400	350	15.1	600
5	380	460	15.5	900

Table 9. Characteristics of crack-like defects in a region of «Urengoy-Centre 2» gas pipeline

Defect No.	Crack	c, mm	a, mm	Position in length of defect, m
6	Longitudinal	110	1.60	10
7	Same	90	1.60	400
8	Circumferential	75	1.50	710
9	Same	150	1.55	820
10	Longitudinal	100	1.55	1000

Table 10. Probability of emergency situation with detected defects in «Urengoy-Centre 2» gas pipeline

Defect No.	Time of service, years				
	0	0.5	1.0	1.5	2.0
1	0 (8)	0.00025 (10)	0.0055 (9)	0.052 (9)	0.179 (9)
2	0 (8)	0 (12)	0.0015 (11)	0.0142 (10)	0.063 (10)
3	0 (8)	0.00125 (9)	0.026 (8)	0.131 (8)	0.338 (7)
4	0.0041 (5)	0.0562 (3)	0.240 (4)	0.490 (4)	0.758 (4)
5	0 (8)	0.007 (7)	0.0715 (7)	0.263 (7)	0.494 (7)
6	0.013 (1)	0.139 (1)	0.436 (1)	0.796 (1)	0.979 (1)
7	0.005 (2)	0.0962 (2)	0.269 (2)	0.600 (3)	0.864 (3)
8	0.001 (6)	0.0353 (6)	0.0612 (5)	0.462 (5)	0.720 (5)
9	0.004 (3)	0.054 (4)	0.251 (3)	0.317 (2)	0.9369 (2)
10	0.002 (5)	0.0412 (5)	0.177 (6)	0.419 (6)	0.715 (6)
11	0.005 (2)	0.005 (8)	0.005 (10)	0.005 (11)	0.005 (11)
12	0.001 (7)	0.001 (11)	0.001 (12)	0.001 (12)	0.001 (12)

Note. Priority of repair is indicated in brackets.

most dangerous regions (shown in grey) substantially decreases the accident rate of MP.

Conclusions

1. The numeric approach to ranking of defects detected in IPD is suggested within the framework of development of the integrated procedure for planning of repair of MP without its removal from operation. The approach is based on multi-level analysis of the degree of damage of a pipeline in a specific region depending on the completeness of the available data on the actual state of a structure and specification requirements to its carrying capacity.

2. Differing conservatism of the developed procedure makes it possible to take into account, if necessary, specific features of the methods used for diagnostics of the state of linear parts of MP and characteristic peculiarities of their repair under pressure. In particular, the use of the probability estimation of admissibility of the detected

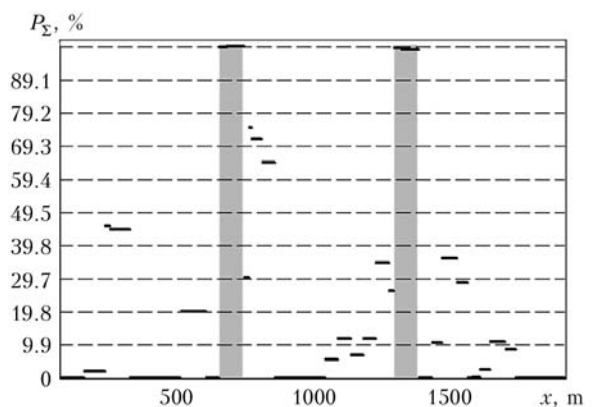


Figure 5. Distribution of total probability of emergency situation in a 10 m base region of bore pit in length of the investigated MP region

defects suggests analysis of the natural spread of data on properties of the pipeline metal and defect parameters.

3. The limits of applicability of the developed procedure and specifics of the predicted devel-



opment of damage in terms of subsequent removal of defects by the methods of repair under pressure are shown by an example of a model problem of ranking of inadmissible defects of the type of local corrosion loss of metal and surface cracks, and on the basis of numeric analysis of the results of diagnostics of the state of the «Urengoy-Centre 2» gas pipeline region (Tables 8–10).

1. Bjornoy, O.H., Marley, M.J. (2001) Assessment of corroded pipelines: past, present and future. In: *Proc. of 11th Int. Offshore and Polar Engineering Conf.* (Stavanger, Norway, June 17–22, 2001), **1**, 93–101.
2. Makhnenko, V.I., Velikoivanenko, E.A., Olejnik, O.I. (2008) Risk analysis as a method for formalizing decision making on unscheduled repair of welded structures. *The Paton Welding J.*, **5**, 2–7.
3. LaMorte, C.R., Boring, M., Porter, N. (2007) *Advanced welding repair and remediation methods for in-service pipelines*: Final report. Columbus: EWI.
4. Makhnenko, V.I., Milenin, A.S. (2009) To the problem of repair of land main pipelines without their decommissioning. In: *Proc. of Sci.-Techn. Seminar on Assurance of Service Reliability of Pipeline Transport Systems* (Kiev, 10–11 June, 2009). Kiev: PWI, 12–18.
5. Aliev, R.A., Belousov, V.D., Nemudrov, A.G. et al. (1988) *Oil and gas pipeline transport*. Moscow: Nedra.
6. *DSTU-N BV.2.3-21:2008*: Directive. Definition of residual strength of main pipelines with defects. Kyiv: Minregionbud Ukrainy.
7. *SNiP 2.05.06–85*: Main pipelines. Construction codes and regulations. Moscow: VNIIST Minneftegazstroj.
8. *VBN V.3.1.-00013471-07:2007*: Main oil pipelines. Methods of repair of defective zones. Kyiv: Ministry of fuel and energy of Ukraine.
9. (2000) *Fitness-for-service*: American Petroleum Institute Recommended practice 579. Washington: API Publ. and Distr.
10. *BS 7910:2005*: British standard. Guide to methods for assessing the acceptability of flaws in metallic structures. London: BSI.
11. Makhnenko, V.I. (2006) *Safe service life of welded joints and assemblies of current structures*. Kiev: Naukova Dumka.
12. Kiefner, J.F., Bruce, W.A., Stephens, D.R. (1994) *Pipeline repair manual*. Houston: Technical Toolboxes.

Received 19.02.2013



PROPERTIES OF THE WELD METAL OF TWO-SIDED WELDED JOINTS ON PIPES MADE FROM INCREASED-STRENGTH MICROALLOYED STEELS

A.A. RYBAKOV, S.E. SEMYONOV and T.N. FILIPCHUK

E.O. Paton Electric Welding Institute, NASU

11 Bozhenko Str., 03680, Kiev, Ukraine. E-mail: office@paton.kiev.ua

Two-pass two-sided welding is widely applied to manufacture large-diameter pipes for main gas and oil pipelines. It is obvious that metal of the welds that are the first to make is subjected to repeated heating in making the subsequent pass. The study is dedicated to evaluation of the effect of repeated heating on properties of the weld metal of the two-sided welded joints on pipes made from increased-strength microalloyed steels. Investigations were carried out on the weld metal of welded joints on the pipes made from ferritic-pearlitic steels of strength category K56–K60 and of different microalloying types (10(09)G2FB, 10G2FT, 10G2T, etc.). Impact toughness, hardness and peculiarities of structural characteristics of the inside weld metal of the welded joints on pipes subjected to repeated heating in making the outside weld were evaluated. It was shown that decrease in impact toughness of test specimens of the two-pass two-sided welded joints on the pipes, the tested section of which comprises the metal of intersection of the inside and outside welds, is caused by the presence of the local embrittlement zones forming in the inside weld metal due to its heating in making the outside weld. Investigations, including by transmission electron microscopy combined with microdiffraction, detected the following two zones present in the inside weld metal: low-temperature zone (heating to 450–650 °C) caused by occurrence of the dispersion hardening processes, and high-temperature zone (heating to 950–1100 °C) related to the MAC-phase containing a substantial amount of a more stressed lath martensite and forming as a result of decomposition of non-homogenised austenite. 8 Ref., 3 Tables, 6 Figures.

Keywords: *gas and oil line pipes, welded joint, weld metal, repeated heating, impact toughness, hardness, structure*

In case of two-pass two-sided welding, which is widely applied in lines of production of large-diameter pipes for main gas and oil pipelines, some regions of the earlier welded, first (inside) weld are subjected to heating to different temperatures in making the second (outside) weld. Naturally, this causes changes in structure and properties of metal in the local zones and in the welded joint as a whole.

In evaluation of impact toughness of the weld metal, the effect of such local zones is most pronounced on the pipes with a relatively small wall thickness (e.g. 12–18 mm), when section of a standard impact test specimen (10 × 10 mm) inevitably includes the metal of the first (inside) weld, in addition to the metal of the second (last) outside weld. However, for the pipes also with a bigger wall thickness, the modern specifications more and more often provide for additional tests of impact specimens cut out from metal of the first weld or from the location where the first and second welds intersect, which comprises regions subjected to repeated heating [1].

Decrease in toughness of the weld metal on microalloyed steel pipes subjected to repeated heating to temperatures of 450–650 °C is a well-known fact. Its nature and the effect of separate microalloying elements are well-studied [2–4]. It is generally recognised that embrittlement of such a weld metal is caused by the dispersion hardening process. The data on properties of metal of the welds subjected to heating to higher temperatures are extremely limited [5].

The purpose of this study was to investigate impact toughness, structural parameters and hardness of metal of the inside weld on the microalloyed steel pipes subjected to repeated heating in making the outside weld, depending on its chemical composition.

Analysed were the results of investigations of welds of the welded joints on pipes with a diameter of 1020–1420 mm and wall thickness of 15.7–30 mm, made from ferritic-pearlitic steels of strength category K56–K60 and of different microalloying types (10(09)G2FB, 10G2FT, 10G2T, etc.), as well as welds of the welded joints on steels of similar microalloying types, made under laboratory conditions. The welds were made by using wire of the Fe–Mn–Ni–Mo or Fe–Mn–Ni–Mo–Cr systems, and aluminate or



Table 1. Experimental compositions of welds (to Figure 1)

Code of welded joint	Steel/wire alloying type (steel thickness, mm)	Content of main alloying elements in weld metal, wt.%						
		C	Mn	Mo	V	Nb	Cr	Ti
3	Mn-V-Nb/Mn-Ni-Mo (18.7)	0.080	1.68	0.30	0.020	0.022	0.09	0.011
4	Mn-V-Nb/Mn-Ni-Mo-Cr (15.7)	0.080	1.75	0.20	0.060	0.033	0.24	0.020
6	Mn-V-Nb/Mn-Ni-Mo (30)	0.070	1.72	0.25	0.050	0.032	0.06	Traces

Table 2. Experimental compositions of welds (to Figure 2)

Code of welded joint	Steel/wire alloying type (steel thickness, mm)	Content of main alloying elements in weld metal, wt.%						
		C	Mn	Mo	V	Nb	Cr	Ti
5	Mn-Ti/Mn-Ni-Mo (15.7)	0.068	1.80	0.19	Traces	Traces	0.01	0.035
6	Mn-V-Nb/Mn-Ni-Mo (30)	0.070	1.72	0.25	0.050	0.032	0.06	Traces
7	Mn-V-Ti/Mn-Ni-Mo (17.5)	0.082	1.75	0.24	0.075	Traces	0.05	0.010

Table 3. Experimental compositions of welds (to Figure 3)

Code of welded joint	Steel/wire alloying type (steel thickness, mm)	Content of main alloying elements in weld metal, wt.%						
		C	Mn	Mo	V	Nb	Cr	Ti
5	Mn-Ti/Mn-Ni-Mo (15.7)	0.068	1.80	0.19	Traces	Traces	0.01	0.035
6	Mn-V-Nb/Mn-Ni-Mo (30)	0.070	1.72	0.25	0.050	0.032	0.06	Traces
8	Mn-V-Nb/Mn-Ni-Mo (17.5)	0.065	1.75	0.18	0.056	0.048	0.06	Same
9	Mn-V-Nb/Mn-Ni-Mo-Cr (15.7)	0.080	1.78	0.20	0.060	0.033	0.24	0.020

high-silicon fused flux (of the AN-60 or AN-67B type). Impact toughness KCV_{-20} of the weld metal of such joints ranges, mainly, from 30 to 100 J/cm².

As the investigations were carried out by using a rather large number of different variants of alloying of the welded joints, for convenience of description of the results the data on chemical composition of metal of the investigated welds are presented separately for each particular case (Tables 1–3 corresponding to Figures 1–3).

For impact bend tests of the two-sided welded joints on pipes, the specimens were cut out on the side of the weld that was the last to make (Figure 1, a; specimen H), as well as from the zone of intersection of the welds (specimen C). The tests often fixed decrease in impact toughness of the metal in a case where the section of a test specimen comprised a certain amount of the inside weld subjected to repeated heating. As an example, Figure 1 shows a characteristic change in the level of impact toughness of metal of the welds of different microalloying types depending on the amount of metal of the first weld contained in section of the test specimen. As follows from the data presented, the values of impact toughness decrease with increase in this amount, espe-

cially at a relatively high content of carbide-forming elements (Figure 1, a; welded joint 4, compared to welded joint 3). This difference in impact toughness increases with decrease in test temperature (Figure 1, b), the drop of average values of impact toughness amounting to 30 J/cm² (here and in other similar parts of the study the average values of KCV are the results of tests of three to six specimens).

Special impact bend tests were conducted on the weld metal of a characteristic chemical composition (with different contents of carbide-forming elements), at which a specimen was located in thickness of the welded joint in such a way that the notch bottom was at a different distance from the penetration line of the second weld, i.e. in regions of the first weld metal subjected to heating to different temperatures.

Figure 2 shows the level of impact toughness of metal of the welds of different chemical compositions depending on the location of the notch bottom in a specimen. It can be seen that in the immediate vicinity of the penetration line of the second weld the impact toughness is even a bit higher than the level characteristic of the weld metal not subjected to heating. As a rule, a minor decrease in hardness of the metal is fixed in this

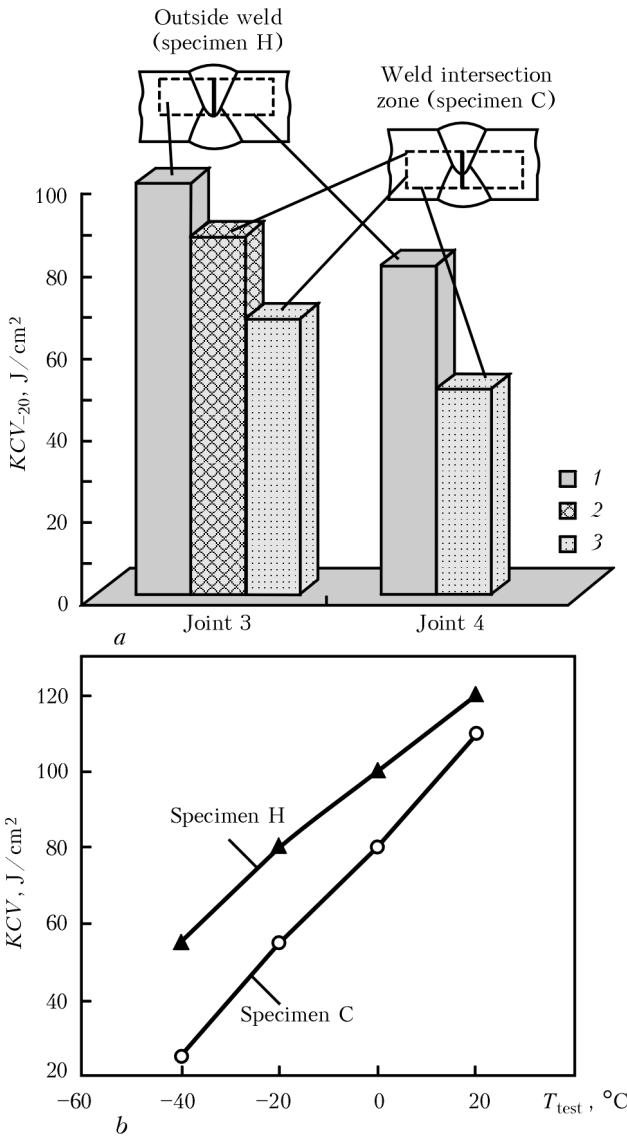


Figure 1. Impact toughness of metal of the welds at different amounts of the inside weld contained in section of test specimen (a), and effect of the test temperature on impact toughness value (b): a – welded joints 3 and 4; b – 6; 1 – 0; 2 – 15; 3 – 25 % of the inside weld

zone (Figure 3). With further distance of the notch bottom from the second weld penetration boundary the zones of decreased toughness are revealed in metal of the first weld. One of such zones is fixed at a distance of 1.5–3.0 mm from the penetration boundary. As the temperature of repeated heating of metal in this zone is 950–1100 $^{\circ}C$, it can be classed with a conditionally high-temperature embrittlement zone (HTEZ).

The said embrittlement was found to occur in base metal of the welds with a relatively increased content of molybdenum and other carbide-forming elements, and, first of all, vanadium, niobium or chromium (e.g. welded joints 6–9 in Figures 2 and 3 with total content of $V + Nb + Cr + Ti + Mo = 0.38-0.56$ wt.%). Impact toughness of the weld metal in this zone is 15–20 J/cm^2 lower than that of the second weld

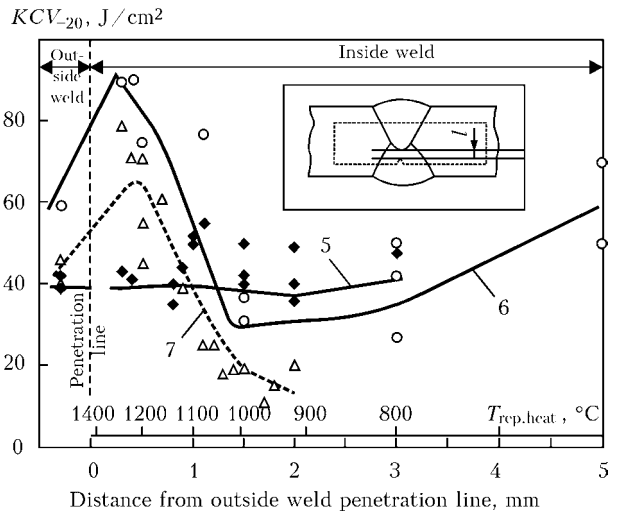


Figure 2. Effect of location of the notch on impact toughness of the investigated weld metal on pipes

metal not subjected to repeated heating, and hardness as a rule is higher by HV 25–35 (see Figures 2 and 3). In the weld metal alloyed only with molybdenum and titanium (e.g. welded joint 5 in Figure 2 with $Ti + Mo = 0.225$ %) no such decrease in impact toughness was fixed.

Another region of decrease in impact toughness of the first weld metal, where embrittlement develops because of dispersion hardening, is located at a distance of 4–6 mm from the second weld penetration boundary. The temperature of repeated heating of metal in this zone is 450–650 $^{\circ}C$. Naturally, the degree of hardening (embrittlement) of metal in this case depends on the content of carbon and carbide-forming elements. Because, as indicated above, the nature of decrease in toughness of the weld metal due to the dispersion hardening processes is well studied, later on the HTEZ of the first weld metal was investigated in more detail.

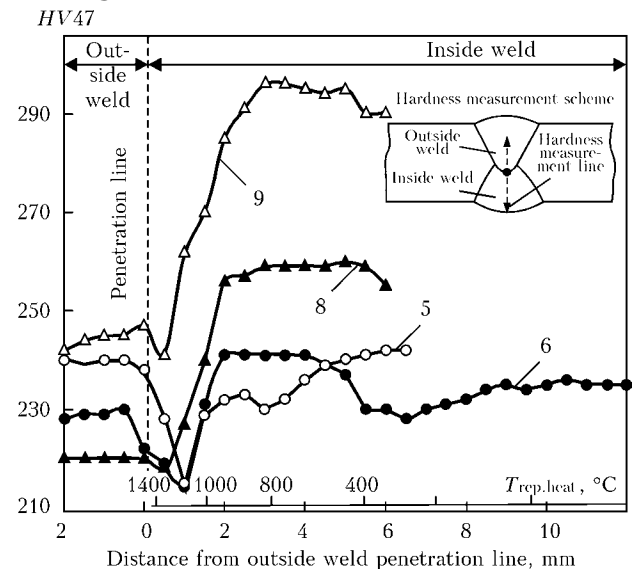


Figure 3. Distribution of hardness in the weld metals of different chemical compositions



HV47

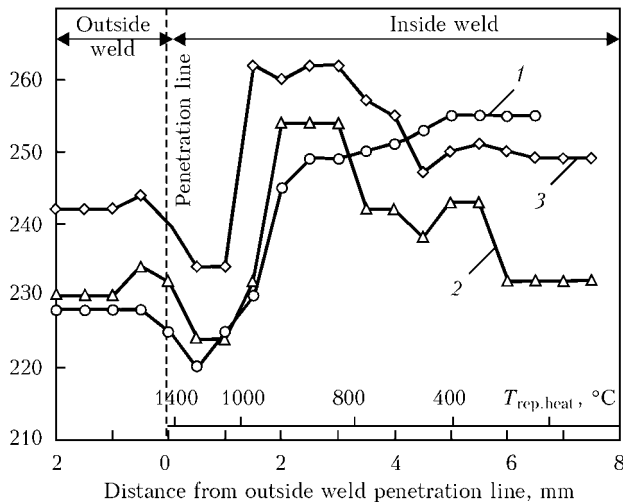


Figure 4. Effect of accelerated cooling on distribution of hardness in the weld metal: 1 – cooling in air; 2 – water cooling; 3 – water-air cooling

As shown by the additional tests, accelerated cooling during the welding process enhances embrittlement of the high-temperature zone. For example, in air, water and water-air mixture cooling of the first weld metal with a total content of vanadium, niobium, chromium, titanium and molybdenum at a level of 0.40 %, the maximum hardening of the HTEZ metal was fixed in a case of cooling by the water-air mixture, i.e. at a higher cooling rate (Figure 4). Also, it should be noted that in a case of cold crack resistance tests by the LTP2-6 procedure [6] providing for accelerated cooling, also an intensive hardening and even cracking were observed particularly in HTEZ (Figure 5, curves 1 and 2) of the first weld metal with a chemical composition close to the indicated one (the total content of carbide-

HV47

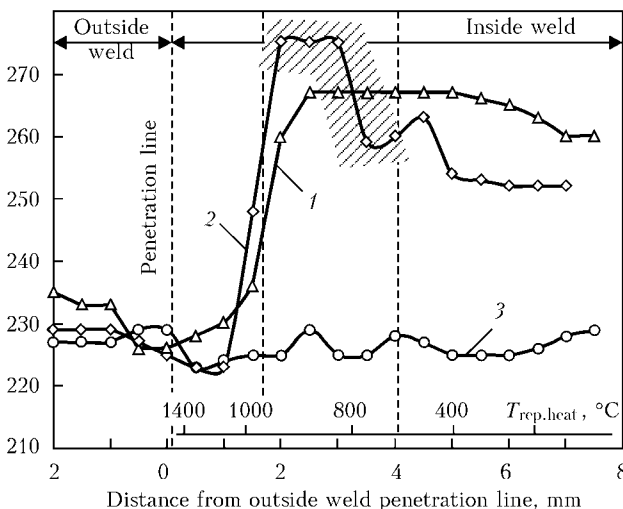


Figure 5. Distribution of hardness in the weld metal subjected to cold crack resistance tests: 1 – as-welded; 2, 3 – after the cold crack resistance tests; 1, 2 – weld of the Mo-V-Nb alloying system; 3 – weld of the Mo-Ti alloying system (dashed region – cold crack formation zone)

forming elements – at a level of 0.39 %). At the same time, under identical test conditions no hardening was fixed, and cracks were absent in the first weld metal alloyed only with molybdenum and titanium and close in chemical composition to the weld of welded joint 5 (the total content of carbide-forming elements – at a level of 0.23 %) (Figure 5, curve 3).

Optical metallography of probable changes in structure of the inside (first) weld metal as a result of repeated heating in making the outside (second) weld revealed no substantial differences in parameters of the structural state of metal of the local zones in the inside weld subjected to heating to different temperatures, where a marked increase in hardness of metal in the high-temperature zone and in the dispersion hardening zone had been fixed. Structural characteristics determining the level of impact toughness of the weld metal [7, 8] (contents of different structural components, i.e. acicular ferrite, intergranular polygonal or lamellar hypoeutectoid ferrite, upper bainite, and sizes of these formations, morphology and distribution of a microphase consisting of the martensite-austenite-carbide complexes (MAC-phase), quantity, size and morphology of non-metallic inclusions) were typical of the welding consumables and materials welded. The exceptions were the welds with a maximal content of molybdenum and niobium, where substantial formations of the carbon phases and structural components (MAC-phase, pearlite, carbides) were fixed in the said regions along the crystalline grain boundaries. Therefore, the local embrittlement zones were additionally examined by the transmission electron microscopy method by using foils, in a combination with microdiffraction).

Examinations were carried out mainly with the welds made by using flux AN-60 and wire Sv-08GNM on steels with a carbon content at a level of 0.1 %, and with different contents of microalloying elements and nitrogen. Such characteristics of the structural-phase state of the weld metal as peculiarities of acicular ferrite and dislocation structure, presence of other austenite transformation products, morphology and distribution of phase precipitates were evaluated.

The examinations showed that at a relatively low content of nitrogen (no more than 0.006 %) and carbide-forming elements ($Ti + V + Nb = 0.04 \%$, where $Ti = 0.03 \%$) the acicular ferrite microstructure with a well-developed sub-structure (sizes of sub-structural elements are approximately $(0.06-1.5) \times 2(.0-7.0) \mu m$, and form-fac-

tor χ is about 2–4) forms in metal of the inside weld, both in HTEZ and in the tempering zone. Dislocation density ρ is at a level of 10^{10} cm^{-2} . The structure is characterised by an ordered distribution of dislocations of volumetric equilibrium configurations. The boundaries of the sub-structural elements, having the form of dislocation networks and webs (inclination and torsion boundaries) are indicative of the relaxation processes occurring in the weld metal. In addition to acicular ferrite and a small amount of polygonal hypoeutectoid ferrite (10–15 %), also microregions of the intermediate transformation products (Figure 6, *a*), containing the indistinct fine-lamellar dispersed carbide inclusions (probably, in content of the MAC-phase), were revealed. Phase precipitates with size of about 0.006–0.012 μm were detected in the tempering zone in ferrite grains. The distance between separate particles of the phase precipitates is approximately 0.06–0.16 μm . The microdiffraction analysis of composition of the phase precipitates allowed identifying them as titanium, iron and vanadium carbides.

Increase in the content of carbide-forming elements in the inside weld metal ($\text{Ti} + \text{V} + \text{Nb} = 0.05 \%$, where there is almost no titanium), leads to formation of acicular ferrite, the grains of which are more elongated ($\chi = 3\text{--}5$, and up to 10 for individual sub-grains) and similarly oriented in some areas. Sizes of the sub-structural elements are about $(0.8\text{--}1.2) \times (3.5\text{--}5.0) \mu\text{m}$. The quantity of bainite microvolumes increases, and twinned martensite (in content of the MAC-phase) appears in the HTEZ region. The dislocation density ρ is at a level of 10^{10} cm^{-2} . The phase precipitates in the tempering zone, which are mostly vanadium, niobium and iron carbides, are 0.02–0.03 μm in size. The distance between the particles is 0.1–0.2 μm .

A simultaneous increase in the contents of nitrogen (up to 0.010–0.012 %) and microalloying elements ($\text{Ti} + \text{V} + \text{Nb} > 0.06 \%$) leads to more substantial changes in the dislocation structure and in the distribution of the phase precipitates. In this case also a dispersed fragmented structure of acicular ferrite forms ($\chi = 3\text{--}5$ on the average, and up to 11 for individual sub-grains). The structure is characterised by high dislocation density ρ – up to 10^{11} cm^{-2} or higher. The distribution of dislocations is mainly chaotic. More microvolumes with the martensite morphology are detected in the structure (Figure 6, *b*). A distinctive feature of structure of such a weld in the tempering zone is a very high density of phase precipitates and their dispersion degree. Sizes of the

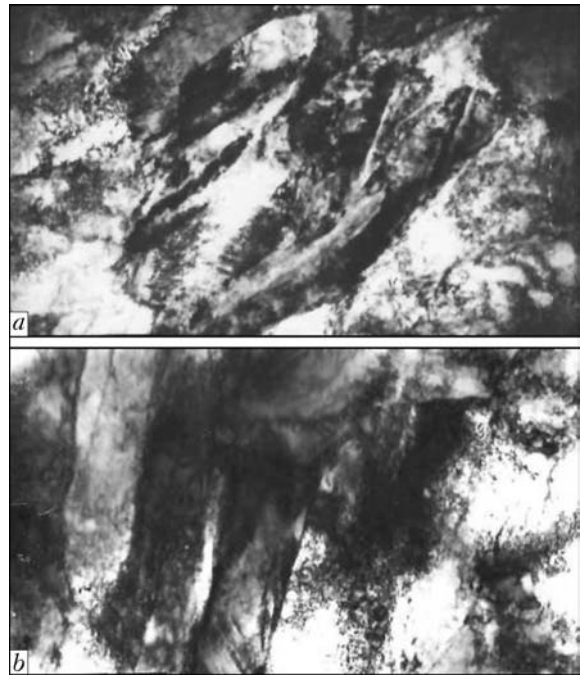


Figure 6. Microstructure ($\times 15,000$) of microphase in the HTEZ of metal of the inside weld at different alloying: *a* – $\text{Ti} + \text{V} + \text{Nb} = 0.04 \%$ ($\text{Ti} = 0.03$); *b* – $\text{Ti} + \text{V} + \text{Nb} > 0.06 \%$ (there is almost no titanium)

phase precipitates are about 0.003–0.007 μm . The distance between the individual particles does not exceed 0.007 μm , which is practically commensurable with sizes of the precipitates proper. The precipitates are mostly titanium, aluminium, niobium and vanadium nitrides (carbonitrides). Such a structural state leads to formation of a more stressed structure of the weld metal, this being related to development of the dislocation, sub-structural strengthening mechanisms, as well as strengthening by the Orowan mechanism (with finely dispersed particles).

Therefore, the investigations confirmed formation of a large number of the dispersed (0.003–0.005 μm in size) particles of the $\text{VNb}(\text{CN})$ type located at a distance of about 0.007 μm from each other in the low-temperature hardening zone of the first weld, which is indicative of occurrence of the dispersion hardening process in the tempering zone.

For HTEZ, increase in the amount of the MAC-phase with the lath martensite microregions prevailing in its content was fixed. Molybdenum carbides and vanadium and niobium carbonitrides observed in this zone are relatively coarse, because the strengthening particles are inefficient.

Based on the data obtained, it seems possible to suggest the following version of the nature of HTEZ: it forms at a repeated heating temperature of about 950–1100 $^{\circ}\text{C}$, when vanadium and niobium



bium carbonitrides, as well as molybdenum carbides have dissolved in the weld metal. Under these conditions a not yet homogenised austenite in the local zones, especially at an increased level of alloying, decomposes in the process of subsequent cooling at decreased temperatures to form the microphase containing a more stressed lath martensite, in addition to the bainite transformation products, this increasing the sensitivity of this zone to embrittlement. Under certain conditions this may lead to formation of cold cracks in the welds.

Conclusions

1. Decrease in impact toughness when testing specimens of the two-pass two-sided welded joints on pipes, the tested section of which comprises the metal of intersection of the inside and outside welds, is caused by a number of factors, the decisive one of which is the presence of the local embrittlement zones forming in metal of the inside welds due to its heating in making the outside weld. The inside weld metal comprises two such zones: in the high- and low-temperature heating ranges.

2. Formation of the low-temperature embrittlement zone is caused by the process of dispersion hardening of metal in repeated heating to temperatures of about 450–650 °C, and its effect is proportional to increase in the content of carbon and carbide-forming elements.

3. Investigations, including by transmission electron microscopy combined with microdiffraction, suggested that decrease in toughness of the high-temperature embrittlement zone forming in repeated heating of the inside weld to temperatures of 950–1100 °C is caused by formation of unfavourable structural components, such as the MAC-phase containing a marked amount of a more stressed lath martensite, due to decomposition of non-homogenised austenite.

1. (2010) *DNV-OS-F101*: Offshore Standard Norskske Veritas. Submarine pipeline systems.
2. Ito, Y., Nakanishi, M. (1975) Study on Charpy impact properties of weld metals with submerged arc welding. *IIW Doc. IX-A-113-75*.
3. Farrar, R.A., Wong, S.Y., Watson, M.W. (1980) How stress relief affects SA weld metal containing niobium. *Welding and Metal Fabr.*, **1/2**, 21–23.
4. Yoshino, Y., Stout, R.D. (1979) Effect of microalloys on the notch toughness of line pipe seam welds. *Welding J.*, **58(3)**, 59–69.
5. Frantov, I.I., Golovanenko, S.A., Moiseev, B.A. et al. (1981) Welding of thick-walled large-diameter pipes made from controlled rolling steel. *Svarochn. Proizvodstvo*, **6**, 11–13.
6. Makarov, E.L. (1981) *Cold cracks in welding of alloyed steels*. Moscow: Mashinostroenie.
7. Garland, J.G., Kirkwood, P.R. (1975) Towards improved submerged arc weld metal. *Metal Constr.*, **5**, 275–283.
8. Denisenko, A.V., Grabin, V.F., Korsun, A.O. et al. (1990) Morphological peculiarities of structure of low-alloy weld metal and their effect on properties of welded joints. *Avtomatich. Svarka*, **10**, 32–37.

Received 27.02.2013



INFLUENCE OF WELD POOL GEOMETRY ON STRUCTURE OF METAL OF WELDS ON HIGH-TEMPERATURE NICKEL ALLOY SINGLE CRYSTALS

K.A. YUSHCHENKO¹, I.S. GAKH¹, B.A. ZADERY¹, A.V. ZVYAGINTSEVA¹ and O.P. KARASEVSKAYA²

¹E.O. Paton Electric Welding Institute, NASU

11 Bozhenko Str., 03680, Kiev, Ukraine. E-mail: office@paton.kiev.ua

²G.V. Kurdyumov Institute for Metal Physics, NASU

36 Acad. Vernadsky Bd., 03680, Kiev, Ukraine. E-mail: Karas@imp.kiev.ua

The main defect, which prevents realization of the advantages of high-temperature nickel alloy single crystals in production of welded assemblies and parts of gas-turbine engine, are stray grains in the weld metal. The objective of this work was studying the features of weld metal structure, depending on curvature of macrofront of weld pool solidification and determination of admissible deviations of the direction of maximum temperature gradient from orientation of predominant crystal growth. Experiments were performed with application of electron beam welding on single-crystal samples from commercial high-temperature nickel alloys JS26 and JS32, containing more than 60 % of strengthening γ -phase. Welded joint structure was studied by optical metallography and X-ray diffractometry methods. It is shown that the main conditions for preservation of single-crystal structure in welding of high-temperature nickel alloy single crystals are correspondence of fusion plane to single crystal high-symmetry axes and coincidence of the direction of maximum heat removal over weld pool solidification front with $\langle 001 \rangle$ orientation of predominant crystal growth. Limit deviations for studied alloys and welding conditions are established. 15 Ref., 9 Figures.

Keywords: *electron beam welding, single crystal, high-temperature nickel alloy, crystallographic orientation, weld, weld pool geometry, dislocation distribution, crystal growth direction, maximum heat removal direction, angle of deviation, stray grains*

Proceeding from analysis of temperature and orientation conditions of growing single-crystals of high-temperature nickel alloys and experimental work on welding conducted earlier [1–4], it is established that the main criteria of evaluation of welded joint quality are preservation of initial crystallographic orientation and single-crystal structure. The latter is evaluated by presence of stray grains in the weld metal, which differ from the initial crystallographic orientation of the material being welded. The best results are achieved under the condition when the fusion surface coincides with the high symmetry axes [4–8]. In this case crystallographic orientation of the plane of edges being welded should be close to $\{110\}$, that is achieved at correspondence of the plane and direction of welding: $\{100\}$, $\langle 100 \rangle$ and $\{110\}$, $\langle 011 \rangle$ (Figure 1). It is established that at such crystallographic conditions stray grains can amount from 2 to 10 % of weld volume. In case of deviation by more than 4° from symmetry conditions, the number of grains can rise up to 60–80 %.

It should be noted that appearance of 2–4 % of stray grains in the weld is possible even with strict following of the above conditions of symmetry. Such disturbances of single-crystal nature of the weld can be due to the fact that the weld pool has a certain curvature, so that over the solidification front the direction of maximum temperature gradient G changes relative to the direction of predominant growth of crystals $\langle 001 \rangle$ (Figure 2). This involves violation of one of the main conditions of directional solidification, namely orientational influence of the substrate on single-crystal growth. Therefore, disorientation between G and direction of predominant growth $\langle 001 \rangle$ on the solidification front leads to formation of high-angle grains.



Figure 1. Microstructure of weld metal of JS26 alloy welded joint with symmetrical crystallographic orientation

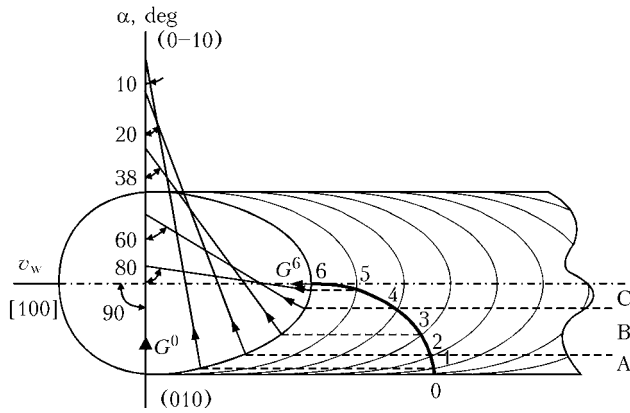


Figure 2. Schematic image of the change of direction of maximum temperature gradient G over weld pool solidification front: A, B, C – characteristic structural zones of the weld; α – deviation angle G

The objective of this work was studying the features of weld metal structure depending on curvature of weld pool solidification macrofront and determination of admissible deviations of the direction of maximum temperature gradient from predominant growth orientation.

Experiments on welding were performed on single-crystal samples from commercial high-temperature nickel alloys JS26 and JS32 of $50 \times 40 \times (1.5-2.5)$ mm size, cut out of blades or blanks produced by the method of high-speed directional solidification with more than 60 % of γ' -phase. The cut area was ground before welding. Samples were heat-treated before welding by standard modes. Welding was performed by the electron beam in vacuum at the speeds of 20–80 m/h. Specific values of welding parameters were selected from the conditions of producing welds of the required geometry. In order to create a more uniform temperature field and lower the welding stresses, welding was performed with preheating to 300–600 °C.

Structure of welded joints was studied on longitudinal and transverse sections with application of optical metallography and X-ray diffractometry methods [5–9]. Distribution of the intensity of scattered X-ray radiation near the reverse lattice nodes was evaluated. Sections were studied at irradiation of a region of 0.3×2.0 mm area and reflection position in the direction normal to butt plane, going sequentially through all the characteristic zones of the welded joint (BM–HAZ–weld–HAZ–BM). The (irradiated) studied area remained parallel to butt edge. 36 sections on sample surface 10 mm wide were studied. Displacement step was 0.28 mm. This procedure is described in greater detail in [4–9].

X-ray analysis was used to orient the samples and select welding direction. Crystallographic orientation of weld metal, presence and number

of stray grains was evaluated, proceeding from pole figure analysis. Dislocation density and their distribution were assessed by the width, shape and uniformity of intensity distribution, i.e. by blackening of X-ray reflections.

Performed metallographic and X-ray investigations allowed identifying individual structural zones of weld metal, associated with weld pool curvature (Figures 2 and 3).

Zone A is part of the weld near the fusion line, characterized by prevalent coincidence of the direction of maximum temperature gradient with $\langle 001 \rangle$ orientation of predominant crystal growth. Directly near the fusion line one can see a narrow (0.3–0.5 mm) strip of epitaxial growth. Further in depth of the weld a finely-dendritic structure of directional solidification with quite accurate inheritance of the initial edge orientation is observed (Figure 4), and high-angle boundaries are absent (Figures 3 and 5). Metal of this zone is characterized by a negligible degree of degradation of single-crystal structure. Despite the marked increase of dislocation density, distribution of the intensity of X-ray reflection $I_{q\perp}$ is relatively smooth and close to base metal. Isointensive lines have the shape of smooth ellipsoidal curves (see Figure 3, b) that corresponds to single-crystal state of the metal with uniform distribution of edge dislocations.

Zone B is that of a critical deviation of maximum temperature gradient from the direction of predominant crystal growth, where the first part of the weld inherits the initial single-crystal orientation, and violation of directional solidification and formation of stray grains with possible cracking along the grain boundaries are found in the second zone (see Figure 3). In terms of roentgenography, this is manifested in additional reflections on pole figures (see Figure 5), presence of intensity deviations for considerable angle values from the maximum one in $I_{q\perp}$ distribution (see Figure 3). For metal of this zone, inheriting the initial orientation of single-crystal being welded, a characteristic feature is the pronounced non-uniformity and localizing of dislocations, that is indicated by irregular isointensive $I_{q\perp}$ curves. Widening of distribution of $I_{q\perp}$ reflections by different azimuthal directions is related to appearance of secondary dislocation systems and increase of their general density. Metal of this zone forms a multilevel dislocation structure that leads to stress localizing in non-uniform dislocation clusters. As a result, the weld forms stray grains with high-angle boundaries. Development of non-uniform disorientation causes an acceleration of deformations and single-crystal

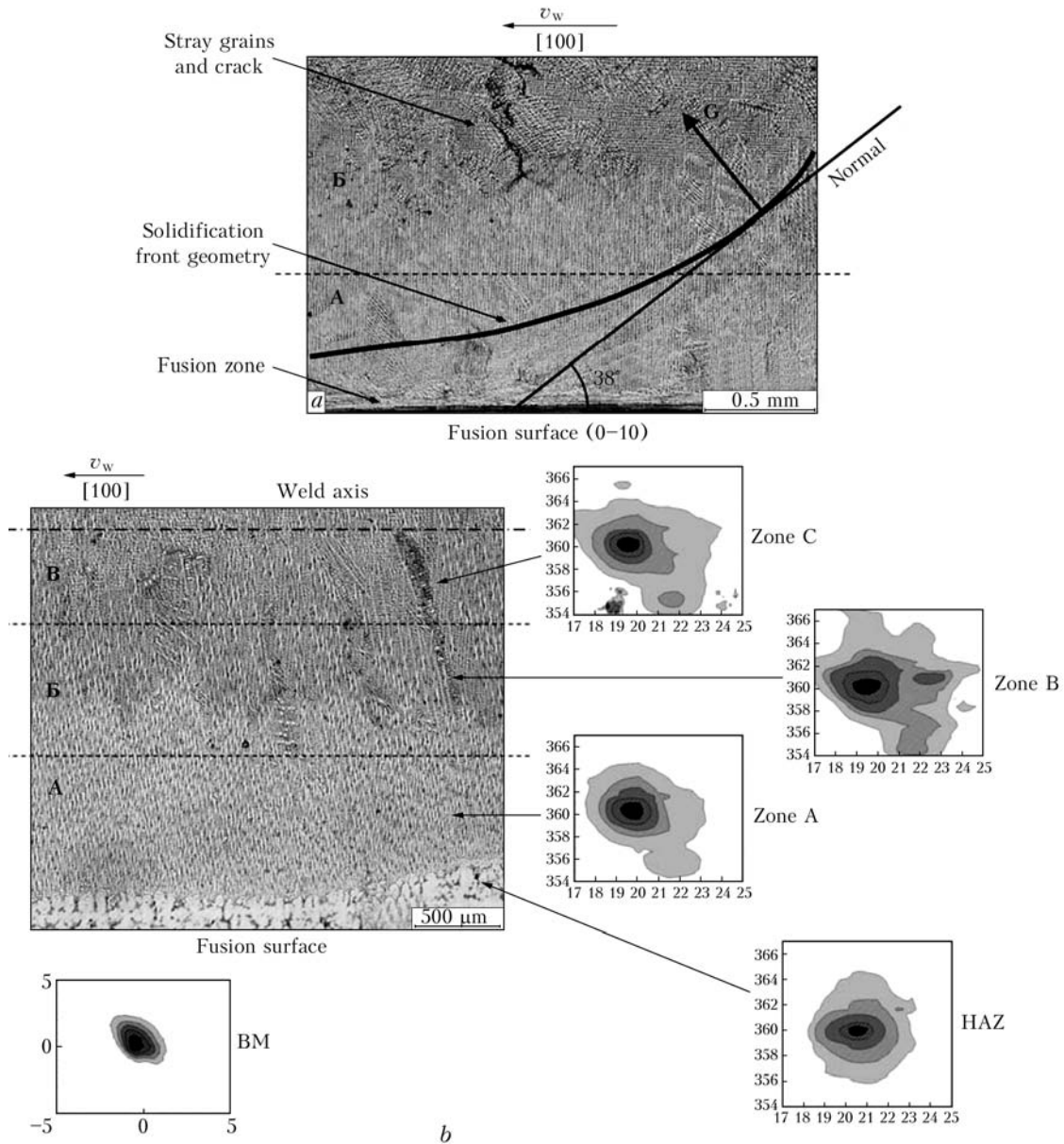


Figure 3. Microstructure (a) and isointensive $I_{q\perp}$ curves (b) of weld metal zones corresponding to different deviations from maximum temperature gradient over weld pool solidification front (acc. to Figure 2) (numerical values along zone axes are shown in degrees)

fracture, as well as crack initiation in welds of these materials [10–15]. In zone B, in addition to stray grain formation in that part which inherits the initial orientation, a successive deviation of crystallographic orientation by 1–2° from the initial one with greater distance from the edges being welded is observed (see Figure 4). Change of orientation characterizes the level of macro- and microstresses, compensation of which can lead to disturbance of single-crystal structure of the metal and formation of high-angle boundaries, because of considerable rotation of crystal-line lattice through more than 5° [10–15].

Zone C is a section of weld metal, in which the direction of maximum temperature gradient practically coincides with crystallographic orientation of ready growth. In this zone formation

of individual high-angle boundaries is possible as a result of mismatch of growing dendrites abutting from different sides of the weld pool.

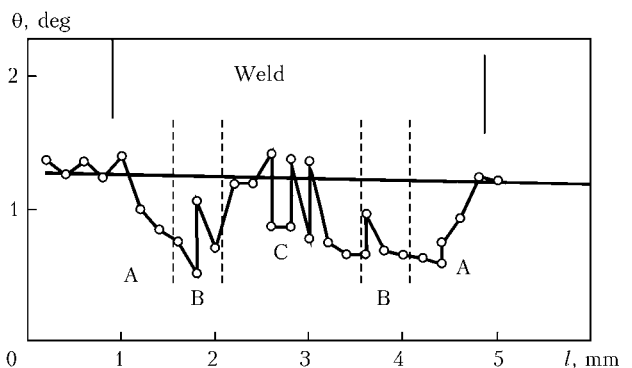


Figure 4. Change of crystallographic orientation close to {100} across welded joint width

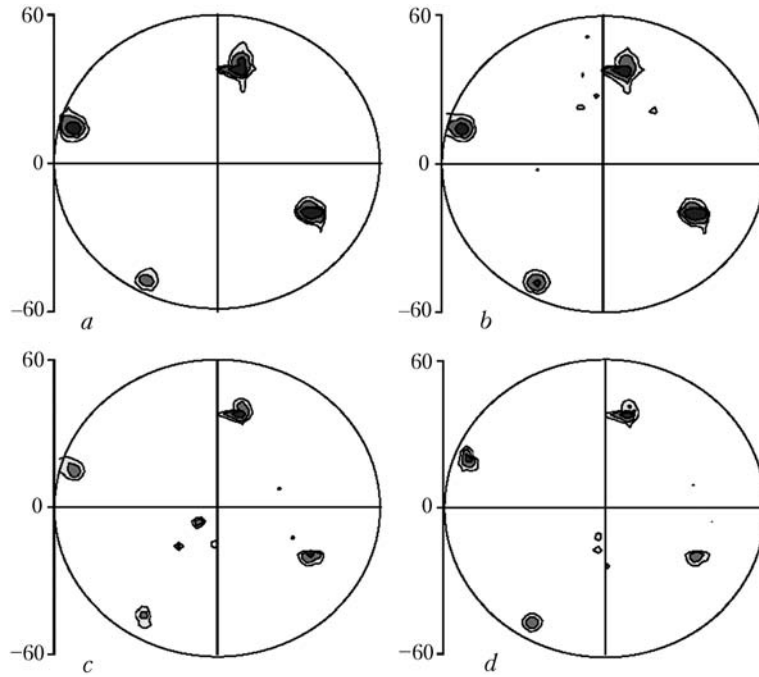


Figure 5. Pole figures for weld metal of welded joint with crystallographic orientation close to $\{100\}$: *a* – base metal; *b–d* – zone A, B, C, respectively (see Figures 3 and 4)

For welded joints with crystallographic orientation differing from high symmetry, the above structural zones are manifested more clearly. In this case, zone B becomes wider, and its position relative to weld axis, as well as the number of stray grains, alongside curvature of weld pool solidification front, also depends on how much

the initial orientation of single-crystals differs (Figure 6) from high symmetry [7].

Thus, formation of single-crystal structure of weld metal is provided at constant direction of temperature gradient in each point of weld pool – a condition of flat solidification macrofront – and its coincidence with crystal growth predominant orientation $\langle 001 \rangle$.

Variation of parameters of EBW modes, beam scanning over single-crystal samples of JS26 and JS32 alloys with different crystallographic orientation allowed forming welds with a flat solidification macrofront, at which the orientation of maximum temperature gradient was constant during solidification. Depending on orientation of welded single-crystal sample and fusion plane, the value of deviation of maximum temperature gradient from the direction of predominant crystal growth $\langle 001 \rangle$ varied from 0 up to 30° .

Studying the structure of the respective welds showed that violation of crystallographic orientation and single-crystal structure is concentrated, mainly, in those weld sections, where the direction of maximum temperature gradient on weld pool solidification front deviates from the predominant growth orientation by more than 15° angles. This allowed establishing admissible disorientation that ensures formation of a weld with single-crystal structure.

Proceeding from analysis of the results obtained during study of weld metal structure formation in single-crystal welding, it was proposed to control weld pool geometry so that the direction of temperature gradient over the entire so-

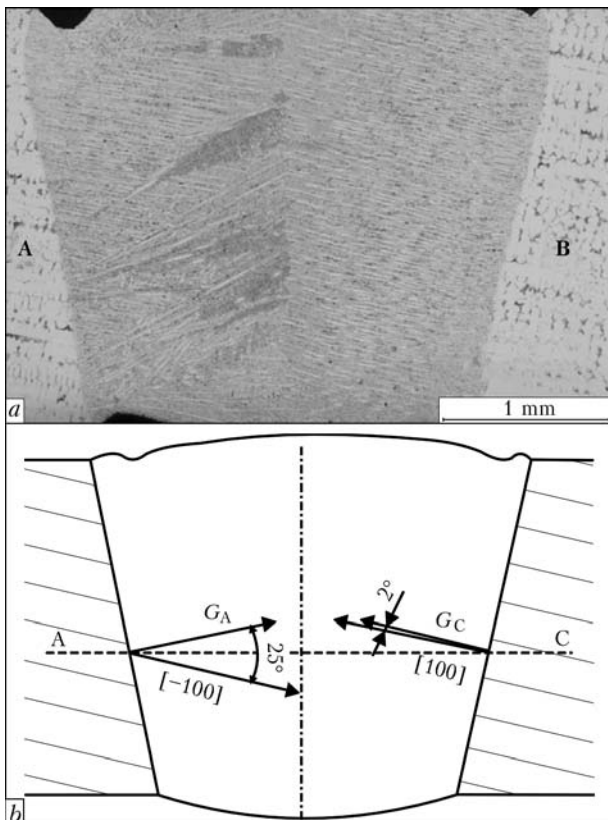


Figure 6. Asymmetry of solidification of metal of JS26 alloy weld: *a* – microstructure; *b* – orientational schematic



lidification macrofront did not deviate from $\langle 001 \rangle$ by angles exceeding the admissible level that will allow preventing critical deviation zone in zone B (see Figure 3), in which stray grains are formed. In terms of technology, this is achievable by adjustment of parameters of EBW and orientation of the joint butt within admissible limits with crystallographic plane (100).

Metallographic (Figure 7) and roentgenographic examinations (Figures 8 and 9) illustrate the positive result of such an approach that is expressed in formation of weld metal with high enough crystallographic perfection and preservation of the orientation of initial material being welded. Comparison of pole figures of base metal and weld metal (see Figure 8) demonstrates preservation of the position of main reflections in absence of reflection reflexes of another orientation. $I_{q\perp}$ distribution of (200) reflection in different zones of the welded joint is indicative (see Figure 9) of uniform distribution of dislocations in the weld bulk, despite an increase of their density. If there is no division of $I_{q\perp}$ X-ray reflection, then the high-angle boundaries are also absent. Level of disorientation of structural components of weld metal is within 2° , and does not exceed the admissible value for high-temperature single-crystals (approximately 5°), at which the single-crystal nature of the material is violation. Principles of selection and control of weld pool

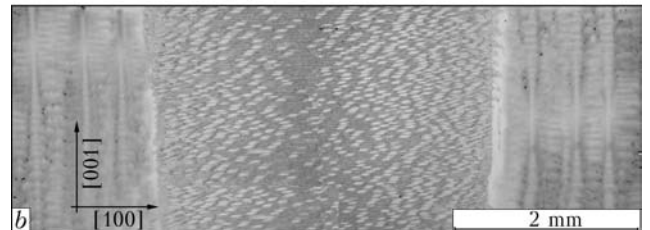
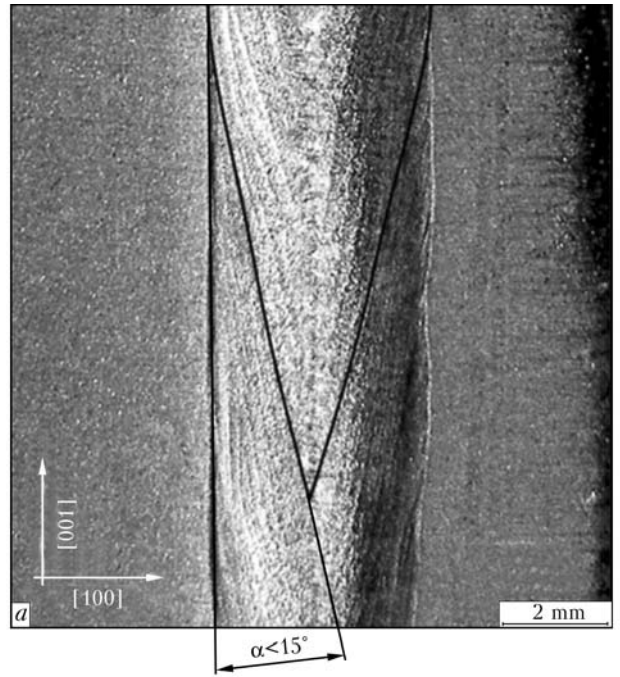


Figure 7. Appearance (a) and microstructure of single-crystal weld (b) of JS32 alloy made with control of weld pool solidification: α – angle of deviation of weld pool solidification macrofront from {100}

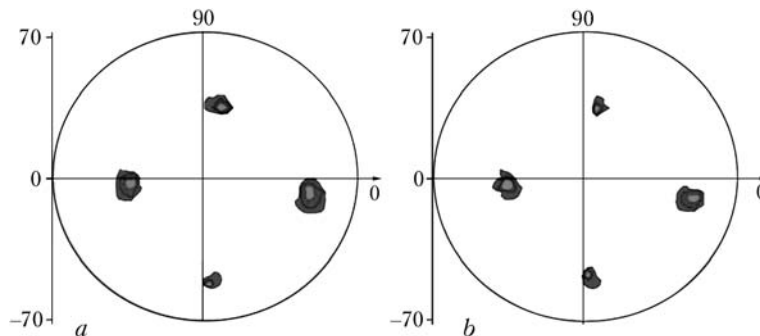


Figure 8. Pole figures {220} of base metal (a) and weld metal (b) made with control of weld pool solidification

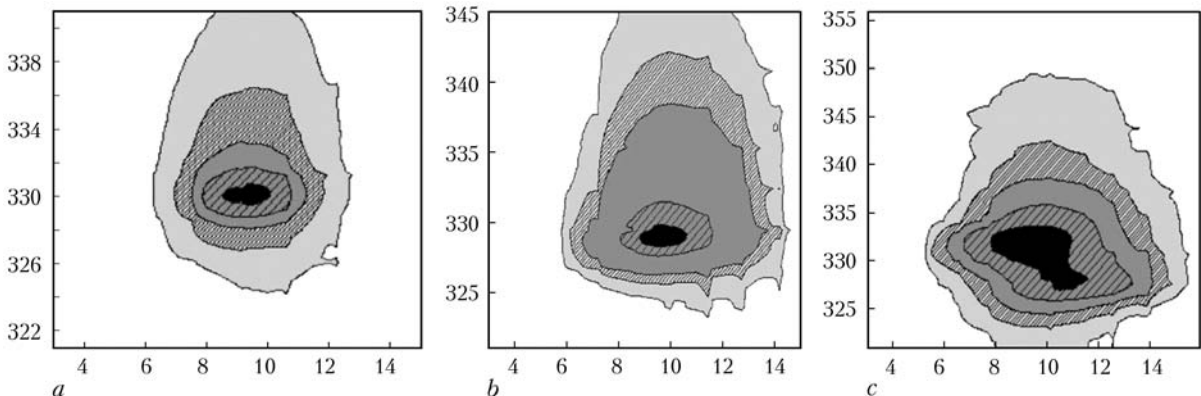


Figure 9. $I_{q\perp}$ distribution of (200) reflection in different zones of the welded joint: a – base metal; b – HAZ metal; c – weld metal (numerical values by axes are given in degrees)



shape were tried out at reconditioning of single-crystal blades from JS32 alloy.

Thus, in EBW of high-temperature nickel alloys the main crystallographic parameters of the welded joint are not only correspondence of the fusion plane to high-symmetry axes of a single-crystal, but also crystallographic orientation at the macrofront of weld pool solidification. There exists a critical angle of deviation of the direction of maximum heat removal relative to the direction of predominant crystal growth $\langle 001 \rangle$. For the studied alloys and their welding conditions the critical angle of deviation is within 15° .

Conclusions

1. Experiments on EBW of single-crystals of high-temperature nickel alloys of JS type with more than 60 % content of γ' -phase revealed that characteristic weld defects is partial inheritance of base metal crystallographic orientation with formation of stray grains and possible formation of grain-boundary cracks.

2. Influence of curvature of weld pool solidification macrofront on inheritance of initial crystallographic orientation by weld metal and perfection of its structure was studied. It is shown that in order to prevent formation of stray grains or cracks, it is necessary to provide weld pool shape, which eliminates the possibility of deviation of the direction of temperature gradient passage over the solidification front from the required direction by an angle, exceeding the admissible one.

3. Results of performed investigations were used in development of basic technology of welding high-temperature nickel alloys, allowing preservation of single-crystal structure with substructure disorientation of $\pm 2^\circ$, as well as absence of cracks or stray grains in weld metal.

1. Shalin, R.E., Svetlov, I.L., Kachanov, E.B. et al. (1977) *Single crystals of heat-resistant nickel alloys*. Moscow: Mashinostroenie.
2. Kablov, E.N. (2001) *Cast blades of gas-turbine engines. Alloys, technology, coatings*. Moscow: MISIS.
3. Pollock, T.M., Murphy, W.Y. (1996) The breakdown of single-crystal solidification in high refractory nickel base alloys. *Metall. and Mater. Transact. A*, **27**, 1081–1094.
4. Gakh, I.S. (2011) *Physical-technological features of electron beam welding of heat-resistant high-nickel alloys with monocrystalline structure*: Syn. of Thesis for Cand. of Techn. Sci. Degree. Kyiv.
5. Yushchenko, K.A., Zadery, B.A., Karasevskaya, O.P. et al. (2006) Structural changes during welding of nickel superalloy single-crystals in crystallographically asymmetrical location of weld pool. *Metallofizika i Nov. Tekhnologii*, **28(11)**, 1509–1527.
6. Yushchenko, K.A., Zadery, B.A., Zvyagintseva, A.V. et al. (2009) Peculiarities of the structure of metal deposited on edges of single-crystal blades made from nickel superalloys. *The Paton Welding J.*, **8**, 36–42.
7. Yushchenko, K.A., Zadery, B.A., Savchenko, V.S. et al. (2008) Welding and cladding of heat-resistant nickel alloys with single-crystal structure. *Ibid.*, **11**, 191–196.
8. Yushchenko, K.A., Zadery, B.A., Zvyagintseva, A.V. et al. (2009) About possibility of inheritance of single-crystal structure of complexly-doped nickel alloys in nonequilibrium conditions of fusion welding. *Metallofizika i Nov. Tekhnologii*, **31(4)**, 473–485.
9. Yushchenko, K.A., Zadery, B.A., Zvyagintseva, A.V. et al. (2008) Sensitivity to cracking and structural changes in EBW of single crystals of heat-resistant nickel alloys. *The Paton Welding J.*, **2**, 6–13.
10. Mughrabi, H. (1983) Dislocation wall and cell structures and long-range internal stresses in deformed metal crystals. *Acta Metall.*, **31**, 1367–1379.
11. Panin, V.E., Likhachev, V.A., Grinyaev, Yu.V. (1985) *Structural levels of deformation of solids*. Novosibirsk: Nauka.
12. Likhachev, V.A., Panin, V.E., Zasmichuk, E.E. (1989) *Cooperative deformation processes and localization of deformation*. Kiev: Naukova Dumka.
13. Malygin, G.A. (1995) Self-organisation of dislocations and localization of sliding in plastically deformed crystals. *Fizika Tv. Tela*, **37**, Issue 1, 3–42.
14. Sarafanov, G.F. (1998) To theory of formation of inhomogeneous dislocation structures. *Fizika Metallov i Metallovedenie*, **85**, Issue 3, 46–53.
15. Koneva, N.A., Kozlov, E.V. (1990) Physical nature of plastic deformation stages. *Izvestiya Vuzov. Fizika*, **2**, 89–106.

Received 01.03.2013



DEVELOPMENT OF LASER WELDING OF ALUMINIUM ALLOYS AT THE E.O. PATON ELECTRIC WELDING INSTITUTE (Review)

V. Yu. KHASKIN

E.O. Paton Electric Welding Institute, NASU
11 Bozhenko Str., 03680, Kiev, Ukraine. E-mail: office@paton.kiev.ua

The works, connected with the development of precision technologies of welding of aluminium alloy structures, allowing minimizing the residual welding deformations, are urgent. They, for example, include the technologies, envisaging the application of a laser welding. The aim of the present article is the review of investigations on welding aluminium and its alloys, applying a laser emission, carried out at the E.O. Paton Electric Welding Institute since the end of the 1960s until now. The stage-by-stage development of these investigations is shown depending on the progress of the laser engineering and growth of level of knowledge of researchers. Three main stages of works on laser welding are distinguished: with application of low-power pulsed lasers (from the end of the 1960s until the end of the 1970s), with application of powerful continuous-wave lasers (from the beginning of the 1980s until the beginning of the 2000s) and with application of hybrid laser-arc and laser-plasma processes (from the beginning of 2000s until now). The offered review illustrates the sufficiently high level of investigations of aluminium alloy welding by applying a laser emission, carried out by the PWI in different years. It is shown that these investigations are continued also at the present time. Their challenges are outlined, including industrial applications of the described methods of welding for manufacture of thin-walled body structures of motor cars, high-speed railway cars, different-purpose ships, aircrafts, rockets and space engineering objects. 16 Ref., 1 Table, 4 Figures.

Keywords: *aluminium alloys, laser emission, hybrid, consumable electrode arc, transferred arc plasma, welding speeds, residual deformations, mechanical properties*

Aluminium and its alloys are widely used in the modern industrial manufacturing. The variety of structures, manufactured of aluminium alloys, required the development of different methods of their welding [1]. Among them a special attention is paid to those, where the laser emission is used. At the E.O. Paton Electric Welding Institute (PWI) the investigations of laser welding of aluminium alloys were carried out since the end of the 1960s. The present paper is devoted to review of these investigations.

At the end of the 1960s–beginning of the 1970s the pulsed solid-body lasers began to be effectively applied for manufacture of products of instrument industry, radio engineering, electrovacuum systems and in other branches of small-object machine building. This promoted the progress of investigations and development of industrial technologies of welding at the PWI, which applied a laser pulsed heating source for heating and braze welding of metallic semi-products.

The technological investigations were headed by O.A. Velichko and V.P. Garashchuk was responsible for the hardware, and the general management of works was realized by V.E. Morav-

sky. Laser installations of UL-2m, SLS-10 and later Kvant-10 were used in experiments. Due to a comparatively low energies of a pulse (to 10 J) the samples were manufactured mainly of foils of 0.1–0.5 mm thickness. The continuous welds were obtained by overlapping of weld spots, forming per one pulse. The coefficient of overlapping was usually from 50 up to 75 %. Welding was performed in shielding gases, helium was often preferable. The distinguished feature of this stage of works was thorough examination of metallographic peculiarities of joints being produced, and also their effect on mechanical properties of the joints.

The example of these investigations is the work [2], in which the data about mechanical properties of butt joints of dissimilar metals, made by laser welding, were published for the first time. The weldability of commercially pure aluminium with such materials as copper M1, bronze Br.B2, austenite stainless steel 1Kh18N9T and carbon steel 08kp (rimmed) was also investigated. It was found that in all these cases the fracture of welded joint is occurred in weld and is brittle. To join the aluminium with copper M1 the relation of tensile strength σ_t of weld metal to appropriate characteristic of the less stronger metal (σ_t of aluminium) was 40 % at 60° bending angle. To join aluminium with bronze Br.B2 and steel 1Kh18N9T the ratio of tensile strength was

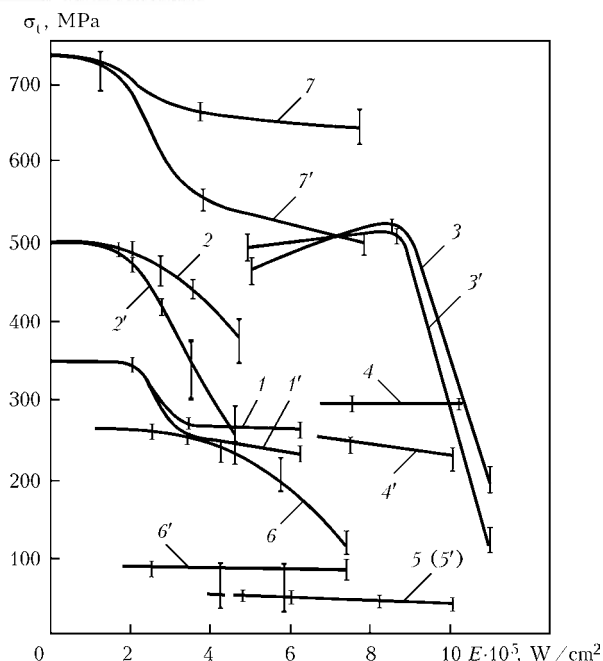


Figure 1. Curves of dependence of weld metal strength on intensity of focused emission, obtained experimentally, in making butt joints [2]: 1 – steel 08kp, $\delta = 0.3 + 0.3$ mm; 2 – titanium, $\delta = 0.3 + 0.3$ mm; 3 – tantalum, $\delta = 0.3 + 0.3$ mm; 4 – niobium, $\delta = 0.2 + 0.2$ mm; 5 – aluminium, $\delta = 0.3 + 0.3$ mm; 6 – nickel, $\delta = 0.3$ mm, with niobium, $\delta = 0.2$ mm; 7 – niobium, $\delta = 0.5 + 0.5$ mm; 1'–7' – welding in argon; 1'–7' – welding in air

60 and 10 % at bending angle of 30° and 5° , respectively. For Al–08kp joint it was 66 % at 80° . To increase the mechanical characteristics of dissimilar joints and to improve the weld geometry, such technological procedure of laser welding was suggested in work [2], as shifting of heat spot from butt axis into the side of one of the metals being joined. Thus, the high-quality butt joints were produced with melting only of one of metals, i.e. so-called process of braze welding. Among these joints, the joints of aluminium with tungsten, molybdenum and steel were noted.

Later, the larger attention was paid to the study of technological features of process of a pulsed laser welding of aluminium alloys. Thus, in work [3] the data about laser welding of aluminium were given for the first time. This work considered the problems of initiation of different types of defects connected with change in process conditions: both the defects of joint formation (cavities, pores, undercuts, thinning) and also of metallurgical origin (structural and chemical changes of metal of weld spot and HAZ, cracks). It was found that at the pulsed laser welding in the condition of heat-conductive penetration the mechanical properties of weld spot metal do not almost depend on intensity of emission, and at transition into the condition of a deep penetration the structure and mechanical characteristics of weld spot can be deteriorated with increase in emission intensity. The susceptibility to the for-

mation of cavities, pores, microcracks and other defects is also increased in this case. It was found that aluminium is very low reacted on the change of emission intensity (Figure 1).

At the PWI even at the initial stage of works on laser welding of aluminium D.M. Rabkin showed a great interest to the obtained results. By the end of the 1980s, when the transition to powerful continuous-wave lasers began and the development of technological procedures of laser welding allowed producing long defect-free welds, he highly evaluated this method of welding and predicted its further progress.

Unlike the pulsed laser welding, the laser welding of aluminium alloys by the continuous emission was considered very problematic almost to 1978–1979. At that time the experiments were carried out in installation OB-1617, designed at the PWI under management of V.P. Garashchuk. In welding of alloy AMg6 by emission of this CO_2 -laser of 1.4 kW capacity the significant microporosity, oxide films and clusters of products of weld metal interaction with air gases in the form of brittle acicular phases were observed in weld. At weld pool shielding with argon the depth of penetration was decreased to zero [4].

At the end of the 1970s the transition began for powerful CO_2 -lasers, generating continuous emission that allowed significant widening of technological capabilities of the laser welding process [5]. For example, at the PWI in 1981 a feasibility of welding of alloy AMg6 ($\delta = 4$ mm) by the continuous-wave laser emission was established in principle [4]. The application of shielding atmosphere of helium at emission power of 5 kW allowed producing at 120 m/h speed the quality keyhole welds, and the microstructure of weld metal by nature and dispersity on alloy AMg6 was identical to weld metal produced in EBW. The attained result was recognized for the first time among the leaders of mastering the laser welding in industrial manufacture of aerospace engineering objects.

The described investigations gave an opportunity to perform nowadays the welding of T-joints of alloy AMg6 by filler wire SvAMg6 (1.2–3.0 mm diameter) in manufacture of stringer panels. In this case, the stiffeners of 5 mm thickness were welded-on to the sheet of 8 mm thickness by double-sided fillet welds using emission of CO_2 -laser of up to 5 kW capacity [5]. To prevent residual welding stresses and deformations the preliminary tension of elements being welded was applied at maximum force of up to 750 kN. It was found that optimum power of emission was 3.8–3.9 kW to produce the quality welds under conditions of carried out experiments. It was also determined that the most effective is the uniform preliminary tension of sheet and stiffeners at

force, whose value was at the level of residual stresses in weld, which was made without preliminary tension of elements being welded [6].

The carried out technological investigations proved the effectiveness and actuality of application of powerful CO₂-lasers with a continuous emission for welding of aluminium alloys. In this connection the CO₂-laser LT104 with HF-pumping of emission power of up to 10 kW was designed under supervision of V.P. Garashchuk in the PWI at the beginning of the 1990s [7]. The power source of this laser was designed at the Department, headed by V.D. Shelyagin.

The further experiments on welding of aluminium alloys became to be conducted by using this equipment. Thus, at the end of the 1990s the peculiar features of laser welding of aluminium-lithium alloys 1410, 1420, 1460, and also alloys 1201, AMg6 and D16 were investigated [8]. The interest to the welding of high-strength aluminium-lithium alloys was caused by the fact that their application in structures makes it possible to decrease the mass of latter by 10–15 % that is especially important in design of aerospace engineering objects. Investigations, carried out at the PWI by the staff members of Welding of Aluminium Alloys and Laser Welding Departments showed that in laser welding of semi-products of the above-mentioned alloys at 2–5 mm thickness of edges the width of the HAZ is 3–4 times decreased as compared with welding by arc methods and by 10–20 % as compared with EBW [8]. In application of laser welding the smaller changes in chemical composition of weld metal are observed [9, 10].

The most significant achievements in the field of welding of aluminium alloys, applying laser emission, were obtained as a result of combination of laser and arc power sources [11]. Thus, it was shown that increase in arc current leads to the increase in welding speed (Figure 2). Here, the transition from comparatively low currents (about 100 A) to the threshold value of 130–150 A is important, after which a very small increase in current leads to the high increase in welding speed. In the opinion of the authors of work [11] it is connected with a threshold value of absorption of laser emission requiring the reaching of a definite level of power density. At exceeding the threshold value the stable welding of aluminium alloys becomes possible. For emission of CO₂-laser this threshold corresponds to the power close to $3 \cdot 10^6$ W/cm². It is evident that the arc source at currents of above 150 A creates conditions for the better absorption of the laser emission by the weld pool.

Experiments on hybrid laser-arc welding of alloys AMg5, AMg6, 1915 and commercially pure aluminium with the range of thicknesses $\delta = 2$ –

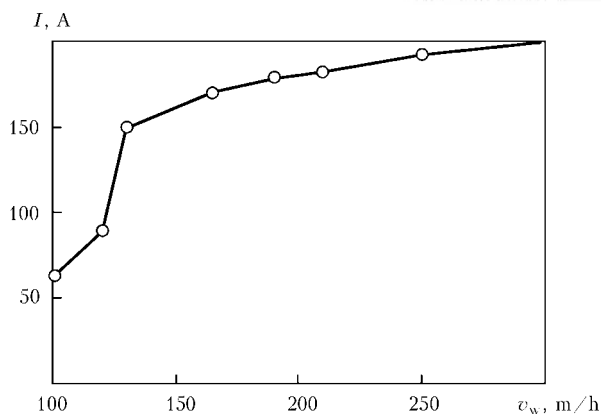


Figure 2. Dependence of speed of hybrid welding of alloy AMg6 2 mm thick on arc current at input of emission power of CO₂-laser of 2.8 kW into metal [10]

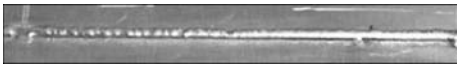



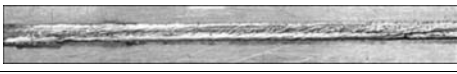

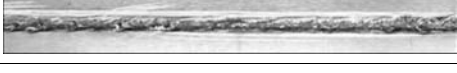






6 mm were carried out by using electrode wire SvAMg6 of 1.0–1.2 mm diameter in argon shielding [11]. It was found that the effect of mutual influence of laser and arc heat sources is manifested in the first turn in a possibility of significant (2–4 times) increase in the process speed. The important aspect was also the determination of the fact that in case of hybrid welding 1 kW of arc power is capable to replace from 0.5 to 1.0 kW of laser emission power. Moreover, the quality of produced welds can be close to laser one.

The further investigations in the field of laser-arc welding showed that in comparison with conventional MIG welding the hybrid welding of butt joints of thin-sheet alloy AMg6 ($\delta = 1.9$ mm) contributes to significant decrease in transverse residual deformations and stresses due to six-fold increase in welding speed (up to 250–300 m/h), 40 % decrease in its energy input and two-fold decrease in weld section [12]. It was found that the values of transverse residual stresses in near-weld zone in hybrid welding do not exceed ± 20 MPa, that is 4–5 times lower than stresses formed in MIG welding. Secondary transverse residual stresses from residual bending of the sample are in the ranges of ± 40 MPa, that is 2–2.5 times lower of values corresponding to MIG welding. Zone with longitudinal tensile residual stresses is 1.5 times narrowed as compared with MIG welding.

For the case of hybrid welding of aluminium alloys by combining the effect of laser emission with transferred arc plasma the investigations of laser-plasma welding of alloys AMts, AMg3, AMg5m, AMg6 of 0.5–3.0 mm thickness using filler wire SvAMg6 of 1.2 mm diameter and without it were carried out at the PWI. In addition, the emission was used from the Rofin-Sinar diode laser DF020HQ of up to 2 kW capacity with wave lengths of 0.808/0.940 μ m and CO₂ laser LT-104 with wave length of 10.6 μ m [7] (Table). It was found that the application of hybrid laser-plasma welding of aluminium allows 2–4



Welding conditions, appearance of face part of weld and transverse macrosections of butt and overlap joints of alloy AMg3 1.5 mm thick made by laser, plasma and hybrid welding [12]

Welding conditions		Appearance of weld on face side	Transverse macrosection
P_L, W	$I_{SP}/I_{RP}, A$		
Welding speed of 108 m/h; diode laser DF020HQ; focused spot diameter of 1.2 mm; focus deepening of 1.0 mm; plasma arc voltage of 20 V			
2000	–		
–	100/50		
1000	50/50		
1500	100/50		
Welding speed of 130 m/h; CO ₂ -laser LT-104; focused spot diameter of 0.5 mm; focus deepening of 1.0 mm; plasma arc voltage of 20 V			
1500	–		–
–	100/50		
1000	60/50		

times increasing the depth of penetration as compared to laser welding, and almost the same increasing the welding speed as compared with plasma welding [13]. Here, the important factor is the use of phenomenon of cathode cleaning of surface from oxide film. Tensile strength for produced joints was $(0.85-0.90)\sigma_t$ of base metal, that exceeds their properties of similar joints, made by arc methods of welding. Structures of welded joints, made by laser-plasma method, are characterized by a fine dispersity of weld metal and narrow fusion zone as compared to those, made by arc methods of welding, thus approaching them to joints made by a laser method.

Except the experiments on welding, the investigations of laser-arc surfacing of aluminium alloys were carried out [14]. The possibility was found for attaining the quality filling of narrow cavities in aluminium products without their mechanical grooving by fixation of electric arc on the cavity bottom using a focused laser emission. The laser-arc surfacing allowed eliminating such drawbacks typical of arc process as the presence of pores and lack of fusion in the lower part of the cavities being filled, as well as reducing the overheating of samples being surfaced.

It was shown in work [15] that increase in depth of penetration in laser welding is directly proportional to decrease in length of emission

wavis Monotonous decrease in depth of penetration with increase in process speed is observed both for laser and also for plasma welding in the range of 18–330 m/h speeds. Comparison of arithmetic sum of depths of penetration for laser and also for plasma processes with depths of penetration, obtained in hybrid laser-plasma process, showed the presence of synergic effect at simultaneous welding into a common pool by laser and plasma components (Figure 3). This effect consists in non-adequate growth of penetration depth and demonstrates the advantage of hybrid welding as compared to welding performed separately by laser and plasma processes.

The investigations of hybrid laser-arc welding of aluminium alloys, where the arc on consumable electrode was used, showed that intensity of evaporation of separate elements of base metal and electrode wire, and also the composition of shielding gas influence greatly the laser emission passing to the metal being welded [16]. Application of arc in argon or at high welding current led to the screening of emission and, consequently, to significant decrease in depth of penetration. To prevent this effect, it occurred to be rational to apply the mixtures of argon with helium or pure helium for the weld pool shielding and also to use the pulsed modulation of laser emission. In this case the hybrid welding in the

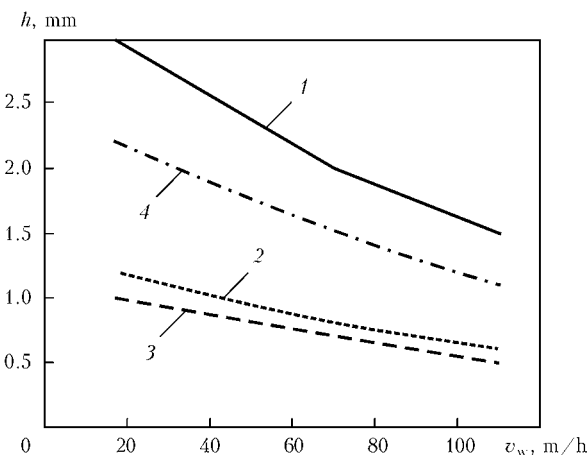


Figure 3. Dependence of penetration depth on speed of welding the aluminium alloy AMg6 ($\delta = 1-3$ mm): 1 – hybrid laser-plasma welding; 2 – laser welding; 3 – plasma welding; 4 – sum of depths of penetrations obtained by laser and plasma welding ($P_L = 1.2$ kW; $I_{SP}/I_{RP} = 50/50$ A; $U_a = 18$ V)

range of 30–60 m/h speeds allowed, as compared with a pulsed-arc consumable electrode welding, 1.8–2.6 times increasing the speed of welding the metal of 6 mm thickness, 1.3–1.6 times decreasing the heat input into metal being welded and reducing significantly the deformations of joints of 4 mm thickness. The investigation of nature of formation of welded joints allowed making conclusion that it is rational to apply the laser emission of more than 4 kW power at hybrid welding of aluminium alloys of 6 mm thickness.

At the present time the investigations of intensities of losses of alloying elements in aluminium alloys at their melting during welding with applying of laser or laser-arc heat sources are carried out. The limits of conditions of laser and hybrid welding are established, at which these losses from evaporation influence negatively the mechanical properties of the joints (Figure 4). It was suggested to eliminate this drawback by control heat input value, including also the application of a pulsed modulation of emission and its scanning, application of hybrid laser-arc processes, gas-dynamic or plasma-chemical processes inside the penetration channel (for example, by development and application of shielding systems with a differential gas supply directly into a vapor-gas channel) as well as processes of weld metal alloying by feeding of filler materials.

The offered review outlines the sufficiently high level of investigations of welding of aluminium alloys using a laser emission at the PWI over the various years. Nowadays these investigations are continued. They include development of the more effective methods of welding for manufacture of thin-walled body structures of motor cars, high-speed railway cars, different-purpose ships, aircrafts, rockets and space engineering objects.

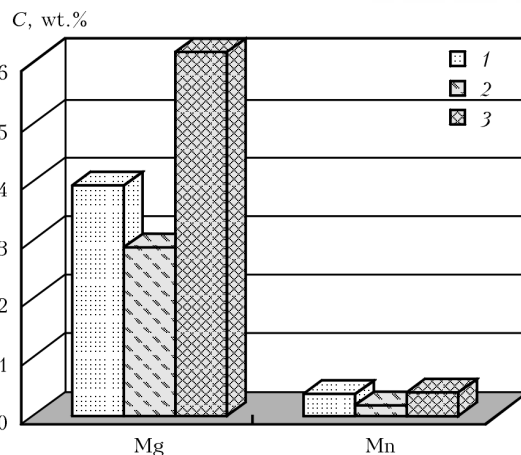


Figure 4. Effect of energy input E of laser welding of alloy AMg6 ($\delta = 1.2$ mm) at density of emission power $W = 2 \cdot 10^7$ W/cm² on content of alloying elements C in weld cast metal: 1 – laser welding, $E = 50$; 2 – laser welding, $E = 120$ J/mm; 3 – base metal

- Rabkin, D.M. (1986) *Metallurgy of fusion welding of aluminium and its alloys*. Kiev: Naukova Dumka.
- Velichko, O.A., Garashchuk, V.P., Moravsky, V.E. (1972) Laser welding of butt joints of dissimilar metal. *Avtomatich. Svarka*, **3**, 71–73.
- Velichko, O.A., Garashchuk, V.P., Moravsky, V.E. (1973) Relation between joint quality and laser welding parameters. *Ibid.*, **3**, 24–27.
- Nazarenko, O.K., Velichko, O.A., Avramchenko, P.F. et al. (1979) *Technological possibilities of welding unit LT1-5*: Information letter. Kiev: PWI.
- Avramchenko, P.F., Molchan, I.V. (1983) Continuous laser beam welding of AMg6 alloy. *Avtomatich. Svarka*, **3**, 68–69.
- Velichko, O.A., Avramchenko, P.F., Molchan, I.V. et al. (1987) CO₂-laser welding of T-joints of aluminium-magnesium alloy AMg6. *Ibid.*, **6**, 34–37.
- Garashchuk, V.P., Shelyagin, V.D., Nazarenko, O.K. et al. (1997) *Technologicac 10 kW CO₂-laser LT104*. *Ibid.*, **1**, 36–39.
- Bondarev, A.A., Boldin, A.A., Shelyagin, V.D. et al. (1998) Peculiarities of laser welding of high strength aluminium-lithium alloys. In: *Abstr. of Int. Conf. on Welding and Related Technologies into 21st Century* (Kiev, Nov. 1998). Kiev: PWI.
- Bondarev, A.A., Bondarev, Andr.A. (2001) Laser welding of aluminium alloys (Review). *The Paton Welding J.*, **12**, 19–25.
- Bondarev, A.A., Bondarev, Andr.A. (2001) Device for a focusing lens protection from sprays and heating in laser welding. *Ibid.*, **12**, 58–60.
- Shelyagin, V.D., Khaskin, V.Yu., Nabok, T.N. et al. (2005) Hybrid laser-arc welding of carbon steels and aluminium alloys. *Dopovidi NAN Ukrainy*, **7**, 97–102.
- Shonin, V.A., Mashin, V.S., Khaskin, V.Yu. et al. (2006) Residual stresses in butt joints of thin sheets from alloy AMg6 after arc and laser-arc welding. *The Paton Welding J.*, **9**, 20–24.
- Krivtsov, I.V., Shelyagin, V.D., Khaskin, V.Yu. et al. (2007) Hybrid laser-plasma welding of aluminium alloys. *Ibid.*, **5**, 36–40.
- Khaskin, V.Yu. (2009) Application of laser-arc cladding for filling up narrow cavities in aluminium alloy items. *Ibid.*, **2**, 31–34.
- Krivtsov, I.V., Shelyagin, V.D., Khaskin, V.Yu. et al. (2009) Hybrid laser-plasma and laser-arc welding of various aluminium alloys. In: *Laser technologies in welding and materials processing*. Kiev: PWI, 47–49.
- Shelyagin, V.D., Khaskin, V.Yu., Mashin, V.S. et al. (2009) Features of laser-MIG welding of high-strength aluminium alloys. *The Paton Welding J.*, **12**, 21–27.

FRICION STIR WELDING IN AEROSPACE INDUSTRY (Review)

E.V. SERGEEVA

HSC Consulting

1a Ginsterweg, 21407, Deutsch Evern, Germany. E-mail: sergeev.dr@t-online.de

Friction stir welding (FSW) finds ever wider application in industry, especially in manufacture of new engineering objects. In the review the examples of modern application of FSW in aerospace industry are given. They describe capabilities of the process and basic trends in development of FSW technologies existing today. The application of FSW in aerospace industry allows reducing the weight of flying vehicles, reducing number of riveted joints by 65 %, joining materials not welded using known methods, automation of joints control. 10 Ref., 7 Figures.

Keywords: *friction stir welding, aluminium alloys, aerospace industry, advantages of application, reduction of weight, flexibility and automation, increase of productivity*

Speaking about application of FSW in aerospace industry one can take data about any leading world corporations connected with manufacture of aircrafts, rockets, space stations and find numerous examples of application of this welding technology and its advantages.

Why namely FSW finds ever wider application in aerospace industry? Why world concerns contribute large funds into this technology? For example, the Boeing corporation made investments of 15 mln USD into FSW only for welding of tanks of «Delta» rocket-carriers. In the published review the author makes attempts to answer the questions and systemize the applications and basic trends for development of FSW technology existing today in aerospace industry (Figure 1).



Figure 1. First test flight of aircraft «Eclipse 500», in manufacture of which FSW was used [1]

FSW process. FSW was invented and patented in the Welding Institute (TWI) in December, 1991. TWI successfully filed the applications on patents in Europe, USA, Japan and Australia.

The principle of FSW is extremely simple (Figure 2). The cylindrical rotary tool of a specific shape with shoulders and pin in the center is submerged into the joining line of the parts subjected to welding and tightly pressed to each other. Here the amount of generated heat is sufficient for plastic welding of parts without fusion. The metal, heated up to the plastic state, is moved from the zone ahead the pin into the zone after it, then it is formed by shoulders and produces the welded joint during cooling.

Application of FSW in aerospace industry. In aerospace industry FSW finds ever more application for welding body parts, welding-on of transverse and longitudinal stiffeners and also production of:

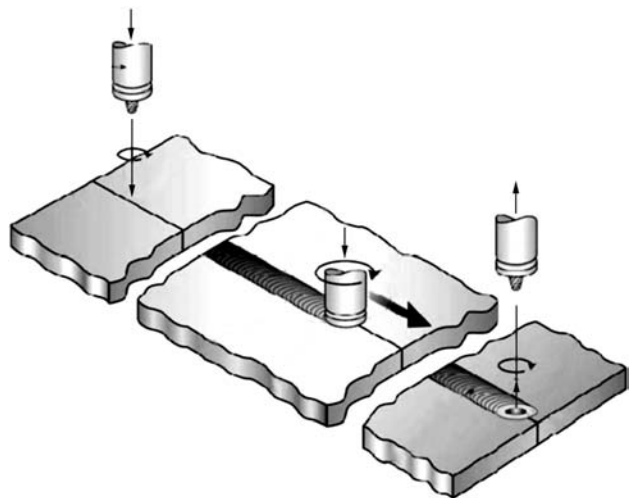


Figure 2. Scheme of FSW process according to DIN EN ISO 25239-1

- wings, fuselages, tail unit of aircrafts;
- cryogenic fuel tanks of space ships;
- fuel tanks for aircrafts;
- external fuel tanks of one-time use for military aircrafts;
- parts for rockets of military and scientific purpose.

One more field for FSW application is repair of defects of welds produced using arc welding.

The production of these design components applying FSW method is more economic as compared to the riveted joints and milling of solid metal. The welding of sheets of available materials with further shape formation is possible.

Application of FSW considerably increases compatibility of products, therefore, the information about practical applications of this welding technology and actual profits are not widely represented. However, from the materials of conferences and symposia on welding technologies [2, 3] the general representation can be obtained about advantages of use of FSW, the main of which are listed below:

- possibility of industrial manufacture of assembly units with high level of readiness;
- high level of repeatability and reproducibility and also assurance of quality at minimal deviations;
- flexibility and functional capabilities of industrial equipment allowing development of new solutions in the shortest terms.

As a rule the welded units and products in general can be verified and approved by such

competent establishments like DNW, RINA and Germanescher Lloyds.

Reasons of ever wider application of FSW in aerospace industry. *Reduction of weight of flying vehicles.* The basic factor determining the ever wider application of FSW in aerospace industry is reduction of weight. The higher is the speed of the flying vehicle, the more rational is the decrease in weight. The direct proportional dependence between the weight of flying vehicles and cost-efficiency of their application can be practically established (Figure 3) [4]. The plot shows the dependence of potential savings due to economy of fuel estimating one or two dollars for gallon per 100,000 miles of way.

The economy of the aircrafts is increased due to economy of fuel. The calculation was made per 100,000 hour service life of fuselage. For the space ships the cost of pound of useful load at the orbit will amount to 20,000 USD. For the space ship «Space Shuttle» of multiple use this cost is decreased to 10,000 USD per pound.

The use of FSW during production of industrial aircraft «Eclipse 500» [5, 6] allows reducing its weight by 50 pounds. The cost of fuel for this aircraft amounts to 89 USD per pound per hour. Therefore, minimization of funds on each pound, saved in welding, estimating per 100,000 h, amounts to 7,000 USD, per 50 pounds — 350,000 USD. The same calculations can be carried out for military aircrafts.

The use of Al–Li alloys in production of fuel tanks of rocket-carriers «Space Shuttle» allowed reducing their weight by 7500 pounds which in

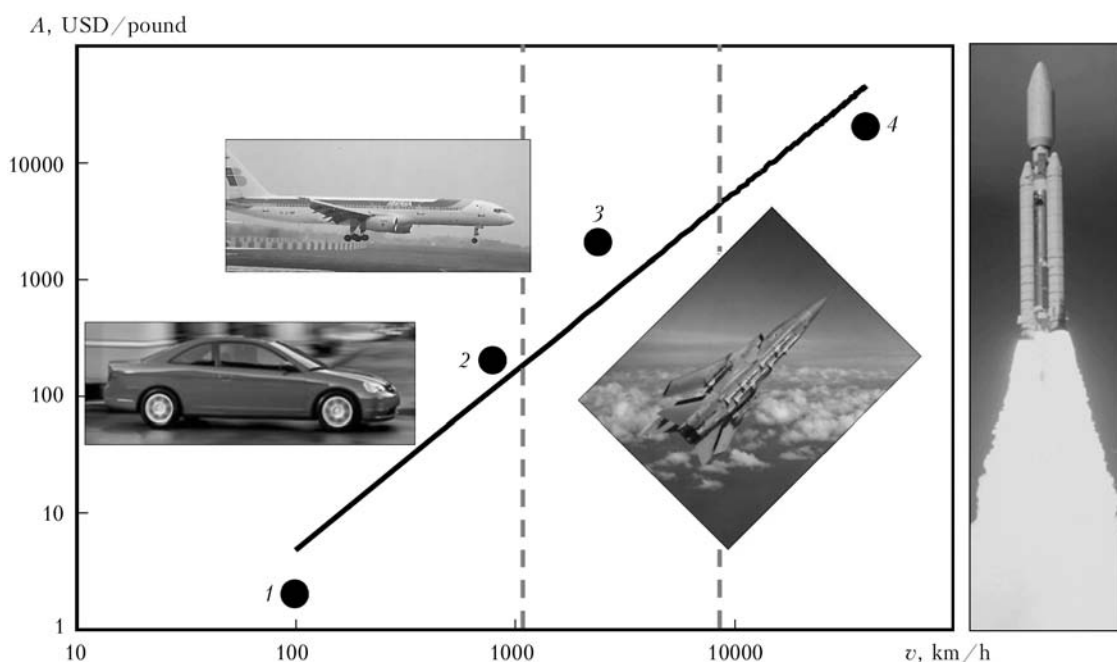


Figure 3. Effect of decreasing weight on economy of service A of motor car and aerospace engineering objects depending on the speed of their flight v [4]: 1 — motor car; 2 — aircraft; 3 — military aircraft; 4 — rocket

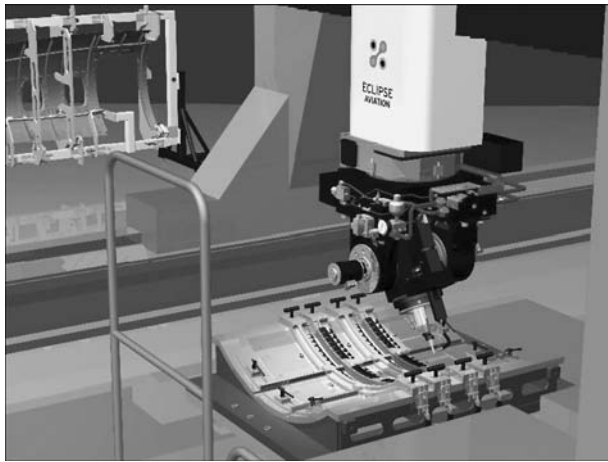


Figure 4. FSW of design components of «Eclipse 500» at the gantry machine tool (access mode: http://www.plm.automation.siemens.com/en_us/Images/Eclipse-fsw_tooling_tcm1023-21267.jpg)

financial relation means saving of 75 mln USD per a launch. This figure is determined by increase in useful load [7].

FSW: welds instead of riveted joints. Among the most important advantages of FSW in aerospace industry, the following fact can be mentioned that its application makes million of rivets redundant.

The FSW technology was at the first time applied in 2002 in production of jet aircraft «Eclipse 500» (Figures 1, 4 and 5) [6].

According to the messages from the management the application of FSW allowed 65 % decreasing the number of riveted joints. During production of each aircraft the FSW is used to weld 135 line meters of welds of cockpit, fuselage, wings and engine. FSW is applied also in the places of fastening of stiffeners and stringers. The welding is performed in automatic mode. As a result, in general 30,000 rivets are eliminated, moreover, the design performance with more rapid and simple mounting is possible. The FSW technology allows joining of design components of the aircraft body 4 times faster than automatic

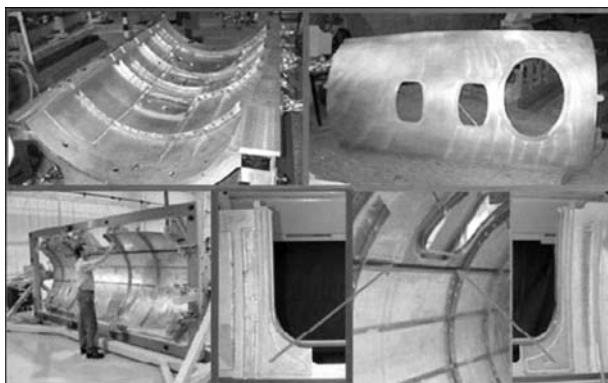


Figure 5. Elimination of riveted joints of overlapped welds using FSW (access mode: <http://www.dvs-ev.de/lvmv/downloads/schweibote0207.pdf>)

riveting and 20 times faster than manual one. Inner arrangement of the cockpit and saloon until the state of readiness for the flight takes not more than hour and a half. Only chairs are left to be mounted into the ready frame of the aircraft body.

The time for assembly of the aircraft «Eclipse 500» from the moment of mounting the body parts into the fastening devices of FSW equipment till the moment of exit of a ready product (with engine, interior, etc.) from the gates of a hangar is reduced to 9 days. If to add here the time for industrial tests and painting works, the general time of industrial cycle from the start of the first weld till the complete readiness to take-off reaches 3 weeks.

One more important message from the Boeing is the following: FSW was successfully applied in 73 projects. The traditional welding methods are connected with application of rivets and materials-fillers, which is inevitably connected with increase in weight of flying vehicles. The Boeing uses millions of rivets. Each day it is required to drill and fill in 1.1 million holes. The cost of each hole considering expenses for design of the structure, drilling, filling in and control amounts to 5–10 USD. The cost-efficiency of FSW is obvious [8].

Application of FSW in welding of two different materials cannot be welded using other methods. Reduction of weight of flying vehicles, in production of which FSW was applied, is not so much due to the absence of rivets, but with possibility of welding aluminium alloys, which cannot be welded using other methods. Using FSW the high-strength aluminium alloys 7XXX and 2XXX can be welded. Using alloys of the higher strength the lighter components meet the requirements to strength of bodies of flying vehicles with walls of a smaller thickness and flanges of a smaller width.

Since the beginning of the 1990s the development of FSW technology is one of the reasons for ever wider spreading of Al–Li alloys in aerospace industry as, for example, AA2195 and AA2198. Lithium has much lower specific weight as compared to aluminium and its presence reduces the mass of alloy simultaneously improving its mechanical characteristics. Al–Li alloys are used in production of fuel tanks of rocket-carriers «Space Shuttle» and «Falcon 9» (Figure 6), as well as in production of design components of fuselage of «Airbus A350 XWB».

Redundancy of expensive operations for control of welded joints. The gas arc welding is connected with fusion of metals and occurring

of gas bubbles inside the welds. In its turn it requires high expenses on elimination of defects. Therefore, the Boeing, for example, decided to replace gas arc by FSW, the application of which completely eliminates the appearance of hydrogen bubbles inside the weld metal. The application of FSW eliminated the expensive X-ray control, as far as inspection of 8900 m welds produced using FSW, showed the complete absence of defects [9].

Monitoring of FSW process parameters for prevention of weld defects. The challenge of problems connected with decrease of cost and weight of flying vehicles and improvement of quality of welds is obvious. The human factor in production of rockets and aircrafts can have irretrievable consequences, therefore, one can understand thriving of producers to automate welding process and control its parameters, increasing speed of welding and considerably decreasing time of production cycle. FSW process parameters are similar to the parameters of treatment using cutting: speed of spindle rotation, feed – welding speed, thickness of parts being welded, inclination of a tool relatively to the part surface, geometry of tool and also preheating of parts and design of clamping devices.

The task of monitoring the parameters of cutting process was successfully solved in modern machine building. There is a great number of enterprises producing systems for monitoring the abovementioned parameters of cutting process and their processing centers reliably operate in the automatic lines. At any output of parameters beyond the field of tolerance the efficient actions on detection and elimination of failure reasons are provided. FSW process can be monitored using the same methods and systems applied for monitoring the parameters of cutting process.

Thus, for example, at the equipment of HAGE Sondermaschinenbau GmbH the monitoring of FSW process is carried out by control of axial load or feed speed of welding head (Figure 7).

During welding at constant load the measuring system controls the preset value of acting axial loading. The monitoring of deviation of movements from the preset values is carried out. When the tolerance is exceeded the processing center is stopped.

In welding at constant feed of welding head the welding is carried out at the constant speed as in milling. The generated forces are changed depending on uniformity of material properties. Using measuring system the monitoring of deviation of movements from the preset values is car-



Figure 6. Tank of rocket-carrier «Falcon 9» of Al-Li alloy (SPACEX), the longitudinal and circumferential welds of which are produced using FSW. Formation of hydrogen bubbles is completely eliminated (access mode: http://en.wikipedia.org/wiki/File:SpaceX_factoryFalcon_9_booster_tank.jpg)

ried out. When the tolerance is exceeded the processing center is stopped.

The switching of monitoring modes is carried out manually or using numerical control program. For example, at the beginning and end of a weld when welding is performed at a constant force. The restricted factor of application of FSW is high axial loads and high forces of clamping of the parts being welded. Here the special clamping devices and special outfit are needed. The experience of HAGE Sondermaschinenbau GmbH for development and production of five-axial gantry processing centers for treatment of parts of steel and aluminium alloys is quite appropriate to solve this problem. The required devices for loading, clamping, feeding, unclamping and unloading of parts are designed and manufactured «key turn» at the same enterprise. The once designed clamping device guarantees the reliability during long service.

Flexibility of FSW process and simplicity of mounting the structure components after welding. The geometry of a tool, optimized to the material and shape of parts, parameters of weld-



Figure 7. Weld monitoring at the gantry center HAGE-MATIC 305 FSW for processing using cutting and FSW



ing process and special outfit allow producing welds of practically any spatial configuration. One of the most convince advantages of FSW is that the design components are ready for mounting just after their welding. The expenses for grinding, polishing and straightening are eliminated.

The application of FSW allowed almost twice decreasing expenses on welding works during production of the rockets «Delta II» and «Delta IV» [10]. It is followed from the materials of report submitted to TWI from the Boeing that application of FSW during production of the rockets «Delta II» and «Delta IV» allowed decreasing their cost by 60 % and reducing period of production cycle from 23 to 6 days.

FSW is also applied to weld external tank of «Shuttle», for «Ares I» and for the stand model of «Orion Crew Vehicle» in NASA and also to weld rockets from «Falcon 1» to «Falcon 9» at SpaceX. In aircraft construction, the FSW was at the first time applied for «Boeing C-17 Globemaster III» and «Boeing 747 Large Cargo Freighter». The roofing panels of military aircraft «Airbus A400M» were also welded applying FSW.

Federal Aviation Administration approved application of FSW for assembly of aircraft «Eclipse 500» already a year earlier before the planned period.

According to the messages from the management of Airbus, the application of FSW allowed reducing the mass of welded elements of flying vehicles by 40 % and decreasing period of production cycle by 20 %.

According to the messages, for «Eclipse 500» the FSW decreases the period of production cycle and production expenses. The period of production cycle of FSW is decreased by 40 % relatively to the period of production cycle with riveted joints. Highly-automated FSW welding allows saving from 50,000 to 100,000 USD for each aircraft.

1. <http://www.twi.co.uk>
2. <http://www.aluplanet.com/documenti/InfoAlluminio/AlGenFeb06Volpone.pdf>
3. <http://techcon.ncms.org/Symposium2005/presentations/Track%202/0810%20Florence.pdf>
4. <http://eagar.mit.edu/EagarPapers/Eagar192.pdf>
5. www.eclipseaviation.comhttp://www.avbuyer.com/PDFs/Eclipse_500_june04.pdf
6. http://www.avbuyer.com/PDFs/Eclipse_500_june04.pdf
7. <http://eagar.mit.edu/EagarPapers/Eagar184.pdf>
8. <http://www.boeing.com/news/frontiers/archive/2004/september/itt.htm>
9. http://www.iiwelding.org/TheIIW/Organization/Document/ISO%20Focus%2010-11_E%20-%20SR-NoMeltMiracle2.pdf
10. http://en.wikipedia.org/wiki/Friction_stir_welding#Applications

Received 06.03.2013

METHOD FOR MEASUREMENT OF DYNAMIC STRAINS IN EXPLOSION WELDING

L.D. DOBRUSHIN, E.D. PEKAR, A.G. BRYZGALIN and S.Yu. ILLARIONOV

E.O. Paton Electric Welding Institute, NASU

11 Bozhenko Str., 03680, Kiev, Ukraine. E-mail: office@paton.kiev.ua

The method is suggested for measurement of dynamic strains by using resistance strain gauges. The working power is supplied by the generator of DC pulses with a voltage of 23 V and duration of 14 ms. The short-time supply of the power allows increasing the working current from 25–50 to 200–250 mA, this leading to almost an order of magnitude increase in sensitivity of the method. The measurement system comprises the DC pulse generator and the digital oscillograph connected to a computer. Calibration tests were carried out, and performance of the measurement system was investigated in a range of elastic and elasto-plastic strains. It is shown that the dynamic strains due to explosion loading of metal structures can be measured at a satisfactory accuracy within $-0.6-0.6\%$ in a time interval of 0–14 ms. In addition, the system makes it possible to fix residual strains of metal of a structure after the dynamic impact. 6 Ref., 1 Table, 8 Figures.

Keywords: *dynamic load, strains, resistance strain gauge, measurement, bridge circuit, pulse generator, sensitivity of method*

Currently, the most widespread method for measurement of dynamic strains is the tensometric one by using resistance strain gauges (RSG), which are connected into the measurement system based on the bridge circuit. Advantages and drawbacks of its practical application are well known [1].

In case of using RSG to measure the stress-strain state of metal structures under explosion loading it is necessary to locate them in close proximity to a charge. The length of wires connecting the working and compensation RSG can be up to several dozens of metres, and their active resistance and reactance can no longer be neglected, as they introduce substantial errors in the measurements. Moreover, in this case the measurement system becomes more sensitive to interferences. In practical measurements, the amplitude of the useful signal differs from that of the interferences, and its identification becomes problematic [2]. Increase in value of the useful signal can be achieved due to increasing the working current powering the bridge. But one of the important factors affecting the measurement accuracy is heating of the RSG by the working current flowing through them. Proper operation of the commercial RSG with the measurement circuit that is permanently on is possible at a current value of 20–50 mA [3].

In structures subjected to explosion loading, as well as in metal during explosion welding the maximal strains last for several milliseconds [4].

Therefore, powering of the measurement circuit can be provided by supplying the pulse voltage for 10–15 ms. In this case it is necessary to synchronise initiation of an explosive charge, starting up of the oscillograph and feeding of the measurement voltage pulse. A short time of supplying the power to the RSG allows increasing the working current to 200–250 mA, this leading to almost an order of magnitude increase in the sensitivity of the measurement method.

The E.O. Paton Electric Welding Institute developed the method for measuring dynamic strains, with which the working voltage is supplied by the generator of DC pulses with a voltage of 23 V and duration of 14 ms [5]. The generator was made by specialists of the Volgograd Technical University. To assess the capabilities of the new method and its fitness for measurement of strains induced in metal structures under explosion loading, its performance was investigated in a range of elastic and elasto-plastic strains.

Calibration tests of the developed method in a range of elastic strains were carried out by using a specially made calibration device (Figure 1) according to the scheme of four-point bending of a prismatic steel beam measuring $400 \times 40 \times 5$ mm, as well as by using the tensile testing machine. Oscillograph Dataman allowing the measurement data to be displayed directly on the computer monitor was employed as recording equipment. The obtained calibration dependences are shown in Figure 2. The Figure also shows the dependence of mechanical stresses on the bridge unbalance voltage, which was derived by calculations from the following expression:

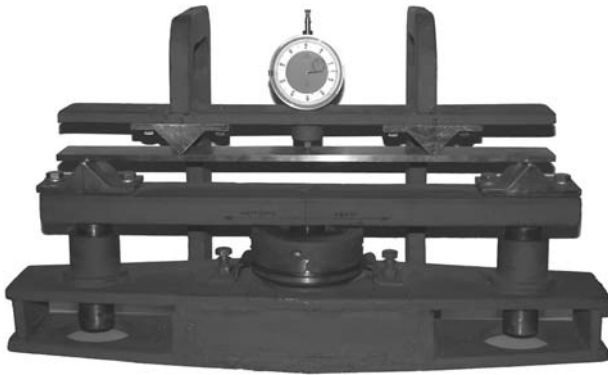


Figure 1. Appearance of the calibration device

$$\sigma = 4E \frac{\Delta U}{s(U - 2\Delta U)}, \quad (1)$$

where σ is the stress; E is the elasticity modulus of the beam steel; ΔU is the measurement bridge unbalance voltage; U is the voltage supplied to

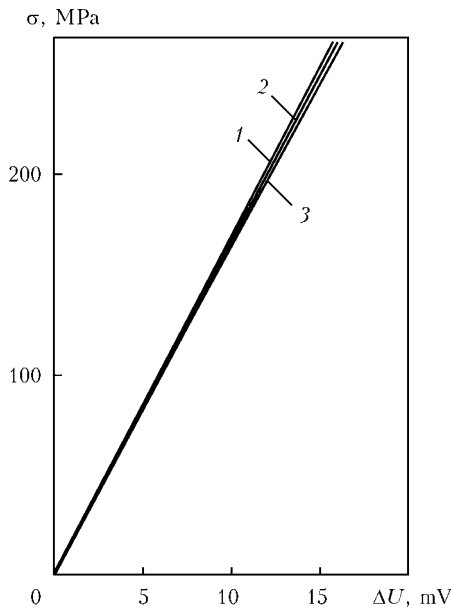


Figure 2. Calibration dependences derived experimentally by using the tensile testing machine (1), by calculations from the coefficient of tensosensitivity (2) and experimentally by using the special device (3)

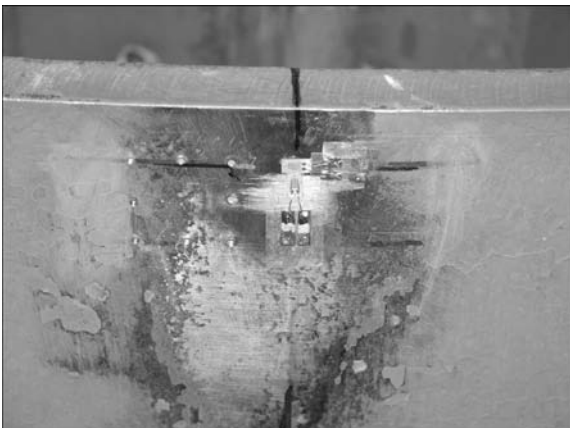


Figure 3. Measurement of strains in the explosion welding support (scale division value – 2 μm)

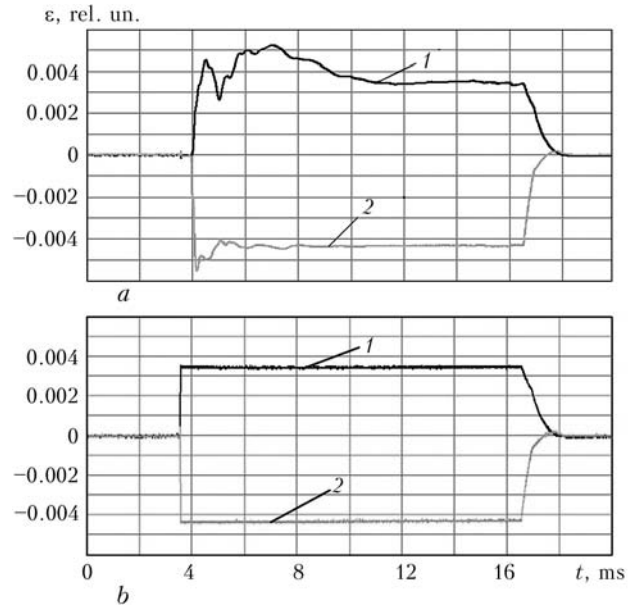


Figure 4. Strains in the supportwall at the moment of explosion of the 50 kg explosive charge (a) and after explosion (b): 1 – horizontal strains; 2 – vertical strains

the bridge; s is the coefficient of tensosensitivity of the resistance strain gauge specified by a manufacturer.

The obtained calibration dependences had a linear form. The calibration coefficient was equal to 17.7 MPa/mV ($56.5 \cdot 10^{-3}$ mV/MPa) in tests by using the tensile testing machine, 17.2 MPa/mV ($58 \cdot 10^{-3}$ mV/MPa) by using the calibration device, and 17.5 MPa/mV ($57.25 \cdot 10^{-3}$ mV/MPa) by calculating the stresses using expression (1).

The difference in the coefficients obtained in calibration tests by using the tensile testing machine and special device was related mainly to

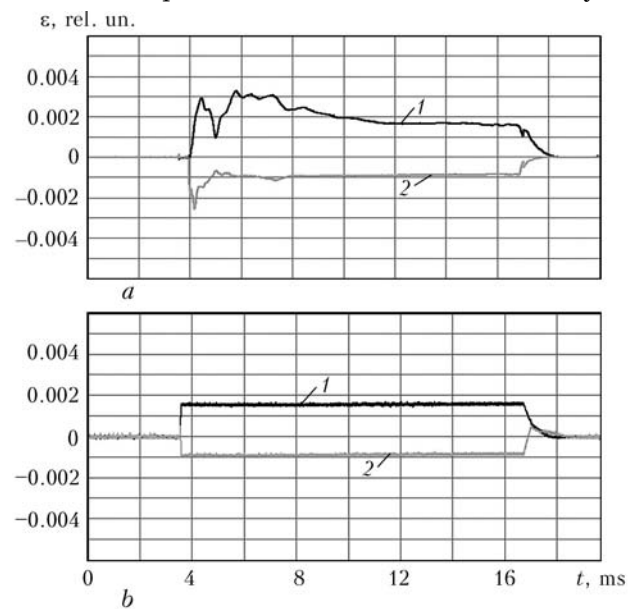


Figure 5. Strains in support wall at the moment of explosion (a) and after explosion of the 20 kg explosive charge (b) (here and in Figure 6 1 and 2 are the same as in Figure 4)

the fact that the tests conducted by using the special device included a great number of geometric parameters, each being measured with some error, as well as to the unavoidable rounding of the calculated values.

Performance of the method in a range of elasto-plastic strains was checked by investigations of the strains taking place in a special support used for explosion welding. The support was a vertically placed steel cylinder 500 mm high and 2 m in diameter, having a bottom. The internal volume was filled up with steel shot. Billets for explosion welding were placed on the shot. Weight of the explosive charge was varied from 20 to 50 kg. Two measurement resistance strain gauges were attached to the support wall near the upper end: in circumferential and vertical directions. Gauge lengths were marked near the RSG to conduct measurements by using a mechanical deformometer with an indicator of the clock type (Figure 3). The deformometer fixed residual strains in the wall of the support after explosions. It should be noted that the method developed allows measuring residual strains in a structure of interest by re-switching on of the measurement circuit after explosion. Figure 4 shows examples of fixation of the strains developing with time at the moment of explosion of a charge and in a stationary state after explosion.

Figures 5 and 6 show similar oscillograms of the strains occurring in the support after explosion of charges 20 and 35 kg in weight.

The Table gives comparative results of measurements of the residual strains.

While evaluating the measurement results, it should be taken into account that the residual strains form due to the plastic strains in the support wall caused by explosion. The plastic strains differ from the elastic ones in a much higher non-uniformity of distribution. Measurements with the deformometer and RSG were conducted at different, although close points in the support wall. The spread of the accumulated strains (the last line of the Table) was smaller compared to the majority of individual measurements. Therefore, the spread of the indications obtained by two different methods can be considered acceptable. The results obtained are indicative of the fact that the developed method allows evaluating the strains that exceed the elastic ones.

Investigations on evaluation of reliability of the time intervals being fixed were carried out by fixing the loading wave generated in a straight cylindrical steel rod due to an impact by a free-falling steel striker. The RSG (gauge length of

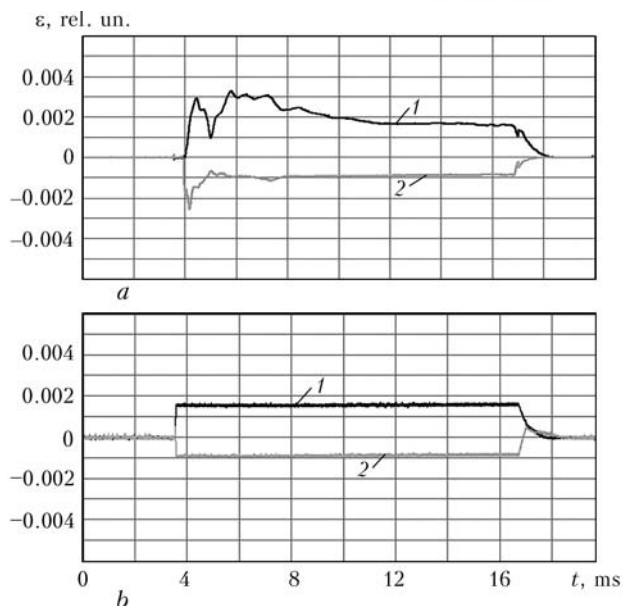


Figure 6. Strains in support wall at the moment of explosion (a) and after explosion of the 35 kg explosive charge (b)

3 mm, resistance of 100 Ohm) was attached to the rod 720 mm long and 18 mm in diameter at a distance of 30 mm from the end hit by the striker. The rod was secured vertically with a clamp through a rubber washer. The striker, which was a cylindrical rod 100 mm long and 10 mm in diameter, was thrown via a guide pipe onto the rod from a height of 1 m (Figure 7). Also, it performed the function of a starting sensor. An example of the loading wave being fixed is shown in Figure 8.

Plastic deformation of the striker and the rod occurs at a moment of their collision, this being evidenced by the resulting dents. Therefore, theo-

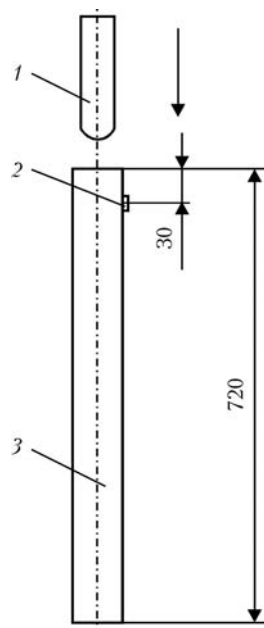


Figure 7. Schematic of generation of the loading wave in the rod: 1 – striker; 2 – RSG; 3 – rod

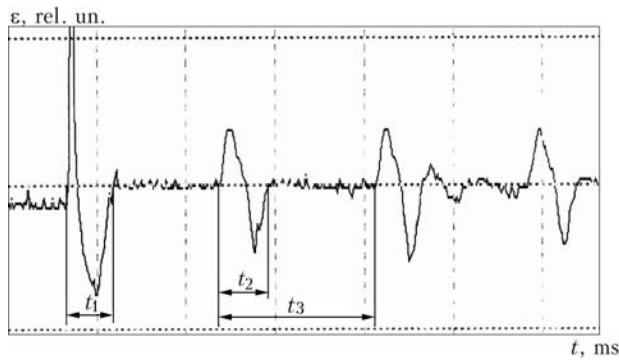


Figure 8. Loading wave in the rod (for designations see the text)

retical calculation of the length of the generated loading wave is problematic. This makes it impossible to compare time t_1 and t_2 with the calculated values (t_1 – time from the moment of collision of the striker with the rod to the moment of departure of the generated loading (compression) wave from the resistance strain gauge; t_2 – time from the moment of entering of the loading (tension) wave reflected from the remote end of the rod to the RSG to the moment of departure from it of the loading (compression) wave reflected from the collision end). The time of passage of the 1380 mm distance by the already elastic wave, which propagates at the sound velocity, characterises t_3 (time of propagation of the loading wave from the RSG to the remote end of the rod and back after reflection). Assuming the rod sound velocity in steel to be equal to 5100 m/s [6] yields that $t_3 = 271 \mu\text{s}$. Time t_3 averaged over measurements by 10 experiments and 3 periods in each experiment (totally 30 values) is 275 μs . Maximal measured time t_3 is 279 μs , and minimal t_3 is 272 μs . Good agreement between the calculated and experimental results, and small spread of the indications make it possible to consider the time measurement accuracy to be sufficient for the range of the problems being solved.

Conclusions

1. The new method developed for measurement of dynamic strains is fit for investigation of the

Comparative results of measurement of residual strains in the explosion welding support

Explosion No.	Strains, %			
	Horizontal		Vertical	
	Deformometer	Resistance strain gauge	Deformometer	Resistance strain gauge
1	–	0.12	–	–0.02
2	–	0.16	–	–0.09
3	–	0.35	–	–0.43
4	0.42	0.39	–0.27	–0.33
5	0.54	0.30	–0.17	–0.12
6	0.23	0.25	–0.29	–0.36
7	0.55	0.60	–0.55	–0.60
8	0.17	0.23	–0.25	–0.30
9	0	0	–0.27	–0.18
10	0	0	–0.56	–0.42
11	0	0	–0.56	–0.33
Total of lines 4-11	1.91	1.77	–2.92	–2.64

stress-strain state of metal structures subjected to explosion loading.

2. The measurement system allows evaluating residual strains induced in structures by pulsed loading.

1. Nedoseka, A.Ya. (2001) *Principles of calculation and diagnostics of welded structures*. Kiev: INDPROM.
2. Kolodyazhny, A.V., Sevryukov, V.I. (1986) *Impact and pulse actions on structures and materials*. Kiev: Naukova Dumka.
3. *TU3.06 Ukraine 7710-0001-93*: Resistance strain gauges. Purpose and field of application.
4. Vorobiov, Yu.S., Kolodyazhny, A.V., Sevryukov, V.I. et al. (1989) *Rapid deformation of structural elements*. Kiev: Naukova Dumka.
5. Dobrushin, L.D., Bryzgalin, A.G., Pekar, E.D. et al. (2012) On the possibility of application of pulse current generator for measurement of dynamic strains in metal structures. *Izvestiya Volgograd. Gos. Tekhn. Un-ta. Series Explosion welding and properties of welded joints*. 5(14), 78–82.
6. Kuchling, H. (1985) *Reference book on physics*. 2nd ed. Moscow: Mir.

Received 13.02.2013